

This document will now be processed through the Hanford Waste Treatment and Immobilization Plant review procedure to produce an interim project report. The full test program will be documented in reports from our sub-contractors, which will be released this summer.

Steve Barnes
PJM Program Manager

SMB/jmp

Attachment:

“Hybrid Mixing System Test Data Supporting the Ultrafiltration Feed Process (UFP-VSL-00002A/2B) and HLW Lag Storage (HLP-VSL-00027A/B) and HLW Blend (HLP-VSL-00028) Vessel Design Efforts”

Distribution

PDC	MS11-B	Hornbuckle, K. w/a	MS5-L
Abodishish, H. w/a	MS5-L	Lavender, J. w/a	MS4-B1
Armstead, M. w/a	MS14-3B	Lawrence, R. w/a	MS8-A
Arnold, J. w/a	MS4-A1	Piccolo, S. w/a	MS14-4C
Barnes, S. w/a	MS5-L	Schneider, J. w/a	MS5-I
Beckman, A. w/a	MS4-A1	Schuetz, P. w/a	MS5-I
Betts, J. w/a	MS14-3C	Slater, C. w/a	MS6-P2
Bronner, A. w/a	MS6-P2	Smith, G. w/a	MS5-L
Corriveau, C. w/a	MS6-P2	Tosetti, R. w/a	MS4-A2
Duncan, G. w/a	MS4-D2	Tamosaitis, W. w/a	MS5-L
Edmondson, A. w/a	MS4-D2	Valentino, T. w/a	MS5-I
Garrett, R. w/a	MS4-B1	Voke, R. w/a	MS9-A
Grabowski, S. w/a	MS4-A2	Wilson, J. w/a	MS12-B
Hoffmann, M. w/a	MS4-D2	Winkler, C. w/a	MS5-G

**Hybrid Mixing System Test Data
Supporting the Ultrafiltration Feed
Process (UFP-VSL-00002A/2B), HLW
Lag Storage (HLP-VSL-00027A/B)
and HLW Blend (HLP-VSL-00028)
Vessel Configurations**

PJM Task Team

March 2004

Table of Contents

1.0 Introduction.....	1.1
1.1 Background	1.1
1.2 Design Goals for the Phase II PJM Hybrid Mixing Systems	1.2
1.3 Operational Scenarios.....	1.3
1.3.1 Operational Processing Modes	1.3
1.3.2 Mixing Operation Modes.....	1.3
1.4 Overview of the PJM-Hybrid Mixing Systems Design Approach	1.4
1.5 Overview of the Scaled Testing Methodology	1.5
2.0 Test Stands and Experimental Methods.....	2.1
2.1 APEL 4 PJM Test Stand.....	2.1
2.2 336 PJM Test Stand Description	2.3
2.3 Scaled Prototypic Test Stands	2.6
2.3.1 UFP Prototype Vessel.....	2.6
2.3.2 Lag Storage Prototypic Vessel	2.10
2.3.3 System Operation and Data Acquisition	2.17
2.3.4 Mixing Effectiveness Determination.....	2.18
2.3.5 Solids Suspension Under Turbulent Conditions.....	2.18
2.3.6 Visual Observations During (Dye) Tracer Tests	2.19
2.3.7 Specific Observations During Gas Retention and Release Tests	2.19
2.4 Sparger Testing.....	2.20
2.5 Gas Retention and Release	2.22
2.6 Tracer Techniques	2.23
3.0 Supporting Data for Mixing System Design Support.....	3.1
3.1 Rheology	3.1
3.1.1 Bounding Conditions.....	3.1
3.1.2 Simulants	3.2
3.2 Prototype Results.....	3.5
3.3 Sparging.....	3.8
4.0 Description of Selected Pretreatment Facility Designs	4.1
4.1 Ultrafiltration Feed Process Vessel (UFP-VSL-00002A/B)	4.1
4.1.1 HLW Lag Storage Vessel (HLP-VSL-00027A/B).....	4.5
4.1.2 HLW Blend Vessel (HLP-VSL-00028)	4.9
5.0 Gas Retention and Release in Selected Prototype Vessel Configurations.....	5.1
5.1 Principle and Approach	5.1
5.2 Gas Holdup in Normal Operations	5.2
5.3 Gas Release after Mixing System Restart	5.4
6.0 References.....	6.1
Appendix A: Technical Basis for Scaled Testing of WTP Mixing Vessels with Non-Newtonian Slurries.....	A.1
Appendix B: Dye Method	B.1

Figures

1.1. PJM-Hybrid Mixing Approach	1.4
2.1. APEL 4 PJM Test Stand.....	2.2
2.2. Photograph of the PJMs Used in the 336 Test Facility	2.3
2.3. Schematic of Experimental System Used to Evaluate PJMs Using Non-Newtonian Simulants	2.3
2.4. Plan View of the Instrument Locations for the 336 Building PJM 4 Test Stand	2.5
2.5. Video System for Detecting Mixed Region in Large-Scale Testing	2.5
2.6. Top View of the UFP Prototypic Test Stand.....	2.6
2.7. Plan View of the UFP Test Stand.....	2.7
2.8. Schematic of the 45° Nozzle Used in the UFP Test Stand	2.9
2.9. Top View of the LS Prototype Test Stand and Nominal Dimensions.....	2.11
2.10. Plan View of the LS Prototype Test Stand and Nominal Dimensions	2.12
2.11. Schematic of the 45° Nozzle in the LS Prototype Test Stand.....	2.14
2.12. Recirculation Pump Discharge Nozzles Used in LS Sequence 20.....	2.15
2.13. Top View of the Recirculation Nozzles in the Tank for LS Sequence 20.....	2.16
2.14. Diagram of Sparging Experimental Setup.....	2.20
2.15. Diagram of Sparging Experiment Concepts.....	2.21
2.16. Summary of Tracer Dye Technique Steps.....	2.24
2.17. Schematic of LS Vessel Tracer Sampling Locations	2.25
2.18. Schematic of Ultrafiltration Process Vessel Tracer Sampling Locations.....	2.25
3.1. Rheogram of Actual HLW Pretreated Sludge Samples with Upper Bound Rheological Curve.....	3.1
3.2. Flow Behavior Comparison of PJM Simulants and Actual HLW Pretreated Sludge	3.3
3.3. Percent Mixed Versus Yield Reynolds Number for UFP Prototype Test Stand During Various Operating Conditions.....	3.7
3.4. Percent Mixed Versus Yield Reynolds Number for LS Prototype Test Stand During Various Operating Conditions.....	3.7
3.5. ZOI and ROB Sparger Diameters at Various Air Flow Rates.....	3.9
3.6. Adjacent ZOI and ROB Interaction Options.....	3.10
4.1. UFP-VSL-00002A/B Mixing System Layout – Plan View	4.1
4.2. UFP-VSL-00002A/B Mixing System Layout – Elevation View	4.2
4.3. Sparge Air Requirements and Resulting Zones of Influence – UFP-VSL-00002A/B	4.3
4.4. PJM Details – UFP-VSL-00002A/B	4.4
4.5. Outer PJM Nozzle Detail – UFP-VSL-00002A/B	4.4
4.6. HLP-VSL-00027A/B Mixing System Layout – Plan View	4.5
4.7. HLP-VSL-00027A/B Mixing System Layout – Elevation View	4.6
4.8. HLP-VSL-00027A/B, HLP-VSL-00028 Recirculation Jet Layout – Plan View	4.6
4.9. Sparge Air Requirements and Resulting Zones of Influence – HLP-VSL-00027A/B.....	4.7
4.10. PJM Details – HLP-VSL-00027A/B, HLP-VSL-00028	4.8
4.11. Outer PJM Nozzle Detail – HLP-VSL-00027A/B, HLP-VSL-00028	4.8
4.12. Specific Location of Spargers in the HLW BV Along with Air Flow Requirements	4.9

4.13. Number and Location of Spargers in the HLW BV Along with Air Flow Requirements	4.10
5.1. Gas Fraction as a Function of Time During and After a Gas Holdup Test in the APEL LS Prototype.....	5.2
5.2. Gas Holdup Test Results in APEL UPF Prototype Using Two Sets of Operating Conditions	5.3
5.3. Gas Release from Gelled Clay in the APEL LS Prototype	5.5
5.4. Gas Release from Gelled Clay in the APEL LS Prototype Showing Additional Gas Release Resulting from Operation of Eight Spargers (Sequence 15).....	5.5
5.5. Gas Release from Gelled Clay at 1.4 H/D in the APEL UFP Prototype (Sequence 5).....	5.6
5.6. Gas Release from Gelled Clay at 1.8 H/D in the APEL UFP Prototype (Sequence 6).....	5.6

Tables

2.1. UFP Test Sequences Presented in this Document and Corresponding PJM, Sparger, and Recirculation Pump Configurations	2.8
2.2. LS Test Sequences Presented in this Document and the Corresponding PJM, Sparger, and Recirculation Pump Configurations	2.13
3.1. Physical and Rheological Properties that Help Define Simulants for Rating or Qualifying Fluidic Mixing Systems	3.2
3.2. Rheological Model Fits for LS Prototype PJM Simulants at Ambient Temperature	3.4
3.3. Rheological Model Fits for UFP Prototype PJM Simulants at Ambient Temperature	3.4
3.4. Rheological Model Fits for LS Prototype PJM Simulants at Ambient Temperature	3.4
3.5. Test Conditions and Percent Mixed Results for Tests Performed in UFP Test Stand	3.5
3.6. Test Conditions and Percent Mixed Results for Tests Performed in LS Test Stand	3.6
3.7. Test Conditions and Results of Solids Lift Tests Performed in UFP Prototype Test Stand.....	3.8
3.8. Test Conditions and Results of Solids Lift Tests Performed in LS Prototype Test Stand	3.8
5.1. Summary of Gas Holdup in the LS Vessel.....	5.3
5.2. Summary of Gas Holdup in UFP Vessel.....	5.4

Acronyms and Abbreviations

acfm	actual cubic feet per minute
APEL	Applied Process Engineering Laboratory
BHRG	BHR Group
BV	blend vessel
cfm	cubic feet per minute
CCN	correspondence control number
CFD	computational fluid dynamics
DACS	data acquisition and control software
DBT	design basis event
FEP	Feed Evaporation Process System
FMP	Fluid mixing Processes
FRP	Feed Evaporation Process System
gpm	gallons per minute
GR&R	gas retention and release
H/D	ratio of slurry height to vessel diameter
HLP	HLW Lag Storage and Feed Blending Process System
HLW	high-level waste
ID	inner diameter
ITS	important to safety
JPP	jet pump pair
LAW	low-activity waste
LRB	laboratory record book
LS	lag storage
OD	outer diameter
PJM	pulse jet mixer
PVC	polyvinyl chloride
PWD	Plant Wash and Disposal System
R&D	research and development
R&T	research and technology
RD	rheological additive
RDP	Spent Resin Collection and Dewatering Process System
RFD	reverse flow diverter
ROB	region of bubbles
scfm	standard cubic feet per minute
TEP	Technetium Eluant Recovery Process
TXP	Technetium Ion Exchange
UHP	ultrafiltration feed process
VFD	variable frequency drive
WTP	Waste Treatment Plant
ZOI	zone of influence

1.0 Introduction

1.1 Background

The Pulse Jet Mixer (PJM) Task Team (R&T, Engineering, R&D, and mixing consultants) developed an integrated strategy for scaled testing to validate PJM mixing in Waste Treatment Plant (WTP) vessels containing non-Newtonian fluids in June 2003. The scaled PJM mixing tests were to provide information on the operating parameters critical for the uniform movement (total mobilization) of these non-Newtonian slurries. In addition, the WTP project funded work to determine WTP-specific hydrogen generation rate source terms and gas transport characteristics in representative scaled prototypic mixing configurations during PJM operation. The gas transport testing included gas retention and release (GR&R) characteristics within non-Newtonian slurries during mixing operations to support design of the PJM mixing systems, to understand these characteristics within the selected mixing system, and to allow for development of normal operation and post-design basis event (DBE) mixing strategies.

Initial (physical) scaled testing confirmed in October 2003 that the baseline pulse jet designs in these vessels did not mix the non-Newtonian slurries to the extent necessary to meet WTP design requirements. Phase I of the PJM program developed an alternative “PJM-only” configuration that mixed the vessels containing non-Newtonian slurries in accordance with WTP design requirements toward the end of November 2003. Phase I scaled gas retention and release testing demonstrated that the WTP could provide safe gas control with these configurations in December 2003. In the same time frame, the hydrogen generation rate source testing was completed using actual waste samples from “expected worst case” tanks, and a better correlation to predict hydrogen generation for use by the WTP Project was developed. While the alternative PJM configuration was acceptable, implementation of the PJM-only mixing systems severely impacted the WTP facility designs due to increased numbers of PJMs, additional piping, and the significantly increased air consumption necessary to operate these systems.

To minimize the impact to the overall project cost and schedule, the PJM Task Team was directed to develop PJM hybrid mixing systems to reduce the WTP impact. Phase II of the PJM program investigated further alternative configurations to assess the effects of slurry rheology changes, reduced tank volume, PJM jet velocity and nozzle size, sparging, and recirculation pump operation. Phase II PJM hybrid mixing systems recently completed additional testing to confirm that the modified configurations mix non-Newtonian slurries in accordance with WTP design requirements. PJM hybrid mixing systems GR&R testing confirmed that the selected PJM configuration provides safe gas control in accordance with WTP design requirements.

This document describes the PJM hybrid mixing systems goals, mixing operation modes, test stands and experimental methods, selected configurations, and testing data supporting the ultrafiltration feed process (UFP) (UFP-VSL-00002A/2B), HLW lag storage (HLP-VSL-00027A/B) and HLW blend (HLP-VSL-00028) vessel configurations selected by the Pretreatment Facility Team and Central Engineering.

1.2 Design Goals for the Phase II PJM Hybrid Mixing Systems

In conjunction with Engineering, Pretreatment and HLW Vitrification Facilities, and Project Management personnel, the PJM Task Team conducted the hybrid mixing systems testing program with the following success criteria and constraints:

- Achieve complete mixing (i.e., no stagnant regions) with turbulent conditions in the majority of the slurry volume. Turbulent mixing conditions enhance heat transfer within the vessel. Turbulent mixing facilitates the suspension of waste particles.
- Use the baseline PJMs to mix in the bottom of the vessels; supplemental mixing would be used to mix the upper portion of the vessels.
- Limit the PJMs to the original baseline design, which includes a 4-inch exit nozzle; however, the standard jet pump pairs (JPPs), which use compressed air as the motive force to drive the pulse tubes, will be upgraded to allow for a nozzle velocity of 12 m/s. The number of PJMs is limited to six in the ultrafiltration feed process (UFP) vessel and eight in the lag storage (LS).
- Target the non-Newtonian slurry rheology in terms of yield stress from 5 to 30 Pa based on actual pretreated waste data from Tanks C-104 and AZ-102, respectively.
- Do not use the UFP recirculation pump above a vessel slurry height (H) over vessel diameter (D) ratio of 1.4.
- Mix the LS and blend vessels to the required H/D ratio of 0.74, with pretreated waste slurries having a yield stress of 30 Pa.
- Operate the air sparge systems within the constraints of the Pretreatment Facility vessel vent system; i.e., total additional air flow of 1520 scfm.
- Consider supplemental mixing technologies that are technically mature above emerging technologies. Eventually, PJMs, sparging, and steady jets (flow provided by recirculation pumps) were selected as the only options.
- Limit the full-scale recirculation pumps to 2200 gpm for each vessel.
- Provide robust mixing systems, i.e., provide for a 40-year operation life in a configuration that can be fabricated readily.
- Keep gas holdup (how much gas is retained at steady state in the mixed waste during normal, continuous PJM operation) as low as possible.
- Control gas release rate (how quickly gas is released upon PJM restart after a period of no mixing) after a post DBE or non-mixing period.
- Minimize air consumption requirements on both the supply and vessel ventilation systems.
- Minimize the number of vessel penetrations.
- Minimize the overall risk to the project.
- Minimize the overall cost and schedule impact to the project.

1.3 Operational Scenarios

1.3.1 Operational Processing Modes

Waste slurries with a sodium concentration of approximately 5 M is delivered to UFP-VSL-00002A/B for separation into solid (HLW) and liquid (LAW) fractions. The waste in the feed vessel is pumped through three bundles of cross-flow filters. The water and other soluble components of the waste permeate pass through the filter media and discharge into one of the permeate receipt vessels. The solids are recirculated into the feed vessels, where additional waste is received from the feed preparation vessels to replace the permeate and maintain a relatively constant volume (corresponding to an H/D of 1.4). While the solids are being concentrated, the filters will be back-pulsed periodically. Back-pulsing pushes permeate back through the filters into the concentrated slurry and dislodges solids that have built up on the filter surface, thus enhancing the overall permeate flux rate. The UFP vessels are equipped with PJMs, cooling jackets, high-pressure steam injectors, and chemical reagent feed lines. The cooling jackets are used to control the slurry temperature while filtering and to cool the waste after leaching. The filter pumps are large and add a significant amount of energy to the waste as heat. The high-pressure steam is used to heat and hold the waste at an elevated temperature during the leach process. The chemical reagents are used for leaching and filter cleaning.

Solids treatment begins after the solids are concentrated to approximately 20 wt% (dry basis) for Envelopes A, B, and D and 15 wt% for Envelope C. The first solids treatment step is to wash the solids with process condensate, using the same steps as solids filtering or concentration to remove soluble components. Process condensate is added to UFP-VSL-00002A/B to replace permeate that passes through the filters. After the Envelope A, B, and D solids are washed, they are leached (Envelope C solids are not leached) if warranted (corresponding to an H/D of 1.8). The first step in leaching is to add 19 molar sodium hydroxide until a calculated value of 3 molar free hydroxide is reached for the batch. The solution is then heated with high-pressure steam to 176°–194°F and allowed to digest for eight hours. After digesting, the slurry is cooled, then filtered until the solids concentration is increased back up to 20%. After the solids are reconcentrated they are washed again with process condensate to remove the residual sodium hydroxide and dissolved solids. The treated solids are then discharged to LS (HLP), and chemical cleaning of the filters, if required, begins.

Normally the LS vessels (HLP-VSL-00027A/B) receive treated solids from ultrafiltration; however, treated solids can be sent directly to the blend vessel (HLP-VSL-00028) if necessary. Backup blend vessel HLP-VSL-00027B can receive the same waste transfers as HLP-VSL-00028. Treated HLW solids, concentrated Cs, and Sr/TRU solids (if available) are blended together in HLP-VSL-00028, sampled, and routed to HLW vitrification.

1.3.2 Mixing Operation Modes

This section discusses the normal and post-DBE mixing operation modes. Normal mixing is that required for routine or normal plant operation. Post-DBE mixing refers to the mixing modes that will be available after a plant upset.

Normal Mixing: The hybrid mixing system will provide for complete mixing of the non-Newtonian slurry within the constraints of the Pretreatment Facility vessel ventilation system. Gas holdup in the waste slurry during normal operation will be low, i.e., gas release will be effective. Normal operations mixing can use a combination of PJMs, sparging, and recycle pump systems.

Post-DBE Mixing: After a DBE, sparging air can be diverted to the cell ventilation system and the incremental air flow constraint of 1520 scfm is lifted. Normal mixing uses equipment that is not rated for important-to-safety (ITS) use. Post DBE, the hybrid mixing system will use ITS-rated systems only and provide for complete mixing of the non-Newtonian slurry to ensure gas release from the slurry. Post-DBE mixing and gas release is limited to PJM and sparger operation.

1.4 Overview of the PJM-Hybrid Mixing Systems Design Approach

The hybrid mixing systems considered in this work involve the combined use of PJMs, steady mixing jets created by recirculation pumps, and air sparging. The mixing technologies were combined to take advantage of their respective strengths.

PJMs are used for mixing the lower region of the vessel contents and facilitating off-bottom suspension of solids. PJMs are ideally suited for these tasks because they discharge downward with nozzles near the vessel floor. The ideal PJM configuration for hybrid systems is one that creates a well-defined, highly turbulent cavern. The material in the upper region of the vessel is then transported to the turbulent cavern by the other systems where it is mixed (spargers and/or steady jets) as illustrated in Figure 1.1.

Having a high degree of turbulence is important to encourage both adequate mixing and gas removal, as well as to minimize scaling issues for prototypic test results that will be applied at full scale (scale-up is discussed in more detail in Appendix A). Additionally, having an obstruction-free interface between the mixed and unmixed regions simplifies the specification of spargers and jet nozzles.

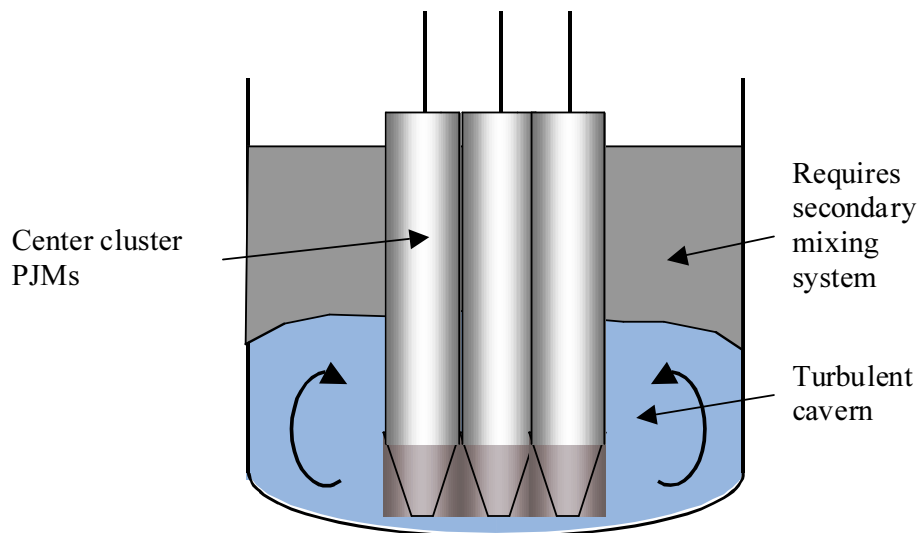


Figure 1.1. PJM-Hybrid Mixing Approach. Central cluster PJMs mix the lower region of the vessel and secondary systems mix the upper region.

A centralized cluster of PJMs with nozzles angled toward the tank wall was found to be the most effective at creating a distinct mixing cavern. Tests with a distributed array of PJMs were also conducted and found to provide good overall mixing (determined by the dye method); however, the uniformity of the cavern was found to be highly sensitive to nozzle impingement angle, and the quality of the turbulence was suspect.

Steady turbulent jets from recirculation pumps are known to be effective in mobilization and mixing applications. In general, mixing effectiveness is improved by increasing either the nozzle diameter or jet velocity. If the flow rate is fixed, the mixing performance is improved only by increasing the nozzle velocity, which implies a subsequent reduction in nozzle diameter.

Mixing performance can also be improved by increasing the number of mixing jets. Jets are a source of linear momentum and tend to be highly directional with relatively small spread angles (about 15 degrees for a free Newtonian jet). Once they impinge on solid surfaces, they tend to follow the contour of that surface. Further, cavern formation (or similar channeling) can occur for non-Newtonian slurries. Single jets can be used to mix entire vessels if the flow rates are high enough; however, a single jet will often break through the fluid surface and dissipate its energy before complete mobilization, particularly in a non-Newtonian slurry. Hence, by distributing the total available flow through multiple jets, more regions of the vessel can be affected and overall mixing can improve.

Ideally, the jet nozzles are located just below the PJM cavern interface, angled upward and aimed between the PJMs and the vessel wall. Material from the lower mixing zone is entrained and mixed into the upper region, a configuration well suited for operation at reduced operating volumes.

Air sparge tubes provide mixing an alternative mechanism. Rising air bubbles produce drag on surrounding fluid, creating an upward pumping effect. Once at the surface, fluid must recirculate downward. The net result is an upward bubble zone of mixing (in this document, this region is referred to as the region of bubbles [ROB]), surrounded by a larger, downward zone (in this document, this region is referred to as the zone of influence [ZOI]). Sparge ZOIs will interact in potentially beneficial ways if neighboring sparge points are spaced close enough. However, these interactions for non-Newtonian fluids are not fully understood and are not addressed in this document. Locating the outlet of the sparge tube near the bottom of the tank and well inside the PJM cavern should provide the capability to completely mix the tank contents.

1.5 Overview of the Scaled Testing Methodology

The scaled testing methodology involved conducting tests in a number of scaled vessels with representative non-Newtonian simulants. Five test stands were tested with PJMs; three were used to investigate the scaling laws and two were scaled versions of the full-scale tanks. Information on sparging was obtained with a single large-scale sparge tube. Scale-up and application of the mixing technologies are based on a mix of well-known theory and developments by the PJM mixing program.

As described in Section 3.1, the two primary simulants were Laponite and a mixture of kaolin/bentonite clay. Laponite is a thixotropic colloidal synthetic clay that forms a transparent gel when left unshered. This simulant was used for assessing the scale-up behavior of the PJMs and visualizing the flow behavior

in the scaled prototypes. The kaolin/bentonite clay mixture exhibits a Bingham plastic rheology that closely represents the rheology of actual waste slurries. This simulant was used to investigate the scale-up behavior of PJMs and GR&R characteristics. It was also used to assess the performance of the scaled prototypes.

The scale-up of the PJM mixing performance and the GR&R characteristics was investigated at three different scales with geometrically scaled test stands containing four PJMs. The largest test stand (described in Section 2.2) is the 12,000 gallon vessel in the Hanford 336 building which is similar in size to the actual concentrate receipt vessel. The intermediate sized test stand (described in Section 2.1) is located in the Applied Process Engineering Laboratory (APEL). It is approximately one-quarter scale (based on linear dimensions) relative to the large tank with a total volume of about 250 gallons. The small-scale tank, which is about one-half scale relative to the APEL test stand, is located at the Savannah River Technology Site.

The basis for scale-up of the mixing induced by PJMs and steady jets is based on modifications to turbulent jet theory to account for the non-Newtonian rheology and non-steady jets from the PJMs. Dimensional analysis (appendix A) was used to identify the important dimensionless parameters and guide the experimental design. The configuration for the sparging systems was based on the results of nearly full-scale tests with a single sparge tube (refer to Sections 2.4 and 3.3).

Scaled prototypes were used to evaluate the various mixing configurations. Both the LS and UFP vessels (both described in Section 2.3) had scale factors in the range of 4 to 5. Approximately 150 separate runs were conducted with these units containing various configurations of PJMs, recirculation pumps, and spargers. Only the mixing results from runs that have a direct bearing on the final configuration are reported in Section 3.2. GR&R results for the scaled prototypes are reported in Section 5. Development of the basis for scale-up of the GR&R results is ongoing and will be included in a future document.

2.0 Test Stands and Experimental Methods

This section contains a description of the test stands and the experimental methods. The APEL 4 PJM and the large-scale PJM test stands are described first and were used to demonstrate the scaling laws for mixing, gas release, and gas holdup. The scaled prototypes are described next and are geometrically scaled models of the full-scale UFP and LS tanks. The prototypes were used to evaluate various mixing configurations. Section 2.4 describes the equipment and methods used to obtain performance data for sparging in non-Newtonian slurries. Section 2.5 describes the methods used to assess GR&R behavior in the simulants. The final section describes the methods used to assess the extent of mixing.

The dimensional information presented in this section is divided into three categories based on (1) standard sizes; (2) measurements made prior to or during, or recreated after the testing; and (3) target values or ranges.

The first category pertains to the internal or external diameters of the stainless steel or PVC tubing/ piping materials used in construction of the pulse tubes, nozzles, recirculation lines, and sparger lines. Although the actual diameters vary from manufacturer to manufacturer, these values are generally within $\pm 5\%$. In the text, tables, and figures, unless otherwise noted, for the diameters of pulse tubes, nozzles, recirculation lines, and sparger lines, only the nominal values are listed.

The second category dimensional measurements are those that can be quantified and are presented as such in the discussion with the appropriate uncertainties.

The third category mainly corresponds to dimensional information that was impossible to measure directly, such as elevations of the vessel internals relative to the vessel bottom (e.g., distance of nozzles from bottom). Although significant effort was made to achieve the target values specified in the testing sequences, no direct as-built measurements were made because of space limitations within the tank (i.e., manned entry was not possible). In addition, this category also includes those measurements that were not recorded at the time of the testing and could not be recreated. The third category of measurements is indicated as approximate in the text, tables, and figures and should only be treated as such.

2.1 APEL 4 PJM Test Stand

The APEL 4PJM test stand (Figure 2.1) is a linearly scaled version of the 4PJM test setup in the 336 test facility. The configuration details, subject to the constraints presented at the beginning of Section 2, are discussed below. The diameter of the tank is 33.8 ± 0.5 inches, which corresponds to a scale factor of ~ 4.57 . This test stand consists of four PJMs constructed of 5-inch (5.29-inch ID) schedule 10 stainless steel pipe tapered to an approximately 60° angle cone truncated to a custom-built nozzle with a 0.88 ± 0.01 -inch ID. The length of the cylindrical section of the PJMs was 48 ± 1 inches. The height was intentionally set longer than the PJMs in the 336 test facility to enable testing at higher H/D ratios (up to H/D of 1.6 and a volume of approximately 180 gallons) than were possible in the large-scale test stands. The PJMs are situated around the center of the tank in a square along a pitch-circle diameter (PCD) of 21 ± 1 inches. The nozzles were approximately 2 inches above the tank floor directly under them.

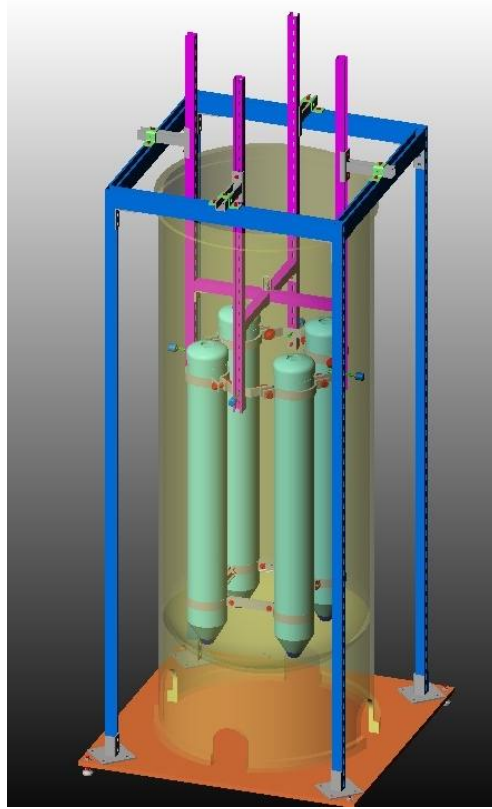


Figure 2.1. APEL 4 PJM Test Stand

Unlike conventional PJMs, whose operation is regulated by JPPs driven by compressed air, the APEL 4 PJM test system used a series of solenoid valves and a combination of an air compressor and vacuum pump to simulate the drive and suction phases of PJM operation. These operations were controlled through a control logic program using DASyLab data acquisition and control software (DACS), which turns on and off the appropriate solenoid valves at specified time intervals. The duration of each phase, the applied pressure, and vacuum are all variables that can be varied independently to simulate the operation of the PJMs.

Each PJM was outfitted with a Drexelbook liquid-level capacitance sensor/transmitter and an Endress+Hauser ceramic pressure transducer, which enabled continuous measurement of the slurry level and pressure inside the PJM during operation. Additional sensors included in the test system are Type K thermocouples that measure the temperature of the tank contents and the ambient temperature.

During the GR&R tests, in addition to the above parameters, the liquid level in the tank and the H_2O_2 (used to generate in situ oxygen bubbles to study gas behavior) flow rate and density were also monitored and recorded digitally. The liquid level in the tank outside the PJMs was monitored continuously using ultrasonic level detectors. The H_2O_2 flow rate and density were monitored using a 0.25-inch Micro-Motion Coriolis mass flow meter. During each mixing test, several variables such as PJM liquid levels and pressures, tank and ambient temperature, and H_2O_2 flow rate and density were monitored continuously and recorded digitally on a computer.

2.2 336 PJM Test Stand Description

The large-scale PJM test stand installed in Battelle's 336 test facility has been described extensively in previous reports (e.g., Bontha et al. 2003); therefore, only a brief description is presented here.

The PJM system consisted of four pulse tubes each with a cylindrical section of ~10 ft length and ~2 ft internal diameter. Each tube has a dished head with a connection to a 2-inch pipe. The bottom end of each pulse tube was tapered at an approximately 60° angle cone truncated to a ~4 inch nozzle. The overall height of the pulse tube, which is shown in Figure 2.2, was approximately 12 ft. A schematic of the experimental system used to demonstrate the PJM system is shown in Figure 2.3. As-built dimensions are detailed in Bontha et al. (2003).



Figure 2.2. Photograph of the PJMs Used in the 336 Test Facility

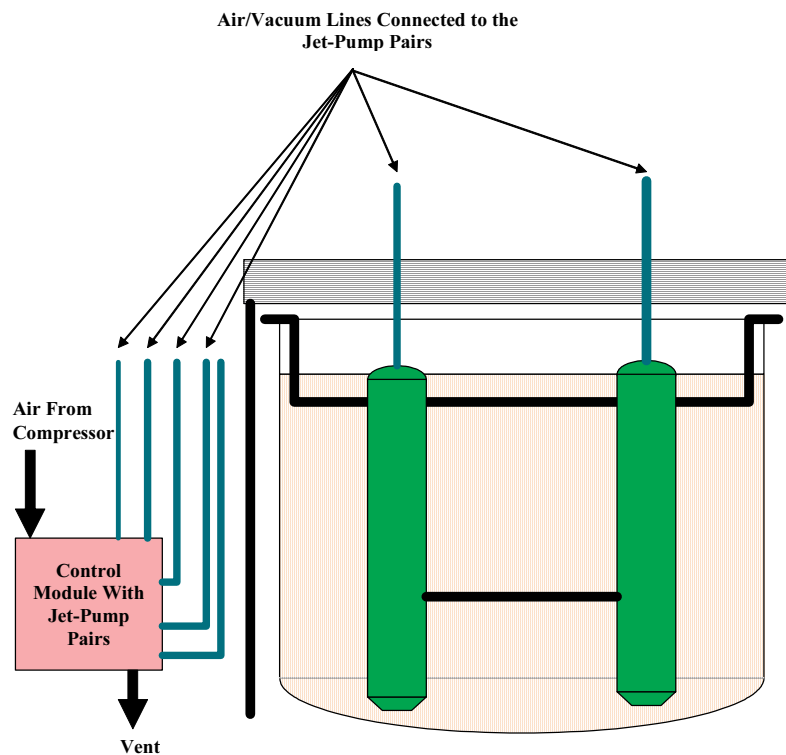


Figure 2.3. Schematic of Experimental System Used to Evaluate PJMs Using Non-Newtonian Simulants

The PJMs are inside a ~12.75-ft-ID x ~15-ft-tall supernate tank with a ~2:1 elliptical dish head. The nominal operating volume of the tank is about 10,000 gallons. The PJMs were held with brackets positioned on top of the tank. The brackets, which traverse the diameter of the tank and are welded to the sides, bear the weight of the tubes. The PJMs were positioned at the center of the four quadrants of the tank approximately 10 inches from the bottom of the tank.

During the operation of the PJMs, the pulse tubes were filled with the slurry by the application of a vacuum. The slurry was then expelled from the pulse tubes with compressed air. The suction and discharge of the slurry to and from the pulse tubes was regulated by JPPs in a control module on the ground level at the side of the tank. The JPPs were connected to the pulse tubes using 2-inch-OD wire-reinforced PVC tubing.

A compressor/accumulator(s) combination was used to regulate the air flow to the JPPs. The compressor chosen for the present study, which was based on the requirements for the air flow to the JPPs, was a Sullair compressor capable of delivering 1600 CFM at an operating pressure of 100 psig. The accumulators were an ASME standard 240 gal Brunner vertical air-receiver tank with pressure relief valves and a timed electronic drain valve. Both the compressor and the accumulators were located outside the 336 Building facility.

During the suction phase, liquid in the pulse tube piping can rise to a level of ~20 ft above the liquid level. To prevent suction of the liquid into the JPPs, the tubing connecting the pulse tubes to the JPPs was routed to the upper catwalk, ~40 ft above the top of the tank.

The sequence of operation and cycle frequency of the PJM and the RFD sampler was controlled by PRESCON™, an AEA Technology proprietary control system. Each PJM was outfitted with a Drexelbook liquid-level sensor/transmitter and a Ccomp pressure transducer that enabled continuous measurement of the slurry level and pressure inside the PJM during operation. Additional sensors included in the test system are Type K thermocouples for measuring the temperature of the tank contents and the ambient temperature. The data were digitally recorded on a computer using DASyLab DACS.

Simulant motion was detected either visually with the use of camera wells or with velocity probes (Figures 2.4 and 2.5). Video systems inserted into the camera wells were generally used to detect the mixed and unmixed regions in transparent simulants. A small video camera was moved up and down the camera well and the images recorded. The boundary of the mixed and unmixed regions was also recorded manually. Velocity probes were used to measure velocity although these results are not reported in this document.

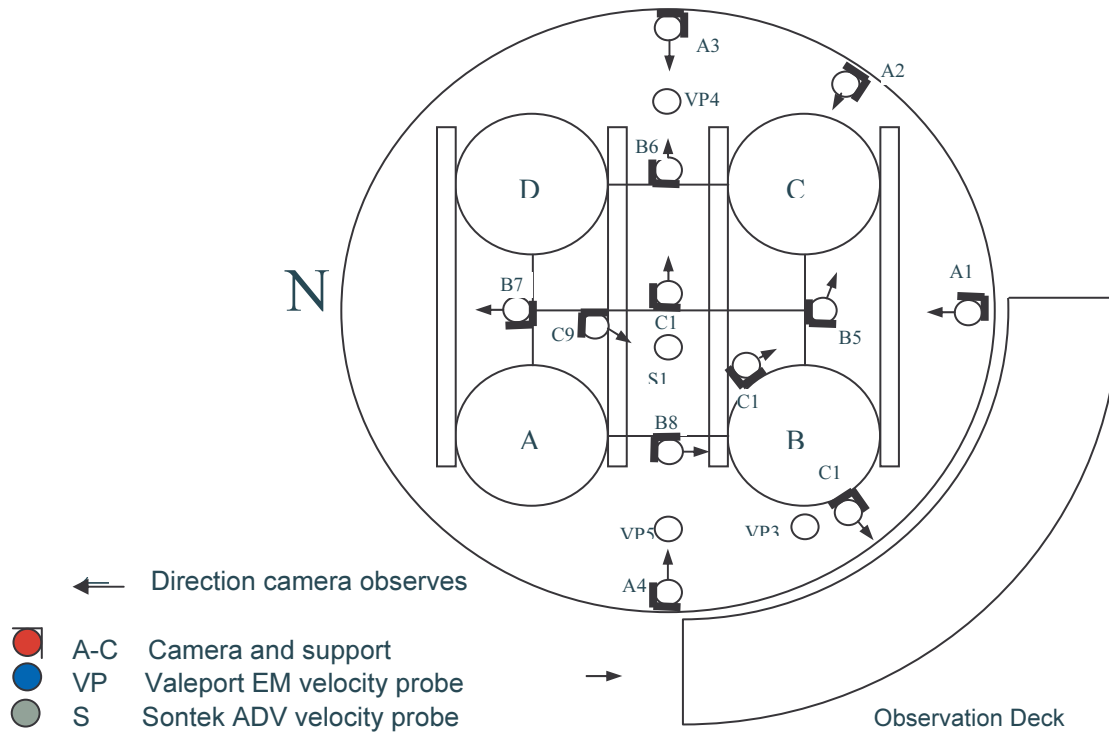


Figure 2.4. Plan View of the Instrument Locations for the 336 Building PJM 4 Test Stand

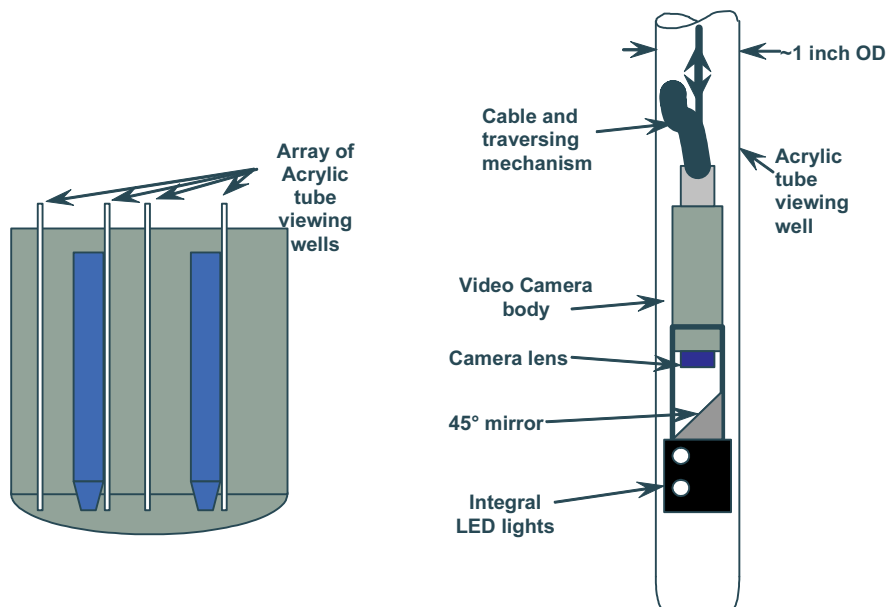


Figure 2.5. Video System for Detecting Mixed (cavern) Region in Large-Scale Testing

2.3 Scaled Prototypic Test Stands

2.3.1 UFP Prototype Vessel

The 168-inch-diameter, full-scale UFP tank was represented by a 34 ± 1 -inch-ID clear acrylic vessel. The geometric scale factor was ~ 4.94 . The scaled UFP prototypic test vessel was 91 ± 1 inches tall with a $\sim 2:1$ elliptical dish head made out of stainless steel. Mixing tests in this vessel were performed using different combinations of PJMs and spargers and a recirculation pump system. Top and plan views of the vessel and internals with nominal dimensions are shown in Figures 2.6 and 2.7. The various test sequences included in this document are presented in Table 2.1. The configuration details, subject to the constraints presented at the beginning of Section 2, are discussed below.

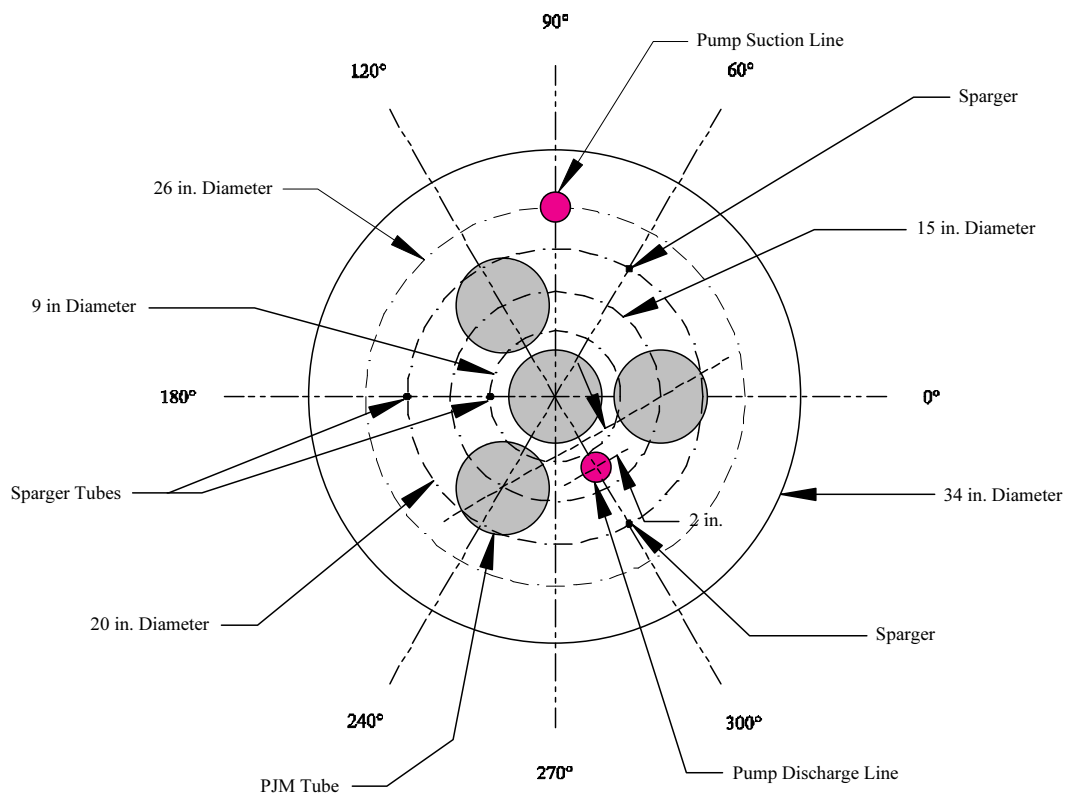


Figure 2.6. Top View of the UFP Prototypic Test Stand Showing Nominal Dimensions (measurement uncertainties are discussed in the text)

2.3.1.1 PJM Configurations

All of the PJMs for the UFP prototype were constructed from 6-inch-diameter (6.065-inch ID) schedule 40 stainless steel pipes with the end connected to an approximately 60° angle cone truncated to a 2-inch-diameter pipe fitting to which the nozzles were connected. The cylindrical section of the PJMs was 37 ± 1 inches tall; this corresponds to a PJM height scale factor of ~ 4.32 . The difference between the UFP tank dimension scale factor and the pulse tube dimension scale factor was due to the need to use

Table 2.1. UFP Test Sequences Presented in this Document and Corresponding PJM, Sparger, and Recirculation Pump Configurations(a,b)

Seq No	Run	Test Type	Test Mode	PJM Configuration			Sparger Configuration			Recirc. Pump Discharge Configuration		
				PJM Arrangement	Nozzle Type	Noz. Dia. (in)	Elevation (in)(c)	No. of Spargers	Radial Pos.	Elevation (in)(c)	Noz. Dia (in)	PCD (in)
2	1	Mixing	PJM Only	Tri-Foil (3+1)	45° (3); Vertical (1)	0.824	2	-	-	-	-	-
2	2	Mixing	PJM Only	Tri-Foil (3+1)	45° (3); Vertical (1)	0.824	2	-	-	-	-	-
2	3	Mixing	PJM + Sparging	Tri-Foil (3+1)	45° (3); Vertical (1)	0.824	2	1 (near center)	Figure 2.6	-	-	-
2	4	Mixing	PJM + Sparging	Tri-Foil (3+1)	45° (3); Vertical (1)	0.824	2	3 (Outer)	Figure 2.6	-	-	-
3B	1	Mixing	PJMs Only	Tri-Foil (3+1)	45° (3); Vertical (1)	0.824	2	-	-	-	-	-
3B	2	Mixing	PJM + Pump	Tri-Foil (3+1)	45° (3); Vertical (1)	0.824	2	-	-	-	1.049	24 0°, Down
3B	3	Mixing	PJM + Pump	Tri-Foil (3+1)	45° (3); Vertical (1)	0.824	2	-	-	-	1.049	24 0°, Down
3B	4	Mixing	PJM + Pump + Sparging	Tri-Foil (3+1)	45° (3); Vertical (1)	0.824	2	1 (near center)	Figure 2.6	4	1.049	24 0°, Down
5	1	GR&R	PJM + Sparging	Tri-Foil (3+1)	45° (3); Vertical (1)	0.824	2	1 (near center)	Figure 2.6	4	-	-
5	2	GR&R	PJM + Sparging	Tri-Foil (3+1)	45° (3); Vertical (1)	0.824	2	1 (near center)	Figure 2.6	4	-	-
5	3	GR&R	PJM + Pump	Tri-Foil (3+1)	45° (3); Vertical (1)	0.824	2	-	-	-	1.049	24 0°, Down
5	4	GR&R	PJM + Sparging	Tri-Foil (3+1)	45° (3); Vertical (1)	0.824	2	1 (near center)	Figure 2.6	4	-	-
6	1	GR&R	PJM + Sparging	Tri-Foil (3+1)	45° (3); Vertical (1)	0.824	2	1 (near center)	Figure 2.6	4	-	-
6	2	GR&R	PJM + Sparging	Tri-Foil (3+1)	45° (3); Vertical (1)	0.824	2	1 (near center)	Figure 2.6	4	-	-
6	3	GR&R	PJM + Sparging	Tri-Foil (3+1)	45° (3); Vertical (1)	0.824	2	1 (near center)	Figure 2.6	4	-	-
6	4	GR&R	PJM + Sparging	Tri-Foil (3+1)	45° (3); Vertical (1)	0.824	2	1 (near center)	Figure 2.6	4	-	-
7(c)	1-4	Solids Lift	PJMs only	Cluster (5+1)	45° (5); Vertical (1)	0.824	2	-	-	-	-	-

(a) Test results discussed in Section 3.
 (b) Configuration spatial and dimensional distances values in table do not reflect the type of measurement or accuracy. See text for details.
 (c) Approximate distance from the bottom of the tank under the nozzle
 (d) Angle from vertical.
 (e) Configuration selected.

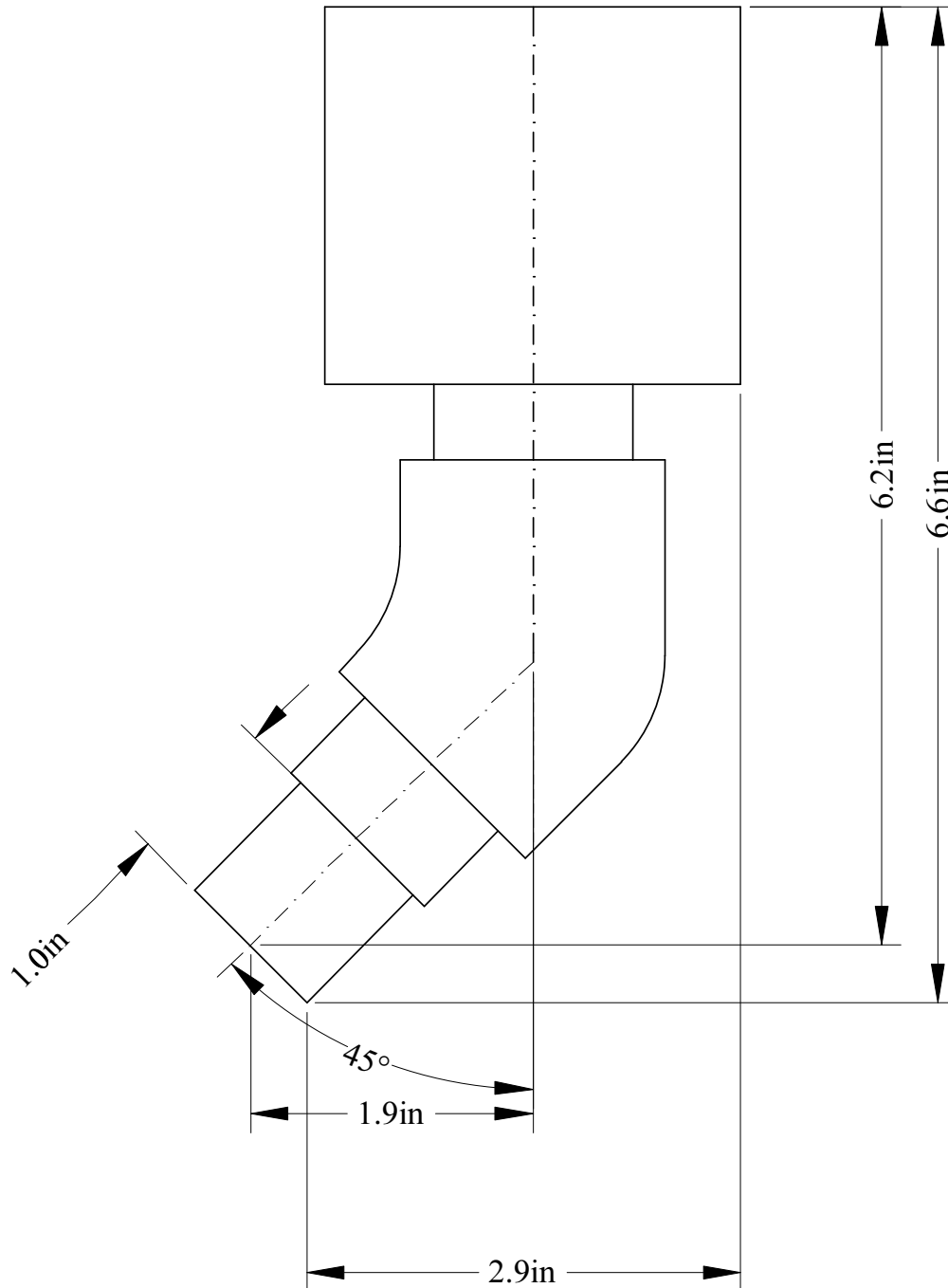


Figure 2.8. Schematic of the 45° Nozzle Used in the UFP Test Stand Showing Nominal Dimensions (measurement uncertainties are discussed in the text)

and sparger hybrid configurations without obstruction of the spargers by additional PJMs. Because the purpose of PJMs was to generate a mixed region at the bottom of the vessel with the spargers extending the mixed region to the vessel surface, four PJMs were suitable for testing. The actual vessel will have six PJMs, which will provide a larger mixed region. The final test sequence (#7 in Table 2.1) used six PJMs.

The center PJM nozzle was constructed from 0.75-inch (0.824-inch ID) schedule 40 stainless steel pipe and was pointed straight down toward the center of the tank bottom and raised approximately 2 inches off the bottom. The perimeter PJM nozzles were constructed from 0.75-inch (0.824-inch ID), schedule 40 stainless steel pipe angled 45° (using a standard 45° elbow fitting) radially outward from the tank center and raised approximately 2 inches off the tank floor. Figure 2.8 is a schematic of the 45° nozzle; all dimensions listed are within ± 0.5 inches. All tests with the PJMs were conducted using a target stroke of 33.5 to 35.5 inches (85 to 90 cm) and a target average nozzle velocity of 8 ± 0.8 or 12 ± 1 m/s.

2.3.1.2 Sparger Configuration

Tests using spargers were performed using an array of four (one center and three perimeter) spargers. The center sparger was approximately midway between adjacent perimeter PJMs at a radial position of approximately 4.5 inches from the tank centerline. The perimeter spargers were placed at approximately midway between adjacent perimeter PJMs at a pitch diameter of 20 ± 1 inches. All of the sparger tubes were made from 0.5-inch-OD (0.37 inch ID) stainless steel tubing, and the lower ends of the sparger tubes were approximately 4 inches above the bottom of the tank as measured from the tank floor (or approximately 2 inches above the tip of the nozzle). Tests with sparging were carried out either with the center sparger operating at a target flow rate of 3 acfm or the perimeter spargers operating at a target flow rate of 1 acfm each.

2.3.1.3 Recirculation System Configuration

The pump recirculation system consisted of two centrifugal pumps placed in parallel and connected in series with a diaphragm pump that served to eliminate cavitation and prime the centrifugal pumps. The recirculation pump system was operated at a target flow rate of 90 ± 5 gpm (which corresponds to ~ 2200 gpm at full scale), and the discharge line nozzle was sized such that the linear velocity exiting the nozzle was ~ 30 ft/sec.

For the test sequences presented in this document, the recirculation configuration consisted of a single discharge line of 2-inch (2.067 inch ID) schedule 40 stainless steel pipe with a 1-inch (1.049-inch ID) schedule 40 stainless steel nozzle pointing down. It was located approximately midway between two of the perimeter PJMs at a radial position of approximately 5.5 inches from the tank centerline and an elevation of approximately 24 inches from the bottom center of the tank floor. The pump suction line consisted of a 2-inch (2.067-inch ID) schedule 40 PVC pipe located at a radial position of approximately 4 inches from the tank wall on the opposite side of the tank from the discharge line and at an elevation of approximately 4 inches as measured from the center of the intake to the tank floor beneath it.

2.3.2 Lag Storage Prototypic Vessel

The 300-inch-diameter, full-scale LS tank was represented by a 70 ± 1 -inch ID clear acrylic vessel. The scale factor was ~ 4.29 . The scaled LS prototype acrylic vessel was 91 ± 1 inches tall with a 100:6 elliptical dish head made of stainless steel. Mixing tests in this vessel were performed using different combinations of PJMs and spargers and the recirculation pump system. Top and plan views of the vessel and internals are shown in Figures 2.9 and 2.10. The various test sequences included in this document are presented in Table 2.2. The configuration details, subject to the constraints presented at the beginning of Section 2, are discussed below.

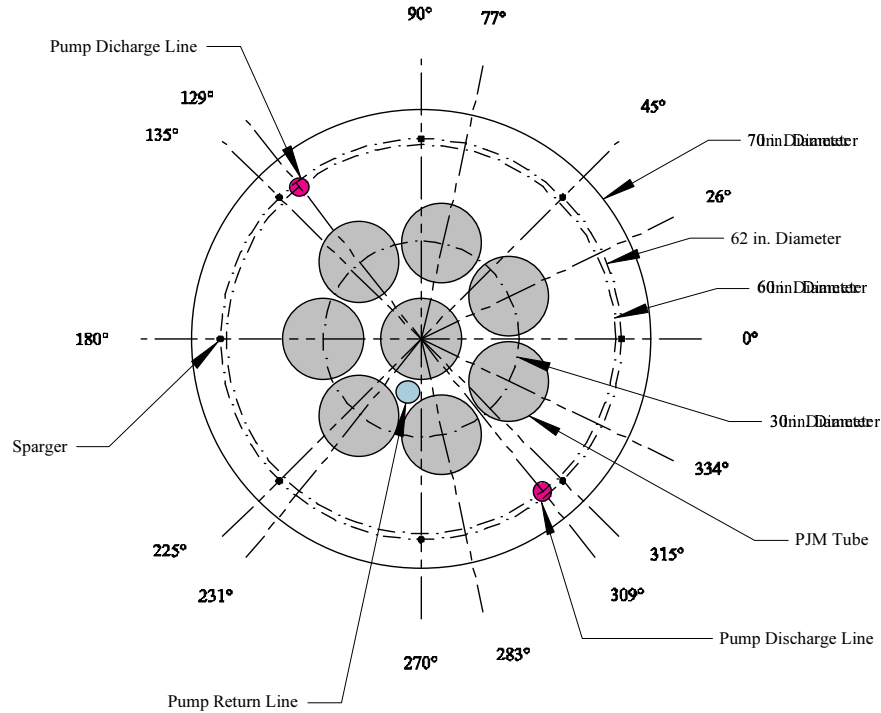


Figure 2.9. Top View of the LS Prototype Test Stand Showing Nominal Dimensions (measurement uncertainties are discussed in the text)

2.3.2.1 PJM Configurations

All the PJMs for the LS prototype were constructed from 12-inch-diameter (12-inch ID) schedule 40 stainless steel pipe with an approximately 60° angle cone truncated to a 2-inch-diameter pipe fitting to which the nozzles were connected. The height of the cylindrical section of the PJMs was 31 ± 1 inches, corresponding to a PJM height scale factor of ~ 4.93 . The difference between the LS tank and pulse tube dimension scale factors is due to the need to use standard pipe sizes for procurement expediency. However, the volume expelled from the PJMs was consistent with the LS scale factor of ~ 4.29 .

For the LS test sequences presented in this document, the PJM array consisted of eight PJMs, with one near the center of the tank and the other seven nearly equally spaced around the center PJM on a pitch diameter of 30 ± 1 inches. This was referred to as the “cluster” configuration.

For all but one test sequence (# 20) presented in this document, the center PJM nozzle was constructed from 1-inch (1.049-inch ID) schedule 40 stainless steel pipe pointed straight down toward the center of the tank bottom and raised approximately 2 inches off the bottom. For sequence 20, a 1-inch (0.957-inch ID) schedule 80 stainless steel pipe was used for the center nozzle. For all test sequences presented in this document, the perimeter PJM nozzles were constructed from 1-inch (0.957 inch ID), schedule 80 PVC pipe, angled 45° (using a standard 45° elbow fitting) radially outward from the tank center and raised approximately 2 inches off the tank floor. Figure 2.11 is a schematic of the 45° angled nozzle; all dimensions in this figure are within ± 0.5 inches. All tests with the PJMs were conducted using a target stroke of 29.5 to 31.5 inches (75–80 cm) and a target average nozzle velocity of 8 ± 0.75 or 12 ± 1 m/s.

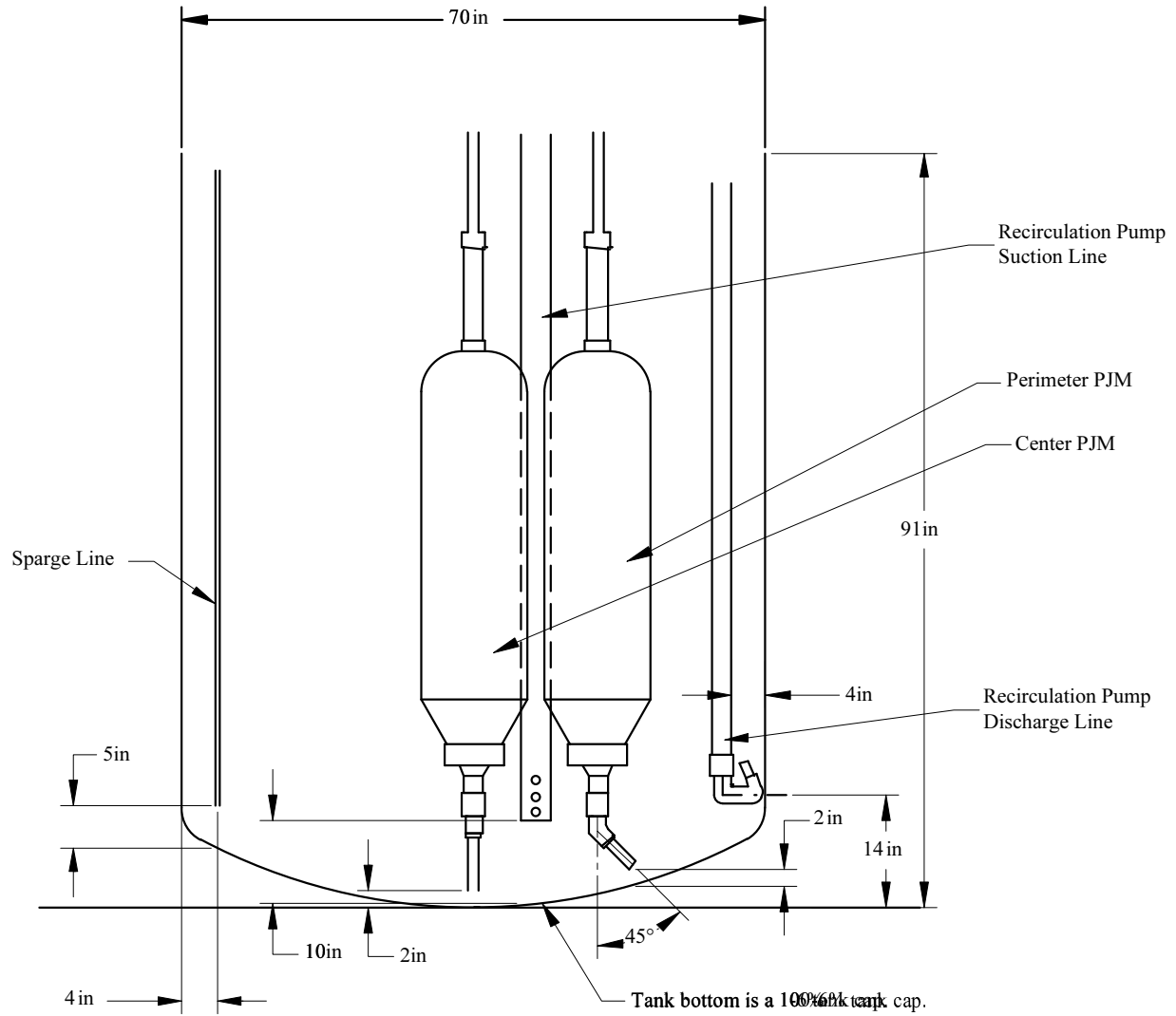


Figure 2.10. Plan View of the LS Prototype Test Stand Showing Nominal Dimensions
(measurement uncertainties are discussed in the text)

2.3.2.2 Sparger Configuration

Tests with spargers were performed using an array of eight spargers nearly equally distributed around the tank circumference at a pitch diameter of 62 ± 1 inches. The sparger tubes were made from 0.5-inch OD (0.37-inch ID) stainless steel tubing. The lower end of the sparger tubes was approximately 5 inches above the tank floor (or approximately 3 inches from the tip of the perimeter nozzles). Sparging tests were carried out using either four alternating or all eight spargers. In both cases, the target air flow rate for each sparger was 3 acfm.

Table 2.2. LS Test Sequences Presented in this Document and the Corresponding PJM, Sparger, and Recirculation Pump Configurations^(a, b)

Seq No.	Run	Test Type	Test Mode	PJM Configuration			Sparger Configuration				Recirc. Pump Discharge Config.					
				PJM Arrangement	Nozzle Type	Noz. Dia. (in)	Elevation (in) ^(c)	No.	OD (in)	PCD (in)	Elevation (in) ^(c)	No. of Nozzles	Nozzle dia (in.)	PCD (in)	Elevation (in) ^(c)	Angle ^(d)
4	1	Mixing	PJMs Only	Cluster (7+1)	45° (7) Vertical (1)	(7) 0.957 (1) 1.049	2	-	-	-	-	-	-	-	-	
4	2	Mixing	PJMs Only	Cluster (7+1)	45° (7) Vertical (1)	(7) 0.957 (1) 1.049	2	-	-	-	-	-	-	-	-	
4	3	Mixing	PJMs + Spargers	Cluster (7+1)	45° (7) Vertical (1)	(7) 0.957 (1) 1.049	2	4	0.5	61	5	-	-	-	-	
4	4	Mixing	PJMs + Spargers	Cluster (7+1)	45° (7) Vertical (1)	(7) 0.957 (1) 1.049	2	8	0.5	61	5	-	-	-	-	
7	1	Mixing	PJMs Only	Cluster (7+1)	45° (7) Vertical (1)	(7) 0.957 (1) 1.049	2	-	-	-	-	-	-	-	-	
7	2	Mixing	PJMs Only	Cluster (7+1)	45° (7) Vertical (1)	(7) 0.957 (1) 1.049	2	-	-	-	-	-	-	-	-	
7	3	Mixing	PJMs + Pump	Cluster (7+1)	45° (7) Vertical (1)	(7) 0.957 (1) 1.049	2	-	-	-	-	4	0.622	60	29	30° Up
7	4	Mixing	PJMs + Pump	Cluster (7+1)	45° (7) Vertical (1)	(7) 0.957 (1) 1.049	2	-	-	-	-	4	0.622	60	29	30° Up
7	5	Mixing	PJMs + Pump + Sparging	Cluster (7+1)	45° (7) Vertical (1)	(7) 0.957 (1) 1.049	2	4	0.5	61	5	4	0.622	60	29	30° Up
7	6	Mixing	PJMs + Pump + Sparging	Cluster (7+1)	45° (7) Vertical (1)	(7) 0.957 (1) 1.049	2	8	0.5	61	5	4	0.622	60	29	30° Up
11	1	Mixing	PJMs + Pump	Cluster (7+1)	45° (7) Vertical (1)	(7) 0.957 (1) 1.049	2	-	-	-	-	2	0.91	60	16	30° Up
11	2	Mixing	PJMs + Pump	Cluster (7+1)	45° (7) Vertical (1)	(7) 0.957 (1) 1.049	2	-	-	-	-	2	0.91	60	16	30° Up
15	1	GR&R	PJMs + Spargers	Cluster (7+1)	45° (7) Vertical (1)	(7) 0.957 (1) 1.049	2	4	0.5	61	5	-	-	-	-	-
15	2	GR&R	PJMs + Spargers	Cluster (7+1)	45° (7) Vertical (1)	(7) 0.957 (1) 1.049	2	4	0.5	61	5	-	-	-	-	-
15A	3	GR&R	PJMs + Pump	Cluster (7+1)	45° (7) Vertical (1)	(7) 0.957 (1) 1.049	2	-	-	-	-	4	0.622	60	16	30° Up
15A	4	GR&R	PJMs + Spargers	Cluster (7+1)	45° (7) Vertical (1)	(7) 0.957 (1) 1.049	2	4	0.5	61	5	-	-	-	-	-
16	1-6	Solids Lift	PJMs Only	Cluster (7+1)	45° (7) Vertical (1)	(7) 0.957 (1) 1.049	2	-	-	-	-	-	-	-	-	-
20	1	Mixing	PJMs	Cluster (7+1)	45° (7) Vertical (1)	(7) 0.957 (1) 0.957	2	-	-	-	-	-	-	-	-	-
20(d)	2	Mixing	PJMs + Pump	Cluster (7+1)	45° (7) Vertical (1)	(7) 0.957 (1) 0.957	2	-	-	-	-	2	0.803	60	14	25° Up

(a) Test results discussed in Section 3.
 (b) Configuration spatial and dimensional distances values in table do not reflect the type of measurement or accuracy. See text for details.
 (c) Approximate distance from the bottom of the tank under the nozzle
 (d) Angle from vertical.
 (e) Configuration selected.

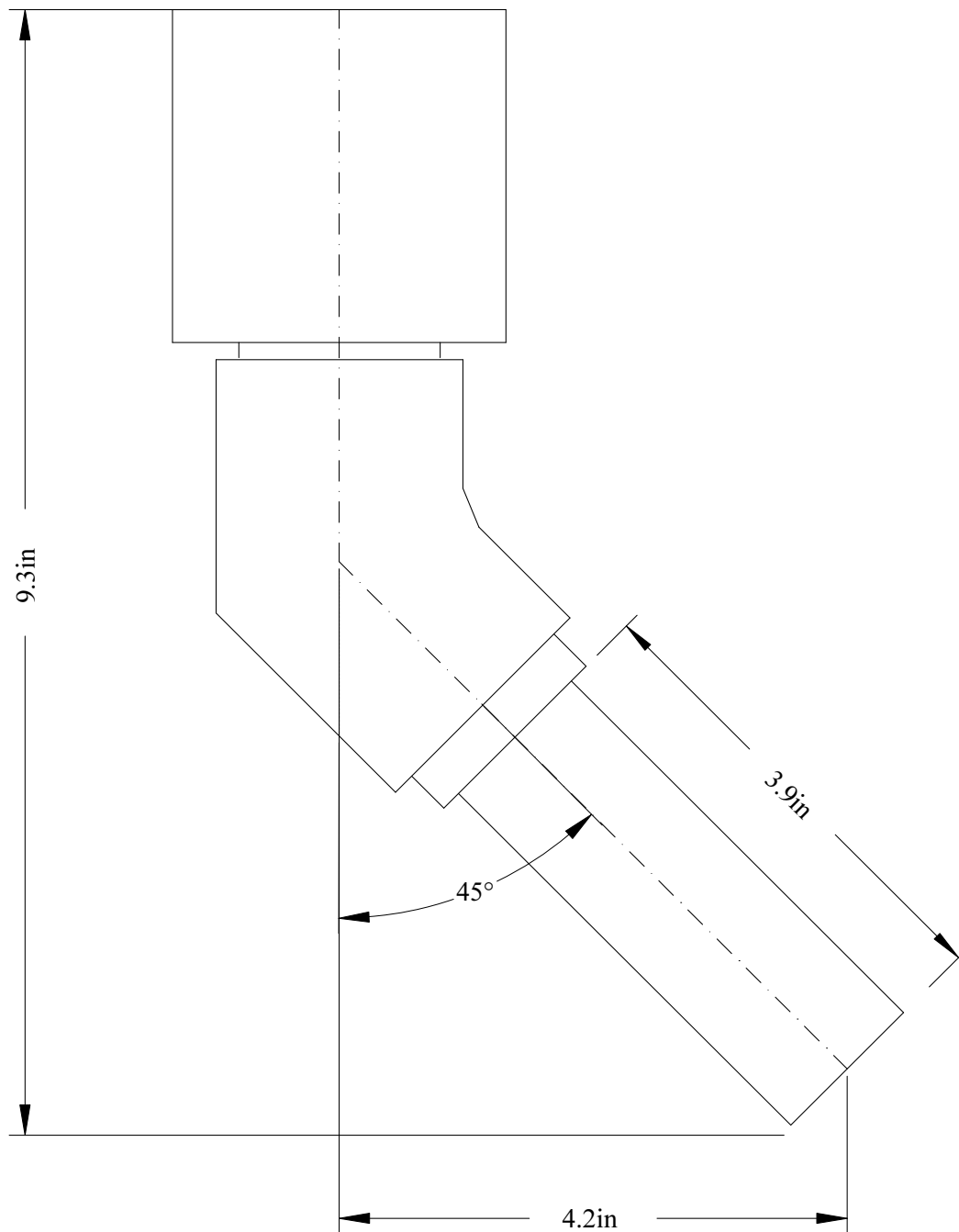


Figure 2.11. Schematic of the 45° Nozzle in the LS Prototype Test Stand Showing Nominal Dimensions (measurement uncertainties are discussed in the text)

2.3.2.3 Recirculation System Configuration

The pump recirculation system consisted of two centrifugal pumps placed in parallel and connected in series with a diaphragm pump that served to eliminate cavitation and prime the centrifugal pumps. The recirculation pump system was operated at a target flow rate of 120 ± 5 gpm (which corresponds to ~ 2200 gpm at full-scale). The nozzles at the discharge were generally sized such that the nominal linear velocity was ~ 30 ft/sec, although during Sequence 20 tests with two discharge nozzles, the nozzle diameter was selected to provide a linear velocity of ~ 40 ft/sec.

For the test sequences presented in this document, the pump suction consisted of 3-inch (2.900-inch ID) schedule 80 PVC pipe. The end of the suction line had several 1.5-inch holes drilled along its side to provide additional area for simulant flow. For all test sequences except Sequence 11, the suction line was in the space between the center and two adjacent perimeter PJMs. For Sequence 11, the suction line was roughly at a distance midway between the two discharge lines at a radial position of about 30 inches from the tank centerline. Except for Sequence 20, the elevation of the suction line varied from 4 to 12 inches above the tank floor during the testing to minimize cavitation due to its proximity to the spargers or to minimize its influence during dye injection near the bottom of the tank. In Sequence 20, the suction line was 10 ± 1 inches off the tank floor, as measured directly under the nozzle and shown in Figure 2.11.

In this document, four sequences of tests conducted with the recirculation pump are presented. This includes two tests with two discharge nozzles (sequences 11 and 20) and two tests with four discharge nozzles (sequences 7 and 15A). A schematic of the recirculation nozzle used in Sequence 20 is shown in Figure 2.12; all dimensions listed in this figure are within ± 0.5 inches.

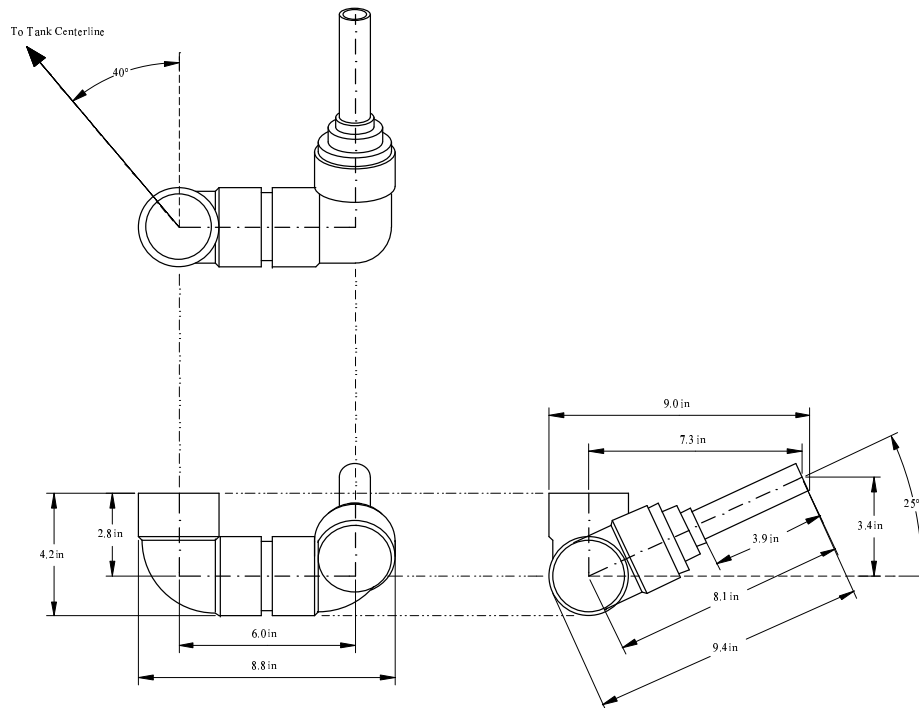


Figure 2.12. Recirculation Pump Discharge Nozzles Used in LS Sequence 20 (measurement uncertainties are discussed in the text)

All discharge lines were constructed out of 2-inch (2.067-inch ID) schedule 40 stainless steel pipe. The first test with two discharge nozzles (Sequence 11) consisted of 0.75-inch schedule 40 stainless steel pipes that were bored out to a 0.91 ± 0.01 -inch ID. The second test with two discharge nozzles (Sequence 20) consisted of 0.75-inch schedule 80 stainless steel pipes that were bored out to a 0.80 ± 0.01 -inch ID. The nozzles for the two test sequences with four discharge lines (Sequences 7 and 15) consisted of 0.5-inch (0.622-inch ID) schedule 40 stainless steel pipe.

For Sequences 11 and 20, the nozzles were diagonally opposite each other in the tank at a pitch diameter of 60 ± 1 inches. For Sequence 11, the nozzles were pointed upward at an angle of approximately 30° and raised to an elevation of approximately 16 inches. The nozzle angles formed by the line from the center of the tank to the center of the discharge line and the line passing through the discharge nozzle were approximately 40° pointing inward. For Sequence 20, the nozzles were pointed up at an angle of $25 \pm 2.5^\circ$ and raised to a 14 ± 1 -inch elevation. The nozzle angles formed by the line from the center of the tank to the center of the discharge line and the line passing through the discharge nozzle were $40^\circ \pm 5^\circ$ pointing inward and are shown schematically in Figure 2.13.

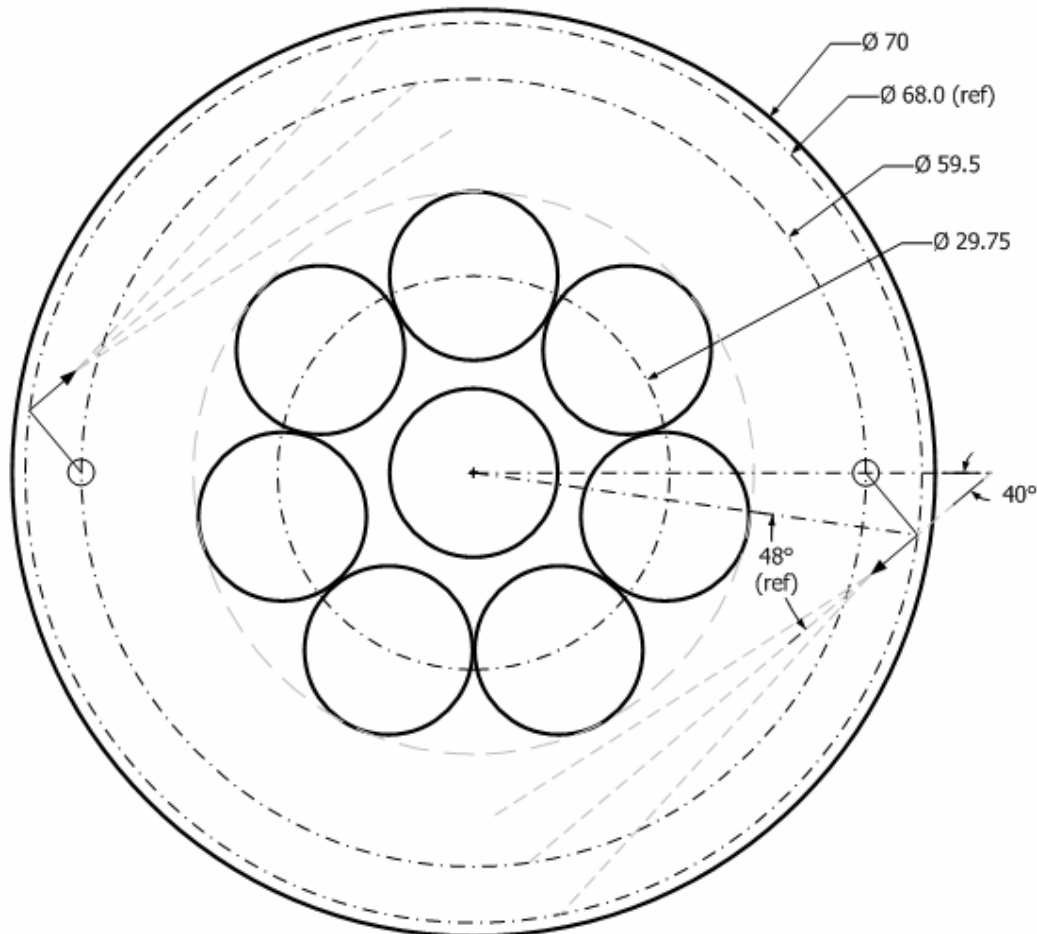


Figure 2.13. Top View of the Recirculation Nozzles in the Tank for LS Sequence 20 (measurement uncertainties are discussed in the text)

For Sequences 7 and 15, the nozzles were located along the four corners of a nearly square rectangle at a pitch diameter of 60 ± 1 inches. For Sequence 7, the nozzles were pointed upward at an angle of approximately 30° and raised to an elevation of approximately 29 inches relative to the bottom center of the tank. The nozzles were pointed approximately tangential to the tank wall. For Sequence 15, the nozzles were pointed up at an angle of approximately 30° and raised to an elevation of approximately 16 inches relative to the bottom center of the tank. The nozzles were approximately tangential to the tank wall.

2.3.3 System Operation and Data Acquisition

Unlike conventional PJMs, whose operation is regulated by JPPs driven by compressed air, the prototype test systems used a series of solenoid valves and a combination of an air compressor and a vacuum pump to simulate the drive and suction phases of PJM operation. These operations were controlled through a control logic program using DASyLab that turns the appropriate solenoid valves on and off at specified time intervals. The duration of each phase, the applied pressure, and the vacuum are all variables that can be independently varied to simulate the operation of the PJMs. The PJMs were operated at a specific average nozzle velocity (\bar{u}_{disch}), which is defined as

$$\bar{u}_{disch} = \frac{\Delta H}{\Delta t} * AR \quad (2.1)$$

where ΔH is the length of the PJM stroke, Δt is the time for achieving the stroke, and AR is the area ratio of the PJM to the nozzle. This equation is the same as Equation A.7 in Appendix A.

In addition to the PJM operation, the recirculation pump flow rates were controlled using a variable frequency drives (VFDs) on the centrifugal pumps and the air pressure to the diaphragm pump. Finally, the sparger air flow rates were controlled using rotameters.

During each mixing test, several variables such as PJM liquid levels and pressures, tank and ambient temperatures, recirculation pump flow rate, and density were monitored continuously and recorded digitally on a computer. The liquid/slurry level inside each of the PJMs was measured using Drexelbook capacitance level probes and transmitters. The functionality of the level probes was checked prior to the start of a sequence of tests which typically ran from 4 to 8 hours. Compressor and vacuum supply pressures and the pressure inside each PJM were monitored using Endress+Hauser ceramic pressure transducers. The tank and ambient temperatures were measured using Type K thermocouples. The flow rate and density of the slurry from the recirculation pump was measured using a 3-inch MicroMotion Coriolis mass flow meter. In addition to these variables, which were digitally monitored, the sparger air flow rates and pressures were recorded manually on the run data log sheets or in the project laboratory record books (LRBs).

During the GR&R tests, in addition to the above parameters the liquid level in the tank and the H_2O_2 flow rate/density were also monitored and recorded digitally. The liquid level in the tank outside the PJMs was monitored continuously using ultrasonic level detectors. In addition, the H_2O_2 flow rate/density was monitored using a 0.25-inch MicroMotion Coriolis mass flow meter.

2.3.4 Mixing Effectiveness Determination

The primary measurement in the scaled prototypic test platforms is the size and extent of the mobilization cavern resulting from PJM operations and PJMs combined with recirculation (i.e., steady jet) and/or sparging. This was achieved using a chemical tracer method discussed in detail in Section 2.6 and Appendix B. This section deals only with the method in which the tracer was injected into the tank and how the samples were collected.

The required amount of tracer (typically Brilliant Blue dye in an amount equal to ~ 5 g per 100 gal of clay simulant in the tank) was mixed with ~2 liters of the same clay simulant that was used in the testing. The concentrated tracer/clay mixture was injected prior to the start of a sequence of tests at lowest nozzle velocity of that test sequence. The concentrated tracer slurry was injected into the center PJM during the vacuum phase of the PJM cycle over a period of approximately 10 minutes. Once tracer injection was completed, the tracer injection line was purged with clean clay to ensure complete transfer of the tracer into the PJM. Once the line was purged, simulant samples from the tank were collected over a period of at least 45 minutes of PJM operation. Samples were withdrawn at various times from five different sample lines installed in the PJMs and the tank. Three of these samples were drawn from three perimeter PJMs and the remaining two samples were drawn from the annulus between the PJM and tank wall at elevations representing the lower and upper halves of the tank, respectively. After completion of the specified run conditions, the tank was completely homogenized and final homogenized samples collected. Comparison of the tracer concentration in the various samples with the final homogenized samples provides the percent mixed as a function of time and run conditions. Complete and successful mixing is defined as 100% as indicated by the chemical tracer method.

2.3.5 Solids Suspension Under Turbulent Conditions

Under some conditions the rheology will be low and solids may settle to the bottom of the tank. PJMs are well designed to pick up such solids because they direct a turbulent jet against the bottom of the tank. Solids suspension in mechanically stirred tanks is characterized by the “just suspended” criteria developed by Zwietering (1958; Atiemo-Obeng 2003), where no solids remain on the bottom of the tank for more than a few seconds. The BHRG-FMP consortium has shown that for steady downward-pointing jets an equation of functionality similar to that of Zwietering can be developed.^(a) The same form and functionalities would be expected to apply for multiple pulsed jets.

$$V_{js} = K * (\Delta\rho)^{0.43} (dp)^{0.2} X^{0.14} \quad (2.2)$$

where

- V_{js} = minimum velocity to suspend solids
- $\Delta\rho$ = density difference between solids and liquid
- dp = maximum particle size
- X = wt% of solids.

To determine the solids suspension characteristics of several of the pulse jet mixed tanks in the WTP area, tests were run similar to those done by Zwietering and FMP. A small concentration of 4-mm glass beads

(a) Personal communication with FMP on “Jet Solid Suspension Design Guide.” FMP report 064.

was placed in the bottom of the tank and the PJM velocity increased in increments until the solids were observed to lift off the bottom. Many workers have shown that visual and instrumentation methods for determining the just-suspended velocity give very similar results (Brown et al. 2003).

The concentrations used in the Zwietering terms were 0.4 to 0.5 wt%. The Zwietering and FMP correlations show that the minimum velocity to pick up solids is a weak function of solids fraction and particle size and mainly depends on the density difference. Thus, using dense glass (2500 kg/m^3) and large particles gives a good estimate of the exact velocity required and makes observation easier.

2.3.6 Visual Observations During (Dye) Tracer Tests

Visual observations of the tank surface and walls supplemented the understanding of the test results. General observations were made to characterize flow conditions on the tank surface, including easily observed upwelling of material due to PJM discharge, recirculation pump operation, or air sparging. Because in all experiments the chemical tracer was Brilliant Blue dye, observations of the slurry surface were made to verify that dye did not prematurely break through the surface during tracer injection. The surface was also monitored during the run to determine whether dye broke through the surface due to upwelling of new slurry onto the surface. A video camera recorded the simulant surface image during each test. The tank walls were monitored during tracer dye injection to verify that the perimeter PJMs were discharging dyed slurry. After dye injection, the tank walls were monitored for evidence of dyed slurry spreading upward and/or laterally along the wall. Dry erase markers were used to map dyed areas on the tank wall and for sketching a cylindrical projection map of the dyed areas on the acrylic tank wall. The markings on the tank wall were also recorded with a video recorder. Mapping tracer locations along the tank walls supplemented interpretation of tracer on the slurry surface for breakthrough due to cavern growth, flow due to the spargers or pump recirculation, and interpretation of tracer sampling results. In some runs, direct evidence was observed of turbulence due to air spargers or PJM discharges, which were seen as a rippling effect extending up the tank wall at specific locations. This supplemented the tracer observations of cavern height at the tank wall. Observations of dark particulates entrained in the slurry at the tank wall were also made to follow flow lines during some of the recirculating pump operations, particularly of flow toward the pump return line.

2.3.7 Specific Observations During Gas Retention and Release Tests

During GR&R tests the tank level changes were monitored to determine the gas fraction in the simulant. The retained gas volume was estimated by measuring the simulant level changes referenced to the simulant level with no retained gas (see Section 2.5 for details). While the liquid levels were recorded digitally by the DACS, observers visually recorded slurry levels along the tank walls at three locations using tape measures attached to the tank wall and/or suspended from the tank rim. In addition, a video recording was made of one of these stations. These observations supplemented data collected from ultrasonic level indicators and were used to interpret gas release and holdup. In addition, periodic general observations were made as appropriate to the run to aid in interpretation of the tests.

2.4 Sparger Testing

To assess the performance of spargers in WTP actual waste rheology bounding non-Newtonian slurries near full scale, an experimental apparatus consisting of a large-scale tank with a single sparge point was used. The tank used had an approximately 10-ft ID conical bottom and a height of about 12 ft. This vessel was filled with a kaolin:bentonite simulant with Bingham plastic rheological parameters of 25 cP consistency and 35 Pa yield stress. A 3/8-inch schedule 40 pipe was used as a sparge point. The tube was immersed in the simulant to a known depth, and air was forced through the pipe. A rotameter coupled with a pressure gauge and thermocouple was used to determine the actual volumetric air flow through the pipe (Figure 2.14).

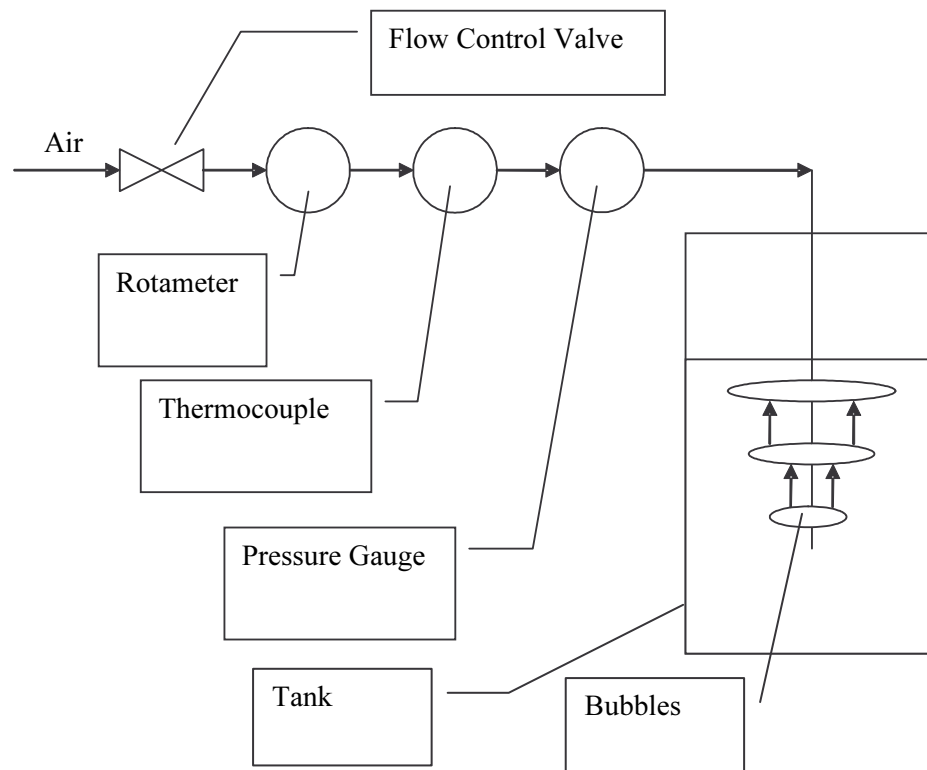


Figure 2.14. Diagram of Sparging Experimental Setup

The rotameter, pressure gauge, and thermocouple readings were converted to the actual volumetric air flow in the slurry at the sparger submergence depth. Isothermal expansion at the sparge tube orifice was assumed. The following equation is used for this calculation:

$$Q_{sparg e} = \frac{Q_{rot}}{\rho_{sim} g h_{sparg e} + P_0} \left(\frac{P_{std} P_{rot} T_{rot}}{T_{std}} \right)^{\frac{1}{2}} \quad (2.3)$$

where

Q_{sparge}	is actual volumetric air flow in the slurry at the submergence depth of sparge tube (ft ³ /min)
Q_{rot}	is the calibrated volumetric flow rate read from the rotameter at standard conditions (ft ³ /min)
P_{std}	is the absolute pressure at which the rotameter is calibrated (1 atm)
T_{std}	is the absolute temperature at which the rotameter is calibrated (530 R)
P_{rot}	is the absolute pressure read at the rotameter
T_{rot}	is the absolute temperature read at the rotameter
ρ_s	is the bulk density of the simulant tested (1.2 g/mL)
g	is the gravitational constant (9.81 m/s ²)
h_s	is submerged depth of the sparge tube
P_0	is atmospheric pressure (1 atm)

Measurements on the surface of the simulant were made to determine the areas of the tank affected by the upward motion of the bubbles. Two major areas were measured. The first area is referred to as the region of bubbles (ROB). This area is the region surrounding the sparge tube that contains the plume of bubbles rising from the sparge point. Surrounding the ROB is an area of induced radial and downward flow. This area is referred to as the zone of influence (ZOI). Both of these regions are reported as diameters. These concepts are portrayed graphically in Figure 2.15.

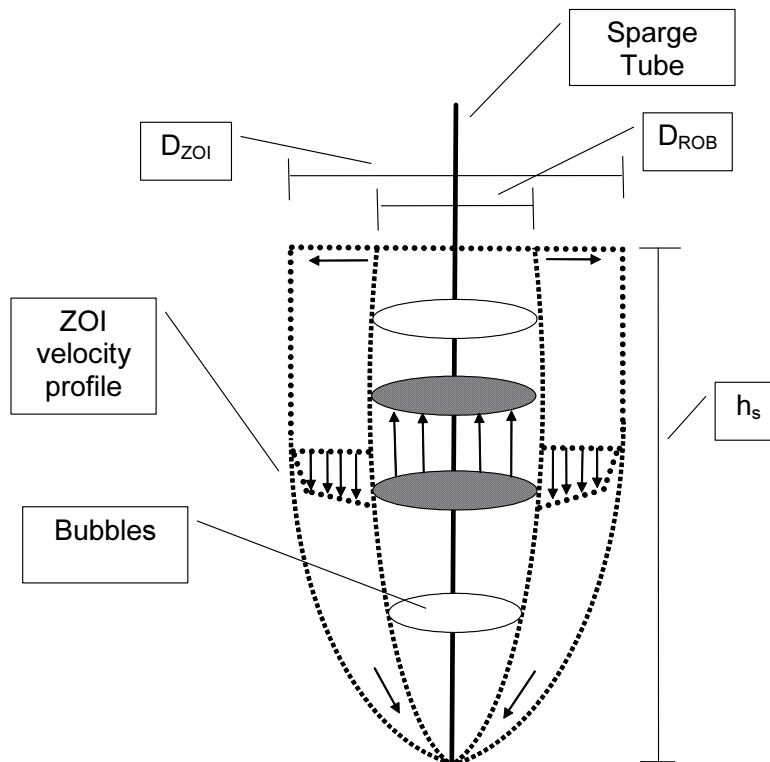


Figure 2.15. Diagram of Sparging Experiment Concepts

The radii of the ZOI and ROB were measured with the sparge tube inserted to several submergence depths and operated with a range of air flow rates. The ROB was measured through the use of a laser reference system coupled with video imaging software. This technique involves placing two laser points

a known distance apart on the surface of the simulant. As testing proceeds, the surface of the simulant is video recorded. The frames from the video images are then analyzed to determine the number of pixels between various features in the frame. By knowing the number of pixels and the actual distance between the laser reference points, the actual distance between two features on the frame were determined.

After the steady-state flow due to sparging was achieved,^(a) the video images of the surface were collected. The technique described above is used to measure the diameter of the bubble plume on the surface of the simulant. Since the bubble plume is dynamic and asymmetric, several images at different times are analyzed to determine the ROB. These values are then averaged to represent a single datum. The ZOI was measured by placing buoyant flow followers on the surface near the sparge tube. The flow followers then move radially outward due to the induced secondary flow. The flow followers stop at the point where the radial flow stops and axial flow downward dominates. A measuring tape was used to determine the distance from the center sparge tube to the flow followers.

2.5 Gas Retention and Release

GR&R tests were completed using ≥ 30 Pa yield stress (Bingham plastic model) kaolin:bentonite clay simulant in the UFP and LS prototype vessels in configurations similar to the selected designs. The basis for the simulant selection is presented in Section 4.1. The vessel configurations and nominal operating conditions and the gas retention and release experimental methods are summarized here.

Of the GR&R test sequences run in the prototype vessels, one sequence in LS (Sequence 15) and two in UFP (Sequences 5 and 6) were closely matched to the final designs. The configurations and nominal or target operating conditions used in the gas retention and release tests are as follows:

- LS Sequence 15– 0.74 H/D initial fill; 8-PJM cluster with 7-45° + 1-vertical nozzles at ~12 m/s; four-nozzle recirculation at ~120 gpm (gas holdup tests only) and four (or eight) air sparge tubes flowing at ~3 acfm each (gas release tests only).
- UFP Sequence 5 – 1.4 H/D initial fill; four-PJM tri-foil configuration with three 45° plus one vertical nozzles at ~12 m/s; single-nozzle recirculation (gas holdup test only) and one center (and three peripheral) sparge tube flowing at ~3 acfm (gas release tests).
- UFP Sequence 6 – 1.8 H/D initial fill; four-PJM tri-foil configuration with three 45° plus one vertical nozzles at ~12 m/s; one center (and three peripheral) sparge tube flowing at ~3 acfm (gas holdup and gas release tests).

Extra sparge tubes (indicated in parentheses above) were used in some tests to release additional gas after the specified release tests with fewer sparge tubes were completed. Unless otherwise specified, the results described in Section 5 were obtained with the nominal operating conditions including fewer sparge tubes.

The decomposition of nominal 30 wt% hydrogen peroxide (H₂O₂) solution was used to generate gas in situ in the kaolin:bentonite clay simulant. The H₂O₂ solution was injected with a peristaltic pump through a single tube into the well-mixed cavern area adjacent to pulse tube nozzles while the PJMs were oper-

(a) Steady state was determined visually by observing that the ZOI flow followers had stopped moving radially from the sparge tube.

ating under prototypic conditions. The amount of H_2O_2 introduced was quantified by weight. In the initial preparation for gas release tests, a specified amount of H_2O_2 was introduced over a short period of time (e.g., 10 to 20 min); after some period of additional mixing (e.g., 10 to 30 min), the system was shut down to allow the H_2O_2 to decompose and gas bubbles to be retained in the quiescent simulant. The accumulated gas was typically released by operating the PJMs and spargers the following day.

In gas holdup tests, H_2O_2 solution was added to simulant at a fixed rate over an extended period of time (e.g., 2 to 3 hours) to continuously generate O_2 gas while the simulant was mixed in the PJM vessel using specified “normal” operating conditions. Injection continued until a new steady-state level was achieved in the test vessel. The rate of H_2O_2 injection was determined by recording the weight of a solution feed container as a function of time. (A MicroMotion flow meter and a data acquisition system were also used to measure and record the solution flow rate.) The mixing system was shut down shortly after the completion of gas holdup tests, resulting in simulant volume growth as residual H_2O_2 decomposed. (Further analysis of the growth profile following shutdown will provide additional information on the apparent gas generation rate.) After a short period of gas retention (30 min or less), a gas release test was typically conducted.

In GR&R experiments, retained gas volume fractions in the prototype vessels were assessed by changes in surface level, which were independently correlated to tank volume. Several methods, including instrumental techniques and visual/camera observations, were used to track changes in surface level over time. Ultrasonic level sensors (Gems Corporation model UCL-200) were deployed in each of the prototype vessels (two in LS and one in UFP), and signals were output to a data acquisition system where they were recorded at 10 Hz. These sensors sample an area of the surface, which increases with the sensor-to-surface separation distance; the sensors were typically placed 0.5 to 1 m from the surface. In both prototypes, the sensors were located in the annular region between the PJMs and the tank wall. Gas volume fractions presented here were determined from the ultrasonic level sensor data. In the case of LS, the results are the average for two sensors located over nearly opposite sides of the tank. Typically, a single volume was determined for each pulse cycle using the minimum level obtained when PJMs were drawn full (suction phase).

A detailed analysis of the uncertainty in reported gas volume fractions and estimated gas generation rates has yet to be completed. The accuracy of reported gas volume fractions is a function of the accuracy of surface level-volume correlations and the accuracy of level measurement techniques. In turn, level measurements are limited by instrument resolution and calibration accuracy and are subject to variability due to surface movement and irregularity during mixing operations. Data fluctuations about central values (e.g., standard deviation in gas holdup tests) give an indication of the variability. These data will be reported in the final DBE strategy.

2.6 Tracer Techniques

Mixing performance in the PJM test vessels was assessed through the use of tracer chemicals. A tracer was injected during the initial stages of the PJM test. Samples of the simulant were taken from several locations during each mixing test to determine the changes in dye concentration as a function of time and operating parameters. At the end of a test cycle, the test vessel was homogenized and a final sample collected. A summary of the technique used is shown in Figure 2.16.

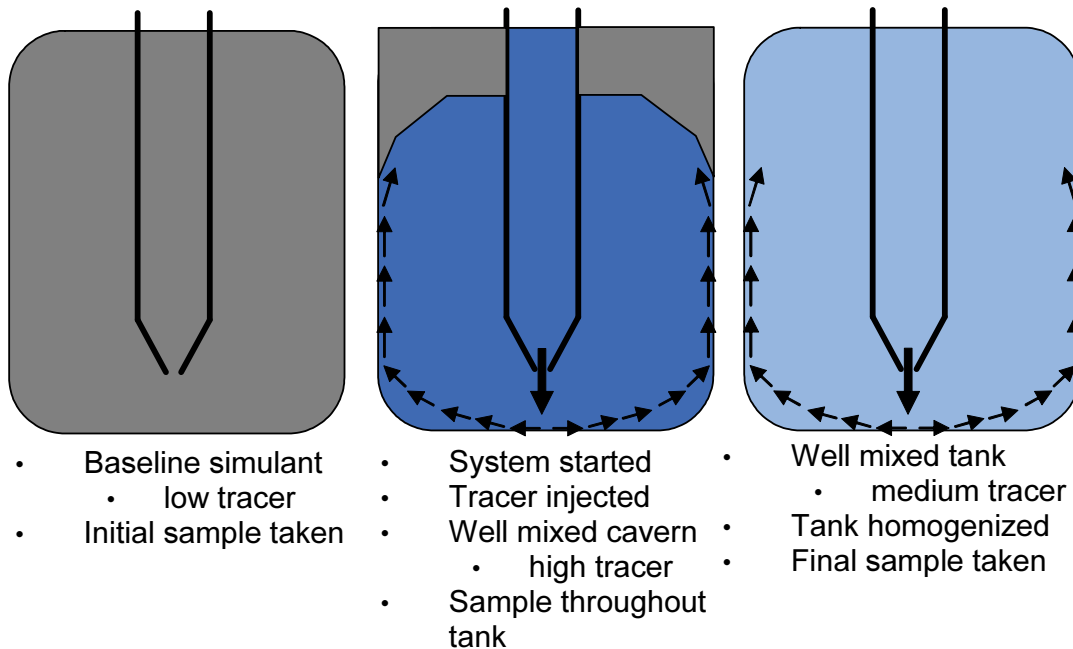


Figure 2.16. Summary of Tracer Dye Technique Steps

The chemicals used were food dye color No. 1, (Brilliant Blue FCF) and sodium chloride (NaCl). Initially, a sample of simulant was drawn from the test vessel to baseline the tracer levels. Next, a stock solution of these materials was prepared by dissolution in water. This stock solution was then blended with a sample of the test simulant to achieve rheological properties close to the actual test simulant. This solution was introduced into the center PJM tube during operation by opening a valve on a sample injection line during the PJM suction phase. During the drive phase, the valve was closed and the injected dye was driven from the PJM tube. Use of this procedure allowed for the gradual introduction of the tracer dye into the system over several drive/suction cycles and minimized the potential for a large amount of concentrated tracer to enter a stagnant region of the tank. This was observed when the concentrated tracer had significantly different physical properties from the bulk simulant. Such physical properties include density, entrained air due to surface tension, and rheological parameters.

After the dye was injected, the experimental clock started and samples were drawn from five locations in each test vessel. Locations 1, 2, and 3 were samples taken directly from three separate pulse tubes. These samples represent the contents of the well-mixed cavern. Sample locations 4 and 5 were placed between the pulse tubes and the tank wall. Location 4 was at a low elevation and location 5 was at a high elevation. Schematic diagrams of the tracer sampling locations are shown in Figures 2.17 and 2.18 for the LS vessel and UFP vessel, respectively.

Multiple run conditions were typically achieved for each tracer injection. The tracer test started with the lowest mixing energy condition to form the initial well mixed cavern. Additional systems (e.g., recirculation pumps or sparging tubes) or increased pulse tube velocities were then used as subsequent run conditions to form larger mixing caverns.

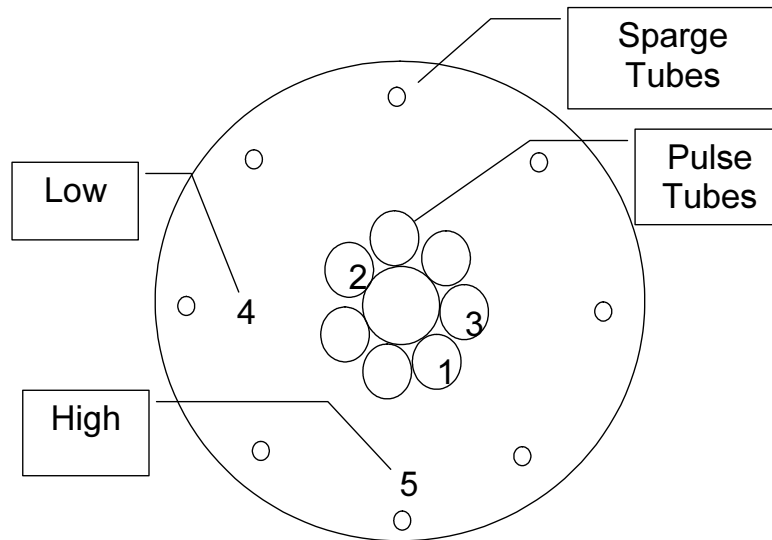


Figure 2.17. Schematic of LS Vessel Tracer Sampling Locations

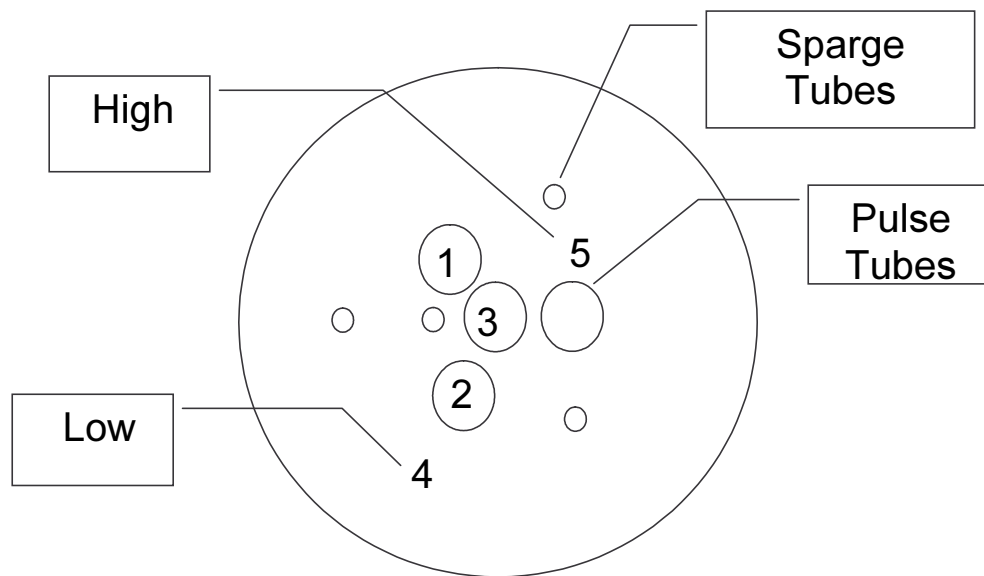


Figure 2.18. Schematic of Ultrafiltration Process Vessel Tracer Sampling Locations

During the initial run condition, samples were drawn from sample locations 1, 4, and 5 taken approximately every 10 minutes after completion of dye injection. After 50 minutes of operation, samples were drawn from all sample locations and the next run experimental condition employed. During subsequent run conditions, samples from locations 1, 4, and 5 were taken every 15 minutes. After 45-90 minutes of operation, samples were drawn from all sample locations, and the next run experimental condition was employed.

This procedure was used to quantify the transient behavior of the mixed regions within the tank. The first run condition was examined in more detail because the anticipated amount of energy required to reach steady state for the first run is greater than subsequent runs where a significant mixed region already exists.

Samples were drawn using a vacuum system. In this system, a vacuum was placed on the sample lines in the tank. The simulant was drawn through the lines and collected in stoppered beakers using a trap. When sampling, the lines were initially purged of simulant into a separate beaker. This step loaded the sample line with simulant from the sample location at the appropriate sample time. A clean beaker was then attached and the newly loaded simulant was collected. The simulant was then transferred into sample containers for tracer analysis. A sample extraction typically took 2 to 5 minutes to complete.

Tracer analysis consists of two measurements, one for the dye and one for the NaCl. The concentration of dye was measured using a UV-VIS spectrometer. This instrument requires a transparent sample. To overcome this limitation, the opaque kaolin:bentonite simulant was centrifuged, and the analysis was performed on the centrifuged liquid portion of the sample. The spectrometer measures the optical absorbance of the sample at multiple wavelengths of light. When the dye is present in the system a peak absorbance is observed at approximately 630 nm. According to Beer's law, the magnitude of this absorbance peak is directly proportional to the concentration of dye in the system.

For the NaCl tracer, a chloride ion selective electrode was used to measure the concentration of chloride present in the samples. This instrument measures the potential difference across an electrode that is surrounded by a membrane that allows chloride ions to pass from the sample material into the electrode cell. Unlike the spectrometer method, this measurement was performed directly on the simulant with no required preparation steps.

The equation used to calculate the fraction mixed is shown below:

$$X_j = \frac{C_f - C_0}{C_j - C_0} \quad (2.4)$$

where

- X_j is the fraction mixed of the j-th tank sample
- C_f is the tracer concentration of the final homogenized simulant
- C_0 is the tracer concentration of the initial baseline simulant
- C_j is the tracer concentration of the j-th tank sample

When the aqueous phase tracer does not absorb onto the solid phase, the liquid phase concentration can be measured with the techniques above, and Equation 2.4 can be used to directly calculate the fraction of the tank mixed. The chloride ion did not appear to absorb onto the simulant particles, and this equation is used for the NaCl tracer. Because the spectrometer measures absorbance, which is proportional to concentration, Equation 2.4 can be rewritten for the dye tracer as follows:

$$X_j = \frac{A_f - A_0}{A_j - A_0} \quad (2.5)$$

where

- X_j is the fraction mixed of the j-th tank sample
- A_f is the optical absorbance of the final homogenized simulant
- A_o is the optical absorbance of the initial baseline simulant
- A_j is the optical absorbance of the j-th tank sample

Unfortunately, the dye tracer absorbs onto the clay particles in significant quantity. In this situation Equation 2.4 still applies, but the concentrations used in the equation must account for both the liquid and solid phases. This is accomplished using the following equation:

$$C = Y_l C_l + Y_s C_s \quad (2.6)$$

where

- C is the tracer concentration
- C_l is the tracer concentration of the liquid phase
- C_s is the tracer concentration of the solid phase
- Y_l is the liquid phase mass fraction
- Y_s is the solid phase mass fraction

The distribution of tracer between the liquid and solid phases is typically described using a distribution coefficient:

$$C_s = K_d C_l \quad (2.7)$$

where K_d is the distribution coefficient.

To complicate matters further, the distribution coefficient is also a function of liquid phase dye concentration. When Equations 2.6 and 2.7 are substituted in Equation 2.4, the following equation results:

$$X_j = \frac{Y_l (A_f - A_o) + Y_s (K_{df} A_f - K_{do} A_o)}{Y_l (A_j - A_o) + Y_s (K_{dj} A_j - K_{do} A_o)} \quad (2.8)$$

where

- K_{df} is the distribution coefficient at the homogenized tank tracer concentration
- K_{do} is the distribution coefficient at the initial baseline tracer concentration
- K_{dj} is the distribution coefficient at the j-th tank sample tracer concentration

When K_d is null or constant, Equation 2.8 reduces to Equation 2.5. Over the small dye concentration ranges observed in the prototype testing, the assumption of a constant distribution coefficient is valid, and Equation 2.5 can be used. Note that as A_j approaches A_f , K_{dj} approaches K_{df} , and the error associated in using Equation 2.5 approaches zero. In addition, the distribution coefficient function varies from batch to batch of simulant, and other factors such as temperature and contact time will also affect the distribution

coefficient function. Lastly, the solids loading of the simulant was often varied for rheological purposes. For these reasons, Equation 2.5 is used to estimate the fraction mixed using the dye tracer. The error associated with this assumption is predicted using estimated values for the liquid and solid mass fractions and the distribution coefficient. Appendix B contains further details on these parameters.

3.0 Supporting Data for Mixing System Vessel Configurations

3.1 Rheology

3.1.1 Bounding Conditions

For all seven WTP vessels that will contain non-Newtonian fluids, it was assumed that the HLW pretreated sludge bounding physical and rheological properties would hold (CCNs 069099, 065607, and 082255).

Normal Plant Operation Rheological Bound: Data from actual radioactive and simulant waste rheograms combined with general engineering design techniques were used to define a set of bounding physical and rheological properties that agree well with actual data (POLOSKI 2004). The non-Newtonian HLW pretreated sludge rheological properties were fit using a linear Bingham plastic model. The bounding conditions were used to develop the waste simulants used in the PJM program. Figure 3.1 is a plot of actual pretreated waste rheograms and the upper bounding rheological properties curve. The linear Bingham plastic model fit parameters are yield stress (y-axis intercept) of 30 Pa and consistency (slope) of 30 cP. Table 3.1 contains a summary of expected physical and rheological properties.

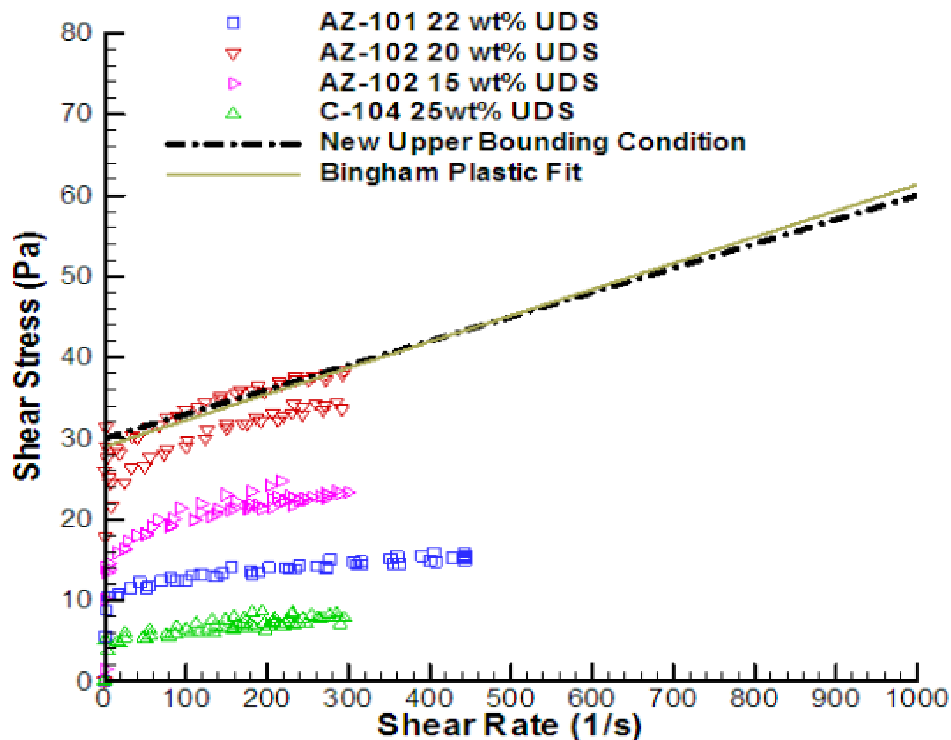


Figure 3.1. Rheogram of Actual HLW Pretreated Sludge Samples with Upper Bound Rheological Curve

Table 3.1. Physical and Rheological Properties that Help Define Simulants for Rating or Qualifying Fluidic Mixing Systems

Property	HLW Pretreated Sludge
pH	≈ 12 ^(a) –14
Particle size distribution (D ₅₀) ^(b)	2 μm
Particle size distribution (D ₉₅) ^(c)	20 μm
Bulk density	1.1–1.6
Supernatant liquid density	≈1.0
Vol% settled solids	10%–90%
Wt% total dried solids	5%–25%
Wt% total oxide	7%–15% ^(d)
Shear stress versus shear rate (ambient and 40°C)	Bingham Plastic
(a) Expected pH after washing leaching in 0.01 M NaOH.	
(b) 50% of particles are smaller than the indicated value.	
(c) 95% of particles are smaller than the indicated value.	
(d) Based on simulant data.	

Because the rheological window is based on only four samples from three tanks, it is possible that slurries from other tanks could exceed the rheological boundary. It has been estimated that 20 to 30% of HLW tanks may have rheological properties higher (yield stress and consistency higher than 30 Pa and 30 cP, respectively) than those documented in the three active tank samples analyzed to date (CCN 082255). This uncertainty will be addressed by laboratory testing prior to receipt of the waste at the WTP to define the extent to which the slurry may be concentrated and stay below the rheological boundary.

Plant Upset Operation Rheological Bound: It is important to note that measured maximum shear strength values (an actual physical property that must be overcome in order for these fluids to flow) for actual HLW pretreated sludge samples when allowed to stand in an unmixed condition, that is, post-DBE, they reach values greater than 30 Pa. For this reason, a bounding yield strength value of 70 Pa should be used (CCN 065607). In addition, the “gel” time (the time required for the actual waste to reach its maximum shear strength value) of actual waste samples will need to be taken into account along with the maximum shear strength values for plant operation considerations.

3.1.2 Simulants

One transparent simulant and one opaque simulant were used in the PJM program. The transparent simulant was Laponite RD (Southwestern Clay Products), a thixotropic colloidal synthetic clay that forms stable gel networks when unsheared. Due to the thixotropic nature of Laponite, the flow behavior of the simulant is dynamic, and it was allowed to gel and reach a target shear strength. Speers et al. (1987) demonstrated that the shear strength of clay drilling muds increases over time following first-order rate kinetics. Laponite shear strength behavior was observed to agree with the Speers et al. (1987) correlation for drilling muds. At this point the PJM system was started and a mixing cavern formed as defined by the gel’s shear strength. After constant shearing, a steady-state flow behavior was approached. Unfortunately, this flow behavior was lower than the bounding rheology of WTP waste streams. This is illustrated in Figure 3.2, where actual HLW pretreated sludge rheograms are compared with PJM simulants. The bounding rheological parameters of the HLW pretreated sludge (Poloski 2004) are defined as Bingham plastic consistency of 30 cP and yield stress of 30 Pa.

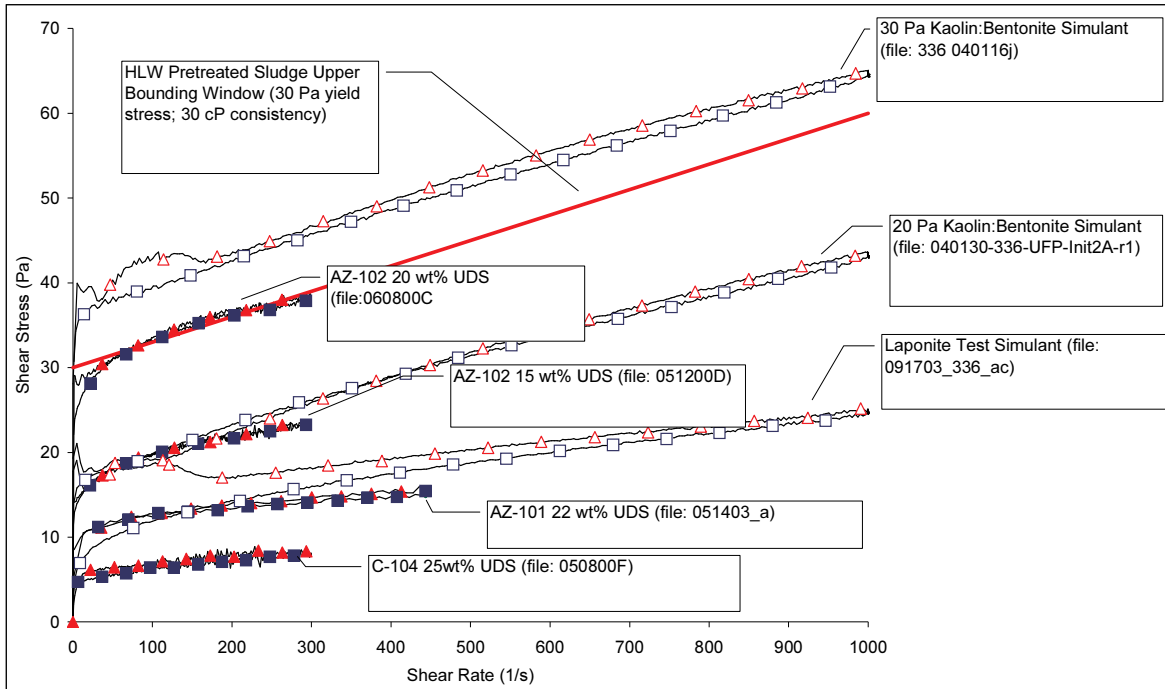


Figure 3.2. Flow Behavior Comparison of PJM Simulants and Actual HLW Pretreated Sludge

In addition to not possessing the target rheological parameters desired for PJM testing, the Laponite composition also does not match other target values given in Table 3.1. The Laponite recipe calls for 1-2 wt% Laponite RD in water where the actual waste is in the 15 to 25 wt% undissolved solids range. And the Laponite simulant consists of particles on the order of tens of nanometers, whereas the actual waste consists of particles in the tens of microns range. These differences may result in varying turbulent flow behavior in the PJM mixing cavern. For these reasons, a more representative particulate slurry was developed to enhance confidence in the PJM testing results. Unfortunately, this simulant is opaque.

The particulate simulant developed consists of a mixture of kaolin clay (EPK Feldspar Pulverized) and bentonite clay (WYO-Ben Big Horn CH-200) in water. To meet the WTP bounding parameters of Bingham plastic consistency of 30 cP and yield stress 30 Pa, a recipe was developed using these two clays. The recipe calls for a composite of 80% kaolin and 20% bentonite mixed with water to a loading of approximately 27 wt%. Water is then added to the simulant to adjust the rheological parameters to other target values. Figure 3.2 compares these simulants with actual waste at various solids loadings to target 30+ and 20 Pa yield stress. A summary of the measured rheological parameters for significant prototype tests and sparging tests is shown in Tables 3.2, 3.3, and 3.4. In addition, the bentonite/kaolin simulant shear strength behavior was observed to agree with Speers et al. (1987) correlation for drilling muds.

Table 3.2. Rheological Model Fits for LS Prototype PJM Simulants at Ambient Temperature

Model/Model Parameter	LS Test 4	LS Test 7	LS Test 11	LS Test 15	LS Test 20
File Name	336 040116j	040123-336- ls-T7-R1	336 04129b	040216 apel- 0002f	040309 apel- r1-0001f
Bingham Plastic:					
τ_O^B - Bingham yield stress (Pa)	37	36	37	36	36
k - Bingham consistency coefficient (cP)	28	27	26	27	24
R - correlation coefficient	1.0	1.0	1.0	9.6 ^(a)	5.8
Herschel-Bulkley:					
τ_O^H - yield stress (Pa)	35	34	35	34	34
k - Herschel-Bulkley consistency coeff. (Pa·s ^{-b})	0.092	0.090	0.082	0.12	0.063
b - Herschel-Bulkley power law exponent	0.83	0.83	0.84	0.79	0.86
R - correlation coefficient	1.0	1.0	1.0	1.3 ^(a)	1.6 ^(a)
(a) Standard error.					

Table 3.3. Rheological Model Fits for UFP Prototype PJM Simulants at Ambient Temperature

Model/Model Parameter	UFP Test 2	UFP Test 3B	UFP Test 5	UFP Test 6
File Name	040130-336- ufp-T2-init-r1	040213 apel- 0003f	040213 apel- 0006f	040213 apel- 0012f
Bingham Plastic:				
τ_O^B - Bingham yield stress (Pa)	34	33	36	37
k c- Bingham consistency coefficient (cP)	27	18	19	20
Rc - correlation coefficient	1.0	6.4 ^(a)	4.8 ^(a)	5.2 ^(a)
Herschel-Bulkley:				
τ_O^H - yield stress (Pa)	33	32	35	36
k - Herschel-Bulkley consistency coefficient (Pa·s ^{-b})	0.086	0.059	0.046	0.053
b - Herschel-Bulkley power law exponent	0.84	0.83	0.88	0.87
R - correlation coefficient	1.0	2.1 ^(a)	1.8 ^(a)	1.7 ^(a)
(a) Standard error.				

Table 3.4. Rheological Model Fits for LS Prototype PJM Simulants at Ambient Temperature

Model/Model Parameter	336 simulant 2-20-04	336 simulant after peroxide addition	336 simulant during gas retention test	336 simulant after gas retention test
File Name	040224 apel- 0007f	040227 apel- 0002f	040301 apel- 0009f	040308 apel- 0001f
Bingham Plastic:				
τ_O^B - Bingham yield stress (Pa)	37	33	33	32
k - Bingham consistency coefficient (cP)	22	21	22	23
R - correlation coefficient	7.7 ^(a)	7.8 ^(a)	7.2 ^(a)	9.1 ^(a)
Herschel-Bulkley:				
τ_O^H - yield stress (Pa)	35	32	32	30
k - Herschel-Bulkley consistency coefficient (Pa·s ^{-b})	0.088	0.082	0.073	0.098
b - Herschel-Bulkley power law exponent	0.81	0.81	0.83	0.80
R - correlation coefficient	1.9 ^(a)	1.8 ^(a)	1.7 ^(a)	2.1 ^(a)
(a) Standard error.				

3.2 Prototype Results

The various mixing tests performed and the percent mixed for both the UFP and LS prototype test stands are summarized in Tables 3.5 and 3.6, respectively. The PJMs, spargers, and recirculation pump configurations for the various sequences listed in the tables are presented in Tables 2.1 and 2.2 (Section 2.3). All tests were performed with a kaolin/bentonite clay simulant, the yield stress of which was determined from thoroughly mixed samples (mixed by PJM overblow and sparging) collected prior to and at the completion of a sequence of runs. The yield stress of the kaolin/bentonite clay simulant is the average of the results for these samples. The H/D_T is the ratio of the simulant fill height to tank diameter.

The nozzle velocities listed in Tables 3.5 and 3.6 were calculated based on the average velocity (\bar{u}_{disch}) as defined by Equation A.7 in Appendix A. The average nozzle velocities are based on averages of all the PJMs (four or six for UFP and eight for LS) taken over typically 25 representative cycles of PJM operation during a run. The cycle times listed in Tables 3.5 and 3.6 for the two test stands were set based on scaling approximately equal to the inverse of the geometric scale factor, that is, 4.94 and 4.24 for the UFP and LS prototype test stands, respectively.

For tests that used a recirculation pump, the pump flow rates were scaled approximately by the square of the geometric scale factor, that is, 4.94^2 (=24.4) and 4.29^2 (18.0) for the UFP and LS prototype test stands, respectively. The recirculation flow rates listed in Tables 3.5 and 3.6 are based on the average of the flow rates measured over the duration of a run. In calculating recirculation pump averages, startup transients were ignored.

For tests that involved sparging, no scaling was applied in setting the operating air flow rates and acfm through the sparger tubes are based on the readout of the rotameters included in-line with each sparger. No corrections were applied to the sparger air flow rates, and a post-calibration of the flow meters indicated the sparger flow rates were within $\pm 15\%$.

Table 3.5. Test Conditions and Fraction Mixed Results for Tests Performed in UFP Test Stand

Seq	Run	Test Mode	H/D	Yield Stress (Pa)	Noz. Vel. (m/s)	Cycle Time (sec)	Sparger Flow Rate (acfm)	Pump Flow Rate (gpm)	Fraction Mixed	Error ^(a) (\pm)
2	1	PJM Only	1.8	35	9.0	27	-	-	0.53	0.093
2	2	PJM Only	1.8	35	12.3	27	-	-	0.64	0.074
2	3	PJM + Sparging	1.8	35	12.3	27	3	-	1.1	0.013
2	4	PJM + Sparging	1.8	35	12.4	27	1	-	0.96	0.0088
3B	1	PJMs Only	1.4	37	9.3	27	-	-	0.65	0.12
3B	2	PJM + Pump	1.4	37	9.3	27	-	90	0.98	0.0074
3B	3	PJM + Pump	1.4	37	14.1	27	-	87	1.0	0.0019
3B	4	PJM + Pump + Sparging	1.4	37	14.1	27	3	95	1.0	0.0038

(a) Estimated error due to assumption of linear isotherm for dye absorption. Experimental error not included.

Table 3.6. Test Conditions and Fraction Mixed Results for Tests Performed in LS Test Stand

Seq	Run	Test Mode	H/D	Yield Stress (Pa)	Noz. Vel. (m/s)	Cycle Time (sec)	Sparger Flow Rate (cfm)	Pump Flow Rate (gpm)	Fraction Mixed	Error ^(a) (±)
4	1	PJMs Only	0.74	38	7.8	45	-	-	0.54	0.15
4	2	PJMs Only	0.74	38	11.3	45	-	-	0.65	0.13
4	3	PJMs + Spargers	0.74	38	11.1	45	3	-	0.87	0.052
4	4	PJMs + Spargers	0.74	38	11.4	45	3	-	0.97	0.014
7	1	PJMs Only	1	36	4.6	55	-	-	0.24	0.11
7	2	PJMs Only	1	36	7	45	-	-	0.42	0.085
7	3	PJMs + Pump	1	36	7	45	-	121	0.55	0.06
7	4	PJMs + Pump	1	36	10.3	45	-	119	1.1	0.01
7	5	PJMs + Pump + Sparging	1	36	10.4	45	3	122	1.1	0.0058
7	6	PJMs + Pump + Sparging	1	36	10.5	45	3	121	0.93	0.0067
11	1	PJMs + Pump	0.74	37	8.2	45	-	121	0.66	0.033
11	2	PJMs + Pump	0.74	37	11.9	45	-	115	0.95	0.0055
20	1	PJMs	0.74	35	12.3	45	-	121	0.96	0.0097
20	2	PJMs + Pump	0.74	35	12.2	45	-	122	1.0	0.00069

(a) Estimated error due to assumption of linear isotherm for dye absorption. Experimental error not included.

The fraction mixed data presented in Tables 3.5 and 3.6 are based on the measurements obtained from the dye/tracer injected into the simulant prior to the start of a test sequence, and the approach is discussed in Section 2.6 and Appendix B. The error in the fraction mixed values is due to a linear isotherm assumption for dye absorption (see Appendix B for details). This error goes to zero as the fraction mixed goes to 100%. Experimental variability due to sampling and analysis is still present. The percent mixed versus yield Reynolds number for the various tests conducted with the UFP prototype test stand are shown in Figure 3.3. Similar results for the LS prototype test stand are shown in Figure 3.4.

It can be seen from the data in Figure 3.3 that with PJMs only an increase in the yield Reynolds number results in an increase in the percent mixed. It can also be in Figure 3.3 that PJMs alone are not sufficient to completely mix the tank. The addition of sparging and/or recirculation generally results in complete mixing. Similar observations can be made for the LS prototype test stand.

The test conditions and results of the various solids lift tests performed in both UFP and LS prototype test stands are shown in Tables 3.7 and 3.8. The PJM configurations for UFP and LS prototype test stands are presented in Tables 2.1 and 2.2 and discussed in Section 2.3. For all the solids lift tests, a slurry of 4-mm glass beads (specific gravity 2.5) in water was used. The concentration of the glass beads was ~0.2 vol%. In Tables 3.7 and 3.8, the nozzle velocities were determined based on the averages described above.

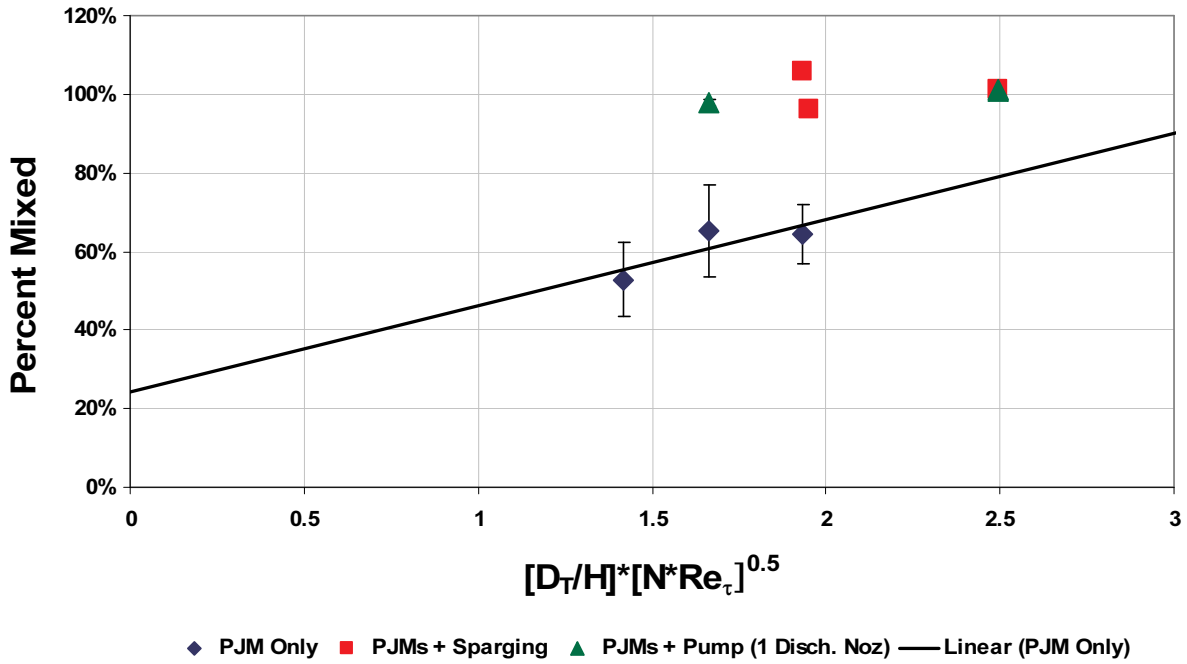


Figure 3.3. Percent Mixed Versus Yield Reynolds Number for UFP Prototype Test Stand During Various Operating Conditions

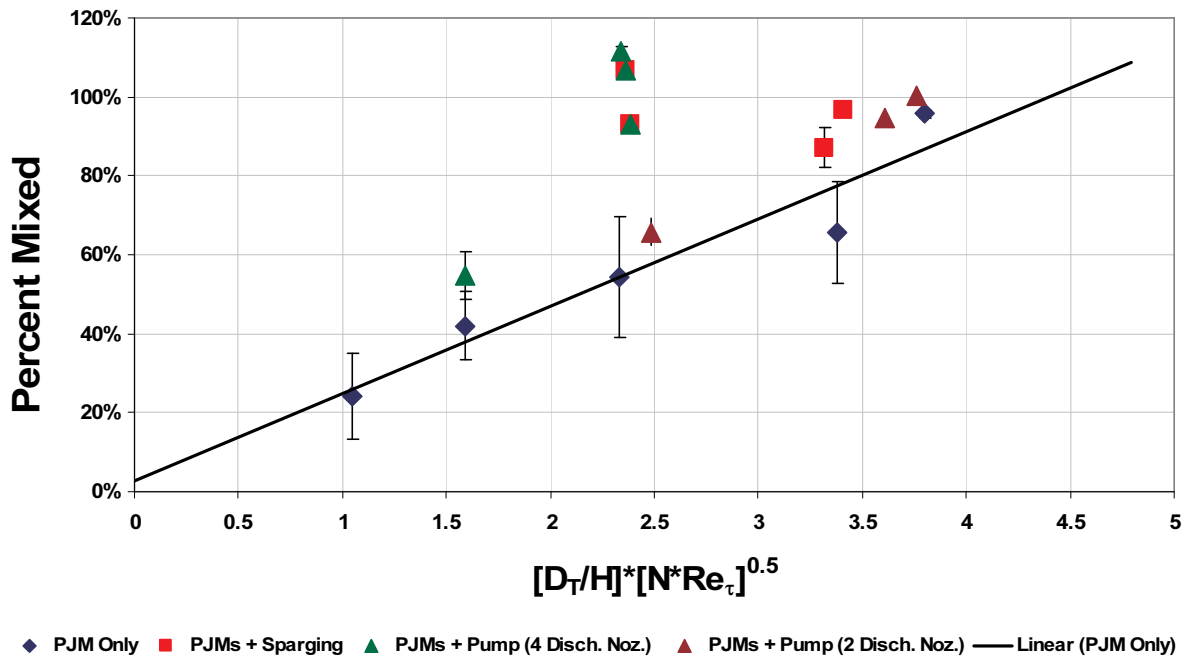


Figure 3.4. Percent Mixed Versus Yield Reynolds Number for LS Prototype Test Stand During Various Operating Conditions

Table 3.7. Test Conditions and Results of Solids Lift Tests Performed in UFP Prototype Test Stand

Seq	Run	Test Mode	H/D	Noz. Vel. (m/s)	Cycle Time (sec)	Solids Lift (Yes/No)
7	1	PJMs only	1.8	4.7	27	No
7	2	PJMs only	1.8	6.1	27	No
7	3	PJMs only	1.8	6.5	27	Yes
7	4	PJMs only	1.8	6.9	27	Yes

Table 3.8. Test Conditions and Results of Solids Lift Tests Performed in LS Prototype Test Stand

Seq. No.	Run	Test Mode	H/D	Noz. Vel. (m/s)	Cycle Time (sec)	Solids Lift (Yes/No)
16	1	PJMs only	0.74	7.8	45	No
16	2	PJMs only	0.74	8.6	45	Yes
16	3	PJMs only	0.74	9.2	45	Yes
16	4	PJMs only	0.74	7.0	45	No
16	5	PJMs only	0.74	7.6	45	No
16	6	PJMs only	0.74	8.0	45	Yes

During the solids lift tests, visual observations were made to assess whether at any moment during the drive phase all the solid glass beads were lifted off the floor. These observations are indicated by Y or N (yes or no) in the last column of Tables 3.7 and 3.8.

The data for the bead lift tests in the UFP test stand using the “cluster” configuration and 45° nozzles indicates that the minimum velocity needed to lift the beads from the floor was between 6.1 and 6.5 m/s. For the LS prototype with cluster PJM configuration and 45° nozzles, the minimum velocity to lift the beads from the floor was found to be between 7.8 and 8 m/s. All the values are below the minimum jet velocity of 8 m/s being considered for the PJMs.

These velocity values can be extended to other concentrations and particle sizes through the functionalities given in Section 2.3.5 and Equation 2.2. FMP found that the effect of scale was given by the function V_j s proportional to $T^{0.3}$ for constant ratio of tank to jet diameter. This scale-up effect is small because of the large scale of the test tanks.

The above data only refers to whether solids are lifted off the tank bottom. How well they are distributed vertically in the tanks depends on different factors with different functionalities. In WTP this has been studied with computational fluid dynamics (CFD) and has shown with slow settling particles that the solids are fairly well distributed. However CFD cannot currently determine whether the solids are lifted off the bottom; this requires the experimental verification discussed above.

3.3 Sparging

The mobilization performance of a single sparge tube in a rheologically bounding WTP simulant was investigated as described in Section 2.4. The rheological properties of the simulant are described in

Section 3.1.2. ZOI and ROB diameter results were plotted against the actual volumetric air flow in the slurry at the end of the submerged sparge tube. These results are shown in Figure 3.5. Examination of the data reveals that the ROB and ZOI diameters are a weak function of submergence depth. This indicates that these regions have a nearly cylindrical submerged vertical profile. The full-scale PJM sparger systems will be submerged deeper than measured in these experiments. Because the ZOI and ROB diameters will increase slightly with submergence depth, this assumption is conservative from a design perspective. A correlation of the ROB and ZOI diameters to actual volumetric flow rate adequately describes the size of these regions (see Equations 3.1 and 3.2).

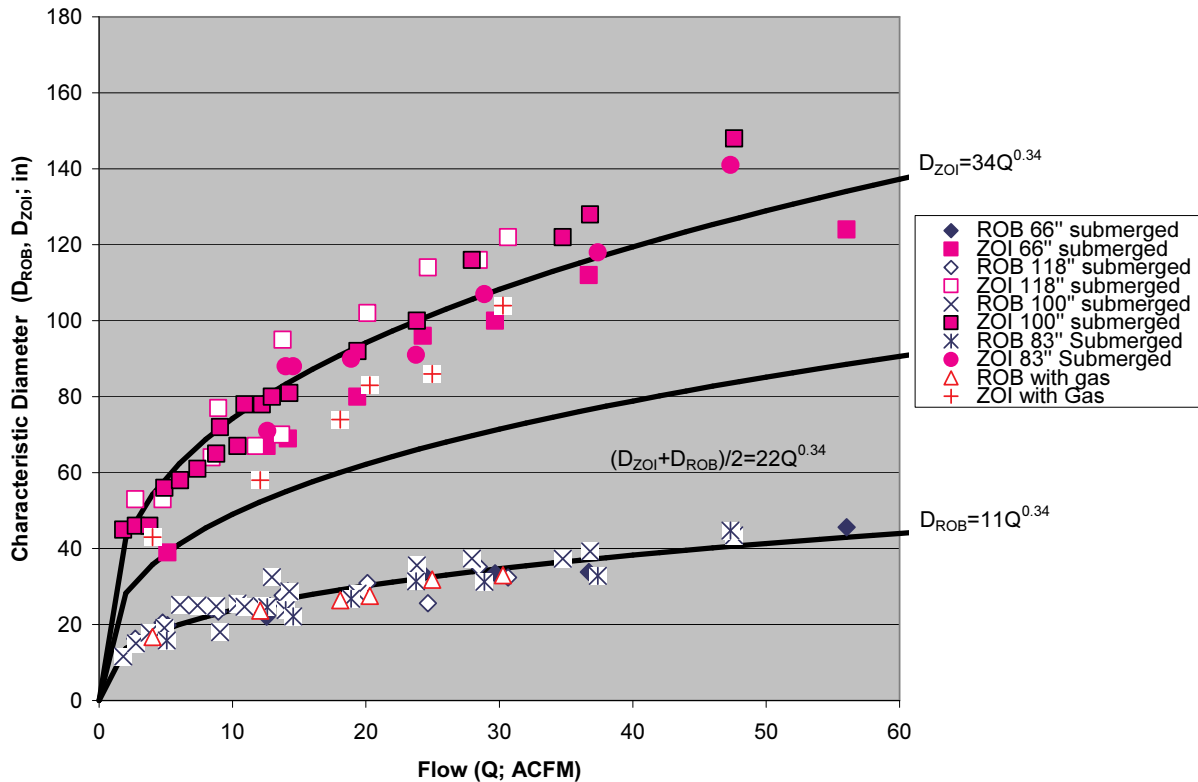


Figure 3.5. ZOI and ROB Sparger Diameters at Various Air Flow Rates

$$D_{ROB} = 11Q_{air}^{0.34} \quad (3.1)$$

$$D_{ZOI} = 34Q_{air}^{0.34} \quad (3.2)$$

where

D_{ROB} is the ROB diameter (in)
 D_{ZOI} is the ZOI diameter (in)
 Q_{air} is the actual volumetric flow rate of the air in slurry at the end of the sparge tube (ft³/min)

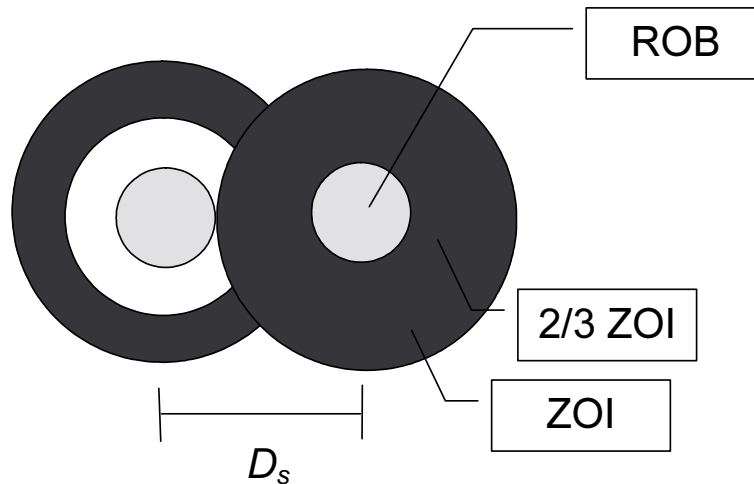


Figure 3.6. Adjacent ZOI and ROB Interaction Options

From these correlations one can see that $D_{ZOI} \approx 3 \cdot D_{ROB}$. If one designs a sparging system such that the ZOI from one sparge tube meets the ROB from an adjacent sparger (Figure 3.6), the sparger spacing shown in Equation 3.3 can be specified.

$$D_s = \frac{D_{ROB} + D_{ZOI}}{2} \quad (3.3)$$

$$D_{ZOI} = 3D_{ROB}$$

$$D_s = \frac{2}{3}D_{ZOI}$$

where

D_s is the sparger spacing
 D_{ROB} is the ROB diameter
 D_{ZOI} is the ZOI diameter

Another single-tube sparging test was performed by mixing hydrogen peroxide with the simulant. The simulant was then allowed to sit undisturbed for a time as the decomposition of hydrogen peroxide proceeded to load the simulant with gas. The sparging experiment was then performed on simulant loaded with gas that had developed a shear strength due to remaining undisturbed for several hours. These results are shown in Figure 3.5 and indicate a significant decrease in ZOI diameter during these tests.

The ROB diameter appears unaffected by the presence of gas. Potential factors that influence the measured ZOI diameter were the presence of gas in the system at startup and increasing shear strength due to gelation of the slurry as it sat undisturbed. Nonetheless, this test illustrates that actual sparger performance in the WTP will be affected by letting the waste remain undisturbed for periods of time, allowing for increasing rheological parameters and gas holdup. Startup procedures to recover from these scenarios should be considered to ensure successful operation of the WTP.

4.0 Description of Selected Pretreatment Facility Designs

The PJM cluster configuration concept, that is, one central pulse tube with the remaining pulse tubes clustered around the central tube, was chosen for both the UFP and LS vessels. This configuration provides a mixed turbulent cavern in the bottom of the vessel that suspends waste particles and is scalable. Supplemental mixing used to mix the upper portion of the vessels relies on recirculation pumps or spargers. This section describes that process.

4.1 Ultrafiltration Feed Process Vessel (UFP-VSL-00002A/B)

Normal operation (without leaching): Under normal operation (without leaching), the UFP operates at or below an aspect ratio of 1.4. The aspect ratio (H/D) is defined by the liquid height (H) divided by the vessel diameter (D). A combination of the PJMs and a recirculation jet will provide adequate mixing up to an $H/D=1.4$. The recirculation pump must provide 2200 gpm to the jet. The jet is sized to provide an exit velocity of 30 ft/sec. Each PJM provides at least a 12 m/s flow during the PJM drive cycle.

During this mode of operation, the sparge tubes will be run in an 'idling' air flow mode using 0.5 to 1.0 acfm (~2 scfm) of air per sparge point. The layout of PJMs, sparge lines, and recirculation lines is shown in Figures 4.1 and 4.2.

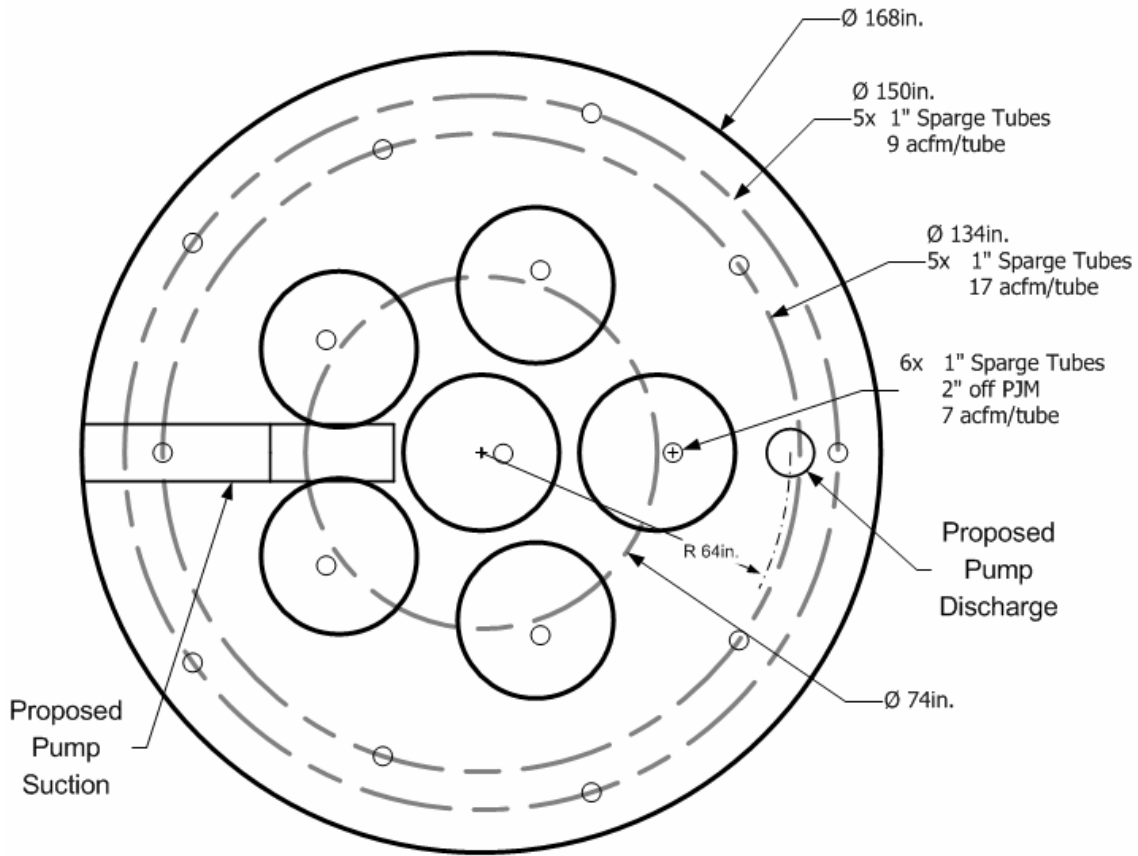


Figure 4.1. UFP-VSL-00002A/B Mixing System Layout – Plan View

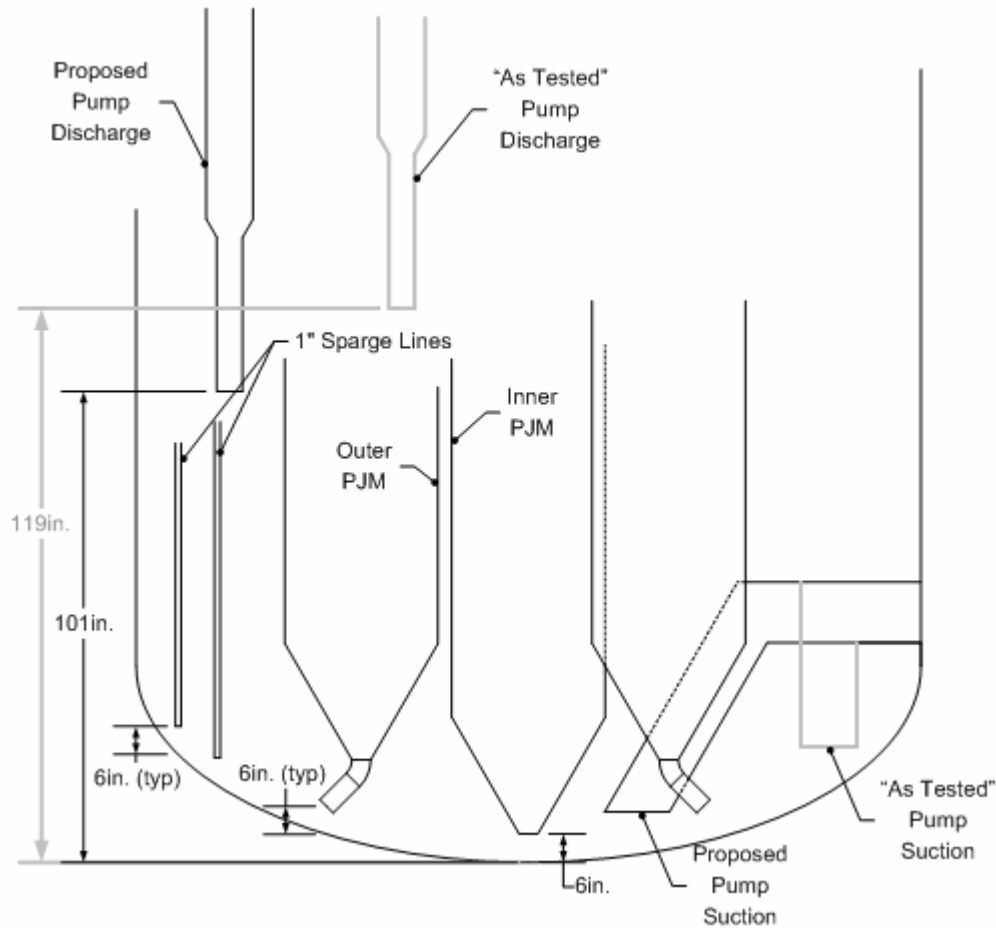
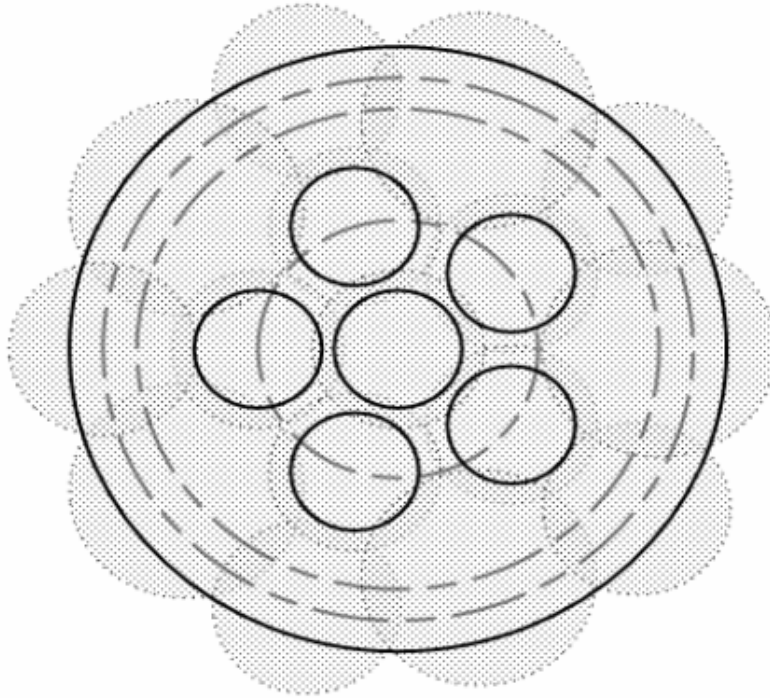


Figure 4.2. UFP-VSL-00002A/B Mixing System Layout – Elevation View

Normal operation (with leaching): When leaching is required, the liquid H/D is above 1.4, the pump is off, and the air sparge system must be used to provide mixing. Varieties of sparge tube layouts were considered for use. The configuration presented in this document was chosen by WTP Engineering to minimize impact with consideration to total air requirement and total number of sparge lines. The selected configuration is shown in Figure 4.3. Hatched circles overlaid in the plan view indicate the size of the ZOI of each particular sparge tube at the flow rates specified in the adjacent table.

The bubble size and resulting mixing zone is based on the air flow (in acfm) at the sparge line exit. The required flow rate measured in scfm is based on the level and density of the liquid in the vessel. The scfm values in Figure 4.3 are based on the overflow level in UFP-VS-00002A/B and a slurry specific gravity of 1.35.

Post-DBE/High Levels: The UFP vessel under post-DBE conditions, or H/D greater than 1.4, requires operation of PJMs and full sparging.



16 Sparge Tubes	# OF TUBES	2/3 ZOI (in.)	flow/tube (acfm)	subtotal (acfm)	Radial Position (in)	Nozzle Elevation (in)	Pressure Corr. Factor	subtotal (scfm)	UFP-VSL-00002A/B
	5	60	17	87	67	23	2.23	195	
	5	48	9	45	75	27	2.22	101	
	6	44	7	42	37	219	1.58	67	
Total Air Flow (scfm):								362	

Figure 4.3. Sparge Air Requirements and Resulting ZOIs – UFP-VSL-00002A/B

PJM Details: The central PJM has a downward-pointing 4-inch nozzle that is 1.5 nozzle diameters (6 inches) off the bottom of the vessel. The outer five PJMs are located on a pitch circle diameter (PCD) of 74 inches. All of their exit nozzles are pointed outward toward the vessel sidewall at 45 degrees; the nozzle openings are also 4 inches and are 6 inches off the bottom of the vessel. Elevation views of the pulse tubes are shown in Figures 4.2 and 4.4 with the outer pulse tube nozzle detail shown in Figure 4.5.

Sparge Line Details: The sparge lines are all 1 inch with the outer two PCD spargers, i.e., 134- and 150-inch PCD, all approximately 6 inches off the bottom of the vessel. Each of the spargers on a single PCD is spaced so that the angle between them is the same; e.g., for a PCD set of spargers equal to 5, the spargers are spaced every 72 degrees. None of the exit tube locations are near pulse tube nozzles or the recirculation pump intake. The spargers above the pulse tubes are approximately 2 inches above the top. Elevation views of the spargers are shown in Figures 4.2 and 4.4.

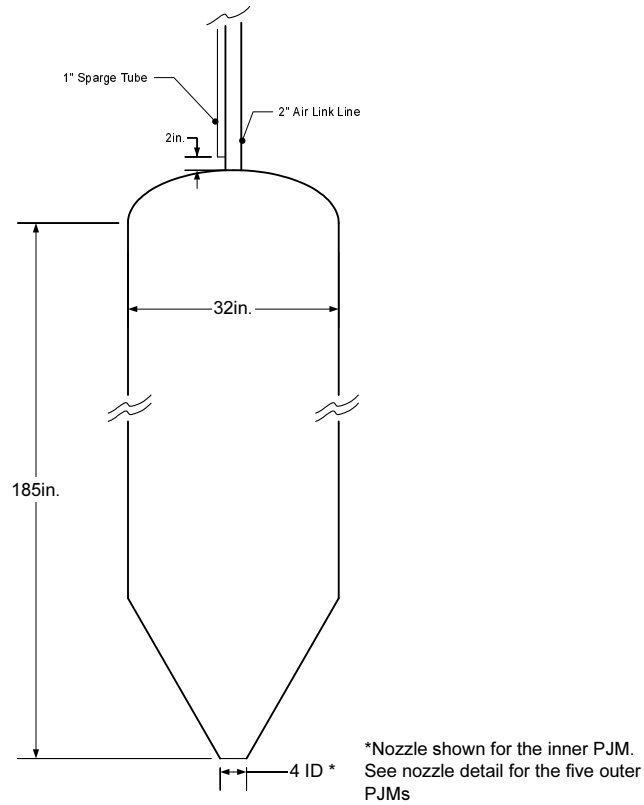


Figure 4.4. PJM Details – UFP-VSL-00002A/B

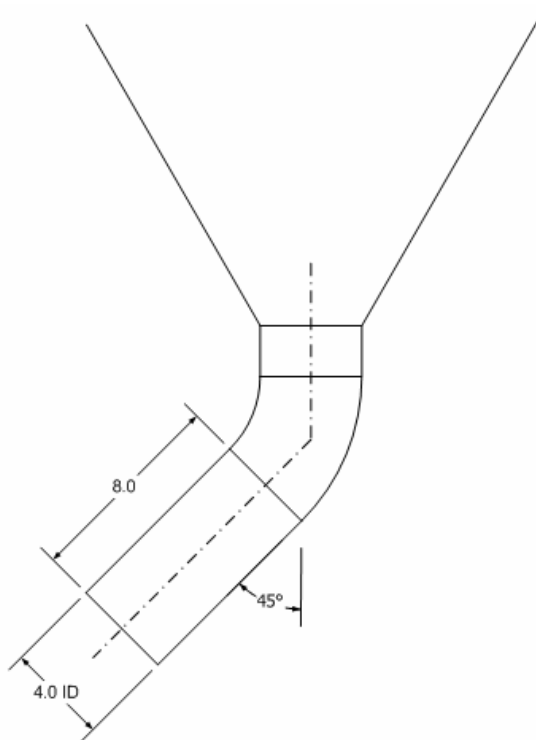


Figure 4.5. Outer PJM Nozzle Detail – UFP-VSL-00002A/B

4.1.1 HLW Lag Storage Vessel (HLP-VSL-00027A/B)

Normal Operation: The HLW LS vessel under normal operation will require eight PJMs and a 2200-gpm recirculation pump with one intake and two terminating nozzles configured to provide an exit velocity of 40 ft/sec to supply the required mixing. PJM nozzle velocities must be at least 12 m/s during the PJM drive cycle. Under normal operation the sparge tubes will be run in an 'idling' air flow-only mode, using 0.5–1.0 acfm (~2 scfm) of air per sparge point. Mixing with PJMs and recirculation jets has been tested up to an H/D of 0.74. The layout of PJMs, sparge lines, and recirculation lines is shown in Figures 4.6, 4.7, and 4.8.

Post-DBE/High Levels: The LS vessel under post-DBE conditions, or an H/D greater than 0.74 requires operation of PJMs and full sparging. Varieties of sparge tube layouts were considered for use. The configuration presented in this document was chosen by WTP engineering to minimize impact with consideration to total air requirement and total number of sparge lines. The selected configuration is shown in Figure 4.9. Hatched circles overlaid in the plan view indicate the size of the ZOI of each particular sparge tube at the flow rates specified in the adjacent table.

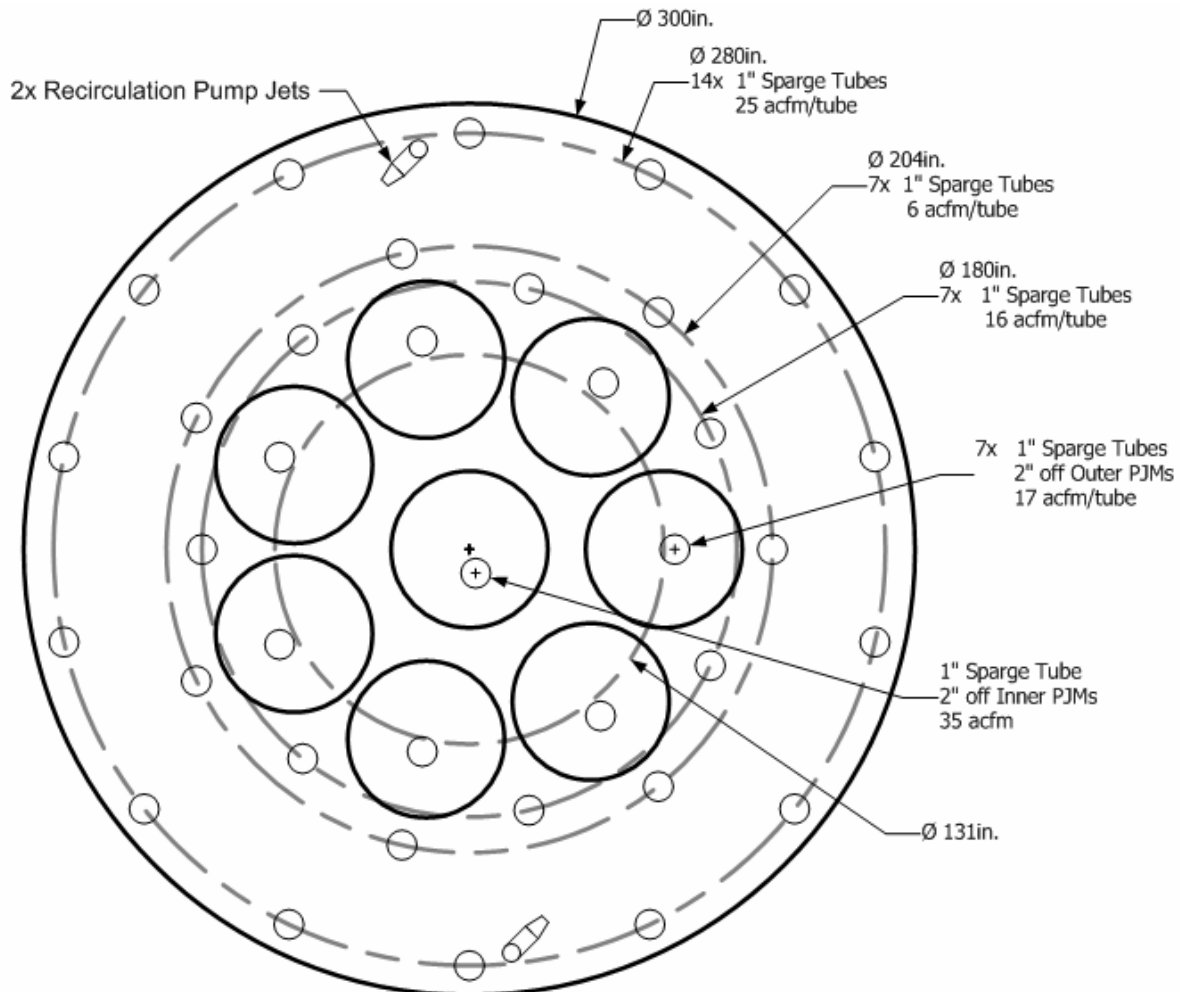


Figure 4.6. HLP-VSL-00027A/B Mixing System Layout – Plan View

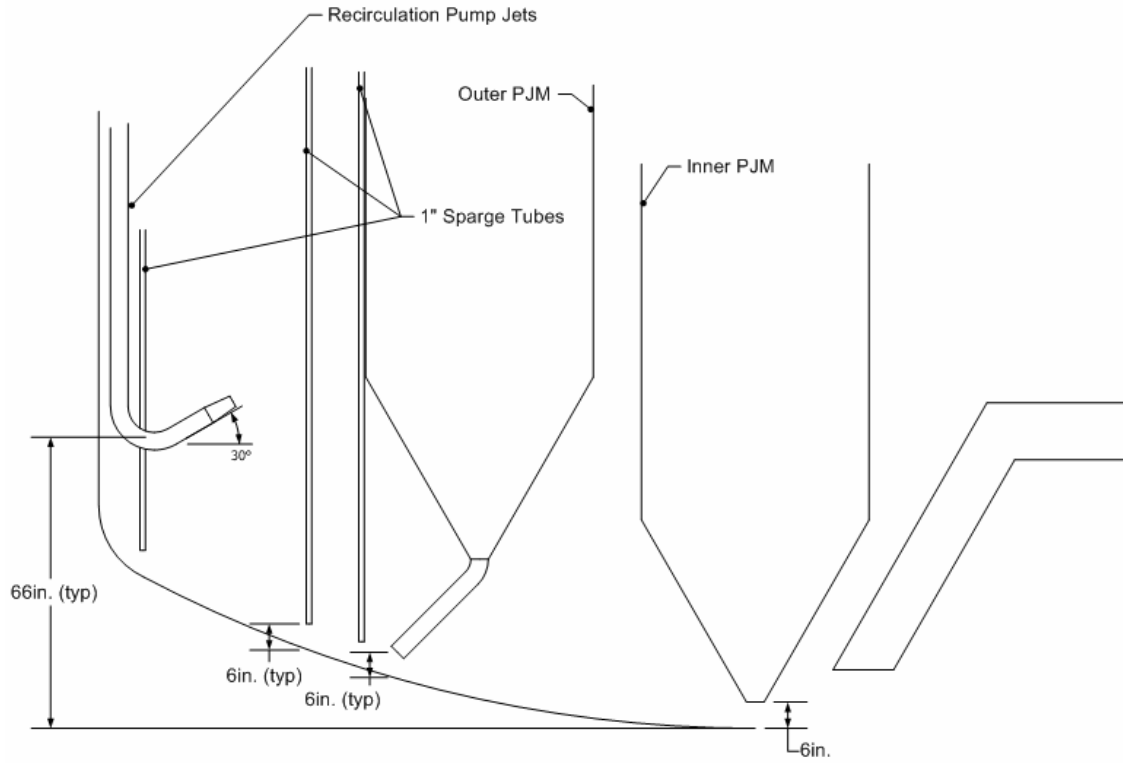


Figure 4.7. HLP-VSL-00027A/B Mixing System Layout – Elevation View

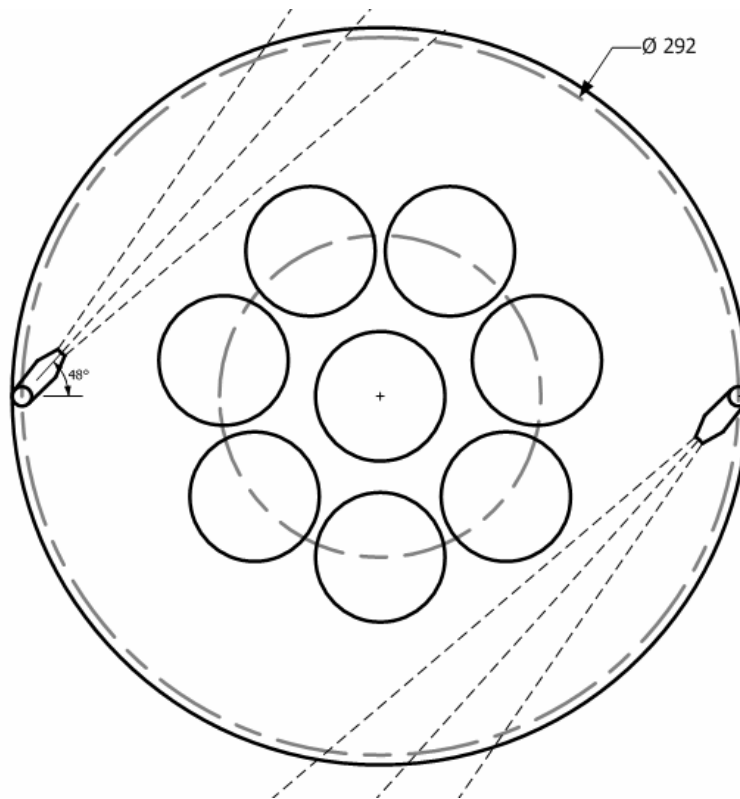
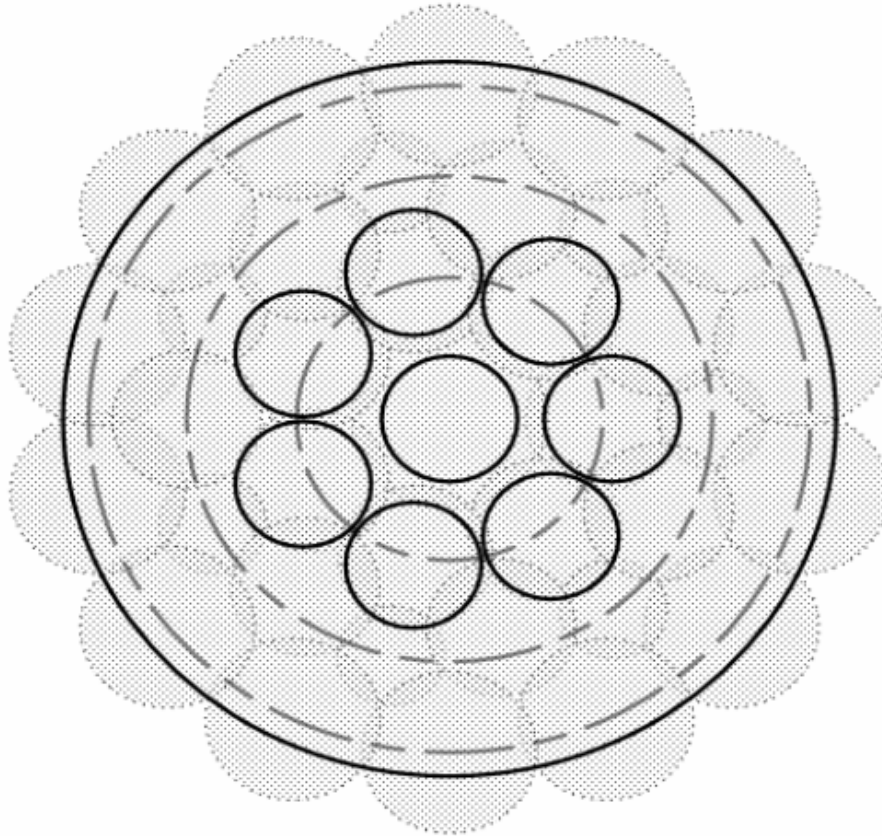


Figure 4.8. HLP-VSL-00027A/B, HLP-VSL-00028 Recirculation Jet Layout – Plan View



36 Sparge Tubes	# OF TUBES	2/3 ZOI (in.)	flow/tube (acfm)	subtotal (acfm)	Radial Position (in)	Nozzle Elevation (in)	Pressure Corr. Factor	subtotal (scfm)	HLP-VSL-00027A/B
	14	68	25	354	140	41	2.15	761	
	7	42	6	43	102	24	2.21	95	
	7	58	16	111	90	20	2.22	246	
	7	60	17	122	66	214	1.58	193	
1	76	35	35	66	214	1.58	55		
Total Air Flow (scfm):								1351	

Figure 4.9. Sparge Air Requirements and Resulting Zones of Influence – HLP-VSL-00027A/B

The bubble size and resulting mixing zone are based on the air flow in acfm at the sparge line exit. The required flow rate measured in scfm is based on the level and density of the liquid in the vessel. The scfm values in Figure 4.9 calculated based on the overflow level in HLP-VS-00027A/B and a slurry specific gravity of 1.35.

PJM Details: The central PJM has a downward-pointing, 4-inch nozzle that is 1.5 nozzle diameters (6 inches) off the bottom of the vessel. The outer seven PJM are located on a PCD of 131 inches. All of their exit nozzles are pointed outward toward the vessel sidewall at 45 degrees; the nozzle openings are also 4 inches and are 6 inches off the bottom of the vessel. Elevation views of the pulse tubes are shown in Figures 4.7 and 4.10; the outer pulse tube nozzle detail is shown in Figure 4.11.

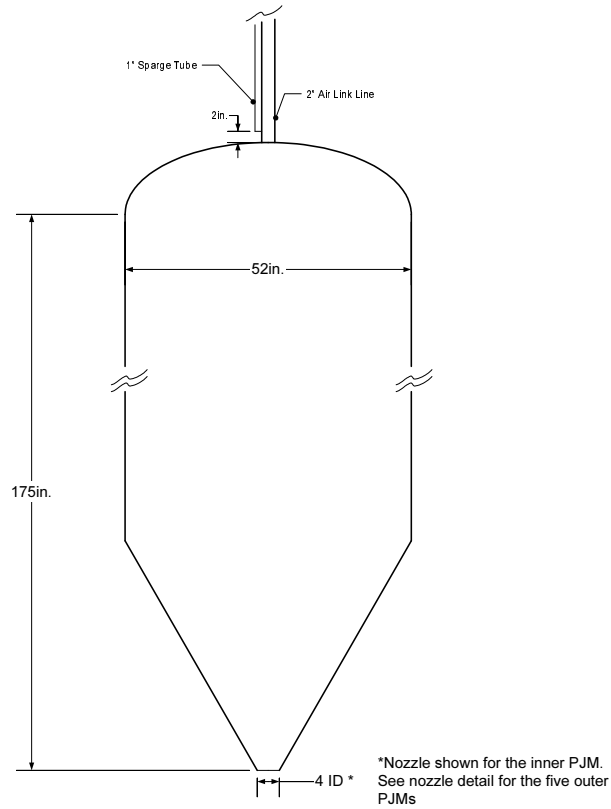


Figure 4.10. PJM Details – HLP-VSL-00027A/B, HLP-VSL-00028

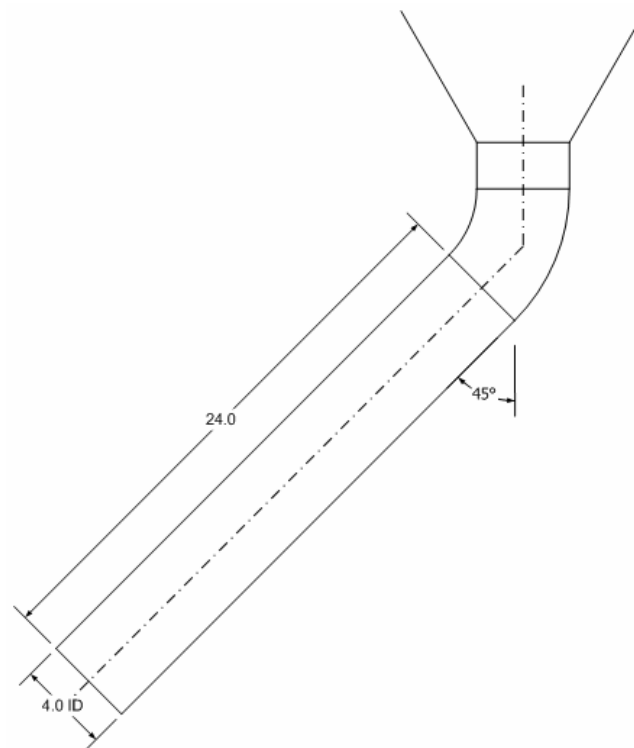


Figure 4.11. Outer PJM Nozzle Detail – HLP-VSL-00027A/B, HLP-VSL-00028

Sparge Details: The sparge tubes are all 1 inch; the outer three sets of PCD spargers, 180-, 204-, and 280-inch PCD, are approximately 6 inches off the bottom of the vessel. The spargers on a single PCD are spaced so the angle between them is the same; e.g., in a PCD set equal to 14 the spargers are spaced every 26 degrees. None of the exit tubes are near pulse tube nozzles or the recirculation pump intake. The spargers above the pulse tubes are approximately 2 inches above the top. Elevation views of the spargers are shown in Figures 4.7 and 4.10.

4.1.2 HLW Blend Vessel (HLP-VSL-00028)

Although a scaled prototypic test platform was not tested, the scaled testing in the LS prototypic platform can be applied to the blend vessel (BV) because the geometry and fluid properties are very similar.

Normal Operation: The HLW BV under normal operation will require eight PJMs and a 2200 gpm recirculation pump with one intake and two terminating nozzles configured to provide an exit velocity of 40 ft/sec to supply the required mixing. PJM nozzle velocities must be at least 12 m/sec during the PJM drive cycle. Under normal operation the sparge tubes will be run in an idling air flow-only mode, using 0.5-1.0 acfm (~2 scfm) of air per sparge point. Mixing with PJMs and recirculation jets has been tested up to an H/D of 0.74 in LS. This level scaled to the BV corresponds to an H/D of 0.70, which is more conservative than using the same H/D as in the LS, and is therefore recommended. The layout of PJMs, sparge lines and recirculation lines is shown in Figures 4.12, 4.7, and 4.8.

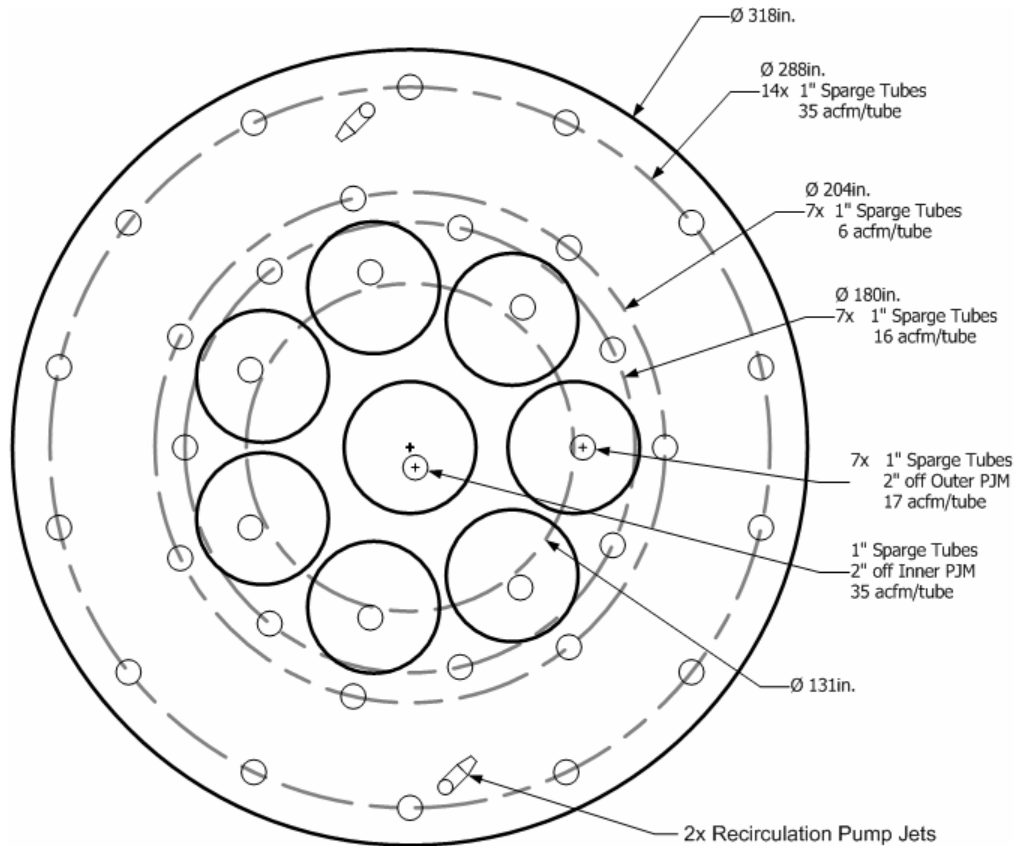
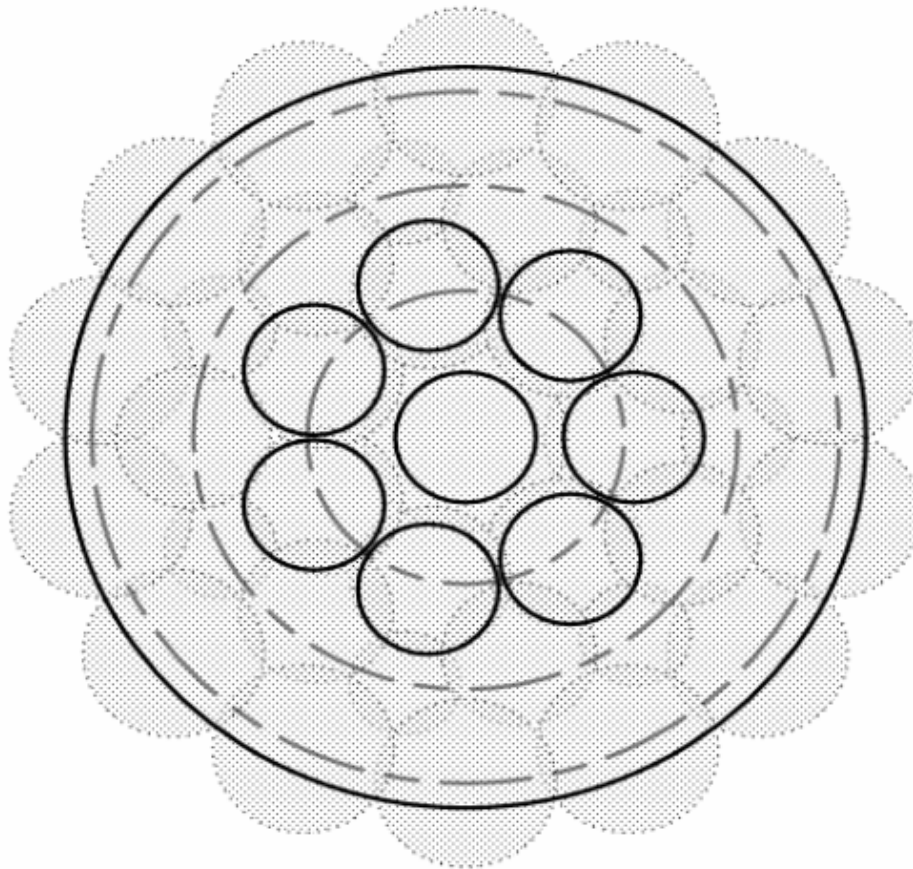


Figure 4.12. Specific Location of Spargers in the HLW BV Along with Air Flow Requirements

Post-DBE/High Levels: The BV under post-DBE conditions, or an H/D greater than 0.70, requires operation of PJMs and full sparging. Varieties of sparge tube layouts were considered for use. The configuration presented in this document was chosen by WTP engineering to minimize impact with consideration to total air requirement and total number of sparge lines. The selected configuration is shown in Figure 4.13. Hatched circles overlaid in the plan view indicate the size of the ZOI of each particular sparge tube at the flow rates specified in the adjacent table.

The bubble size and resulting mixing zone is based on the air flow in acfm at the sparge line exit. The required flow rate measured in scfm is based on the level and density of the liquid in the vessel. The scfm values in Figure 4.13 calculated based on the overflow level in HLP-VS-00028 and a slurry specific gravity of 1.35.



36 Sparge Tubes	# OF TUBES	2/3 ZOI (in.)	flow/tube (acfm)	subtotal (acfm)	Radial Position (in)	Nozzle Elevation (in)	Pressure Corr. Factor	subtotal (scfm)	HLP-VSL-00028
	14	76	35	491	144	40	2.14	1051	
	7	42	6	43	102	23	2.20	94	
	7	58	16	111	90	19	2.21	245	
	7	60	17	122	66	214	1.57	192	
1	76	35	35	66	214	1.57	55		
Total Air Flow (scfm):								1638	

Figure 4.13. Number and Location of Spargers in the HLW BV Along with Air Flow Requirements

PJM Details: The central PJM has a downward-pointing, 4-inch nozzle that is 1.5 nozzle diameters or 6 inches off the bottom of the vessel. The outer seven PJM are located on a PCD of 131 inches. All of the exit nozzles are pointed outward toward the vessel sidewall at 45 degrees; the nozzle openings are 4 inches in diameter and 6 inches off the bottom of the vessel. Elevation views of the pulse tubes are shown in Figures 4.7 and 4.10 with the outer pulse tube nozzle detail shown in Figure 4.11.

Sparge Details: The sparge tubes are all 1 inch with the outer three sets of PCD spargers, 180-, 204-, and 288-inch PCD, all approximately 6 inches off the bottom of the vessel. All of the spargers on a single PCD are spaced so that the angle between them is the same; e.g., for a PCD set of spargers equal to 14, the spargers are spaced every 26 degrees. None of the exit tube locations are near pulse tube nozzles or the recirculation pump intake. The spargers above the pulse tubes are approximately 2 inches above the top. Elevation views of the spargers are shown in Figures 4.7 and 4.10.

5.0 Gas Retention and Release in Selected Prototype Vessel Configurations

The GR&R activity is focused on developing an understanding of flammable gas (e.g., hydrogen) retention and release in pulse-jet mixed tanks containing non-Newtonian wastes. Testing to date includes bench-scale development activities and experiments in PJM vessels covering a range of configurations and scales, all using non-Newtonian waste simulant. Several tests have been conducted to assess the volume fraction of gas retained in simulant during continuous gas generation and steady state PJM operation (i.e., gas holdup tests), and the gas release characteristics (volume and rate) after the restart of mixing following a stoppage (i.e., gas release tests). The following summarizes kaolin: bentonite clay simulant gas holdup and gas release tests completed in the UFP and lag storage prototype vessels using near-final design configurations and operating conditions. The basis for scale-up of the GR&R results is not fully reviewed and could not be included in this document.

5.1 Principle and Approach

To assess gas holdup and gas release in PJM tanks, gas bubbles are generated in situ in the simulant. The gas bubble generation technique is based on the decomposition of hydrogen peroxide (H_2O_2) on catalytic surfaces according to the following reaction:



Once sufficient H_2O_2 has decomposed to supersaturate the simulant in O_2 , bubbles nucleate and existing bubbles grow. Further decomposition of H_2O_2 leads to additional bubble nucleation and/or bubble growth as O_2 diffuses through the simulant to the bubbles. Generated gas will be retained or released depending on many factors, including the degree of mixing in the system, the retained gas volume fraction, the size of bubbles, and simulant rheology.

In gas holdup tests, H_2O_2 solution is added continuously for a period of time while the PJM system is operated normally to establish a constant gas generation rate. At steady state, the rate of gas generation equals the gas release rate (e.g., from bubbles migrating to the surface), and the steady-state gas volume fraction is termed the gas holdup. In gas release tests, the mixing system is shut down after an amount of H_2O_2 solution is added to allow gas bubbles to be retained in the quiescent simulant. The release of gas upon restart of the mixing system is tracked to assess gas release volumes and rates.

The primary data obtained in gas holdup and gas release tests are on the simulant surface level as a function of time. Through independently established correlations, the level measurements are used to calculate retained gas volume and gas volume fractions. The gas volume fraction α referenced to the initial simulant volume is defined as

$$\alpha = \frac{V_{gas}}{V_o} = \frac{V_{gas}}{V_{sim} + V_{sol}} \quad (5.2)$$

where V_{gas} is the volume of retained gas (e.g., O_2 bubbles), and the total initial slurry volume V_o includes the bubble-free simulant volume V_{sim} and the volume of H_2O_2 solution V_{sol} . In many cases V_{sol} is negligible compared with the large volume of gas-free simulant. However, in gas holdup experiments where H_2O_2 solution is added continuously for an extended period of time, a correction is made for the added solution volume.

According to the expected reaction stoichiometry (shown in Equation 5.1), two moles of H_2O_2 decompose to produce 1 mole of O_2 and 2 moles of H_2O . Using this relationship, the nominal H_2O_2 solution concentration (30 wt%), and ideal gas law considerations, the equivalent volumetric rate of O_2 gas generation can be determined for a given rate of H_2O_2 decomposition. Assuming instantaneous H_2O_2 decomposition or a steady process where a steady-state concentration of H_2O_2 is established in the slurry, O_2 gas is generated at a rate equivalent to H_2O_2 introduction. The latter is assumed to occur in gas holdup experiments, and reported steady-state volumetric gas generation rates (at 22°C and 1 atm) are calculated from measured H_2O_2 injection rates. Normalizing the gas volume generation rate by the volume of simulant in the vessel gives the specific volumetric gas generation rate (volume of O_2 gas/volume of simulant/time).

5.2 Gas Holdup in Normal Operations

This section demonstrates that gas is released regularly and controllably in normal operation of the LS and UFP prototype systems, resulting in relatively low gas holdup. Figure 5.1 plots the measured gas volume fraction as a function of time during and after a gas holdup test in the LS scaled prototype (Sequence 15). At elapsed time 0, a hydrogen peroxide addition rate was established to provide an effective O_2 gas generation rate of 0.18 vol%/min (normalized to atmospheric pressure and 22°C). The specific gas generation rates used in the prototype experiments exceed the expected maximum actual

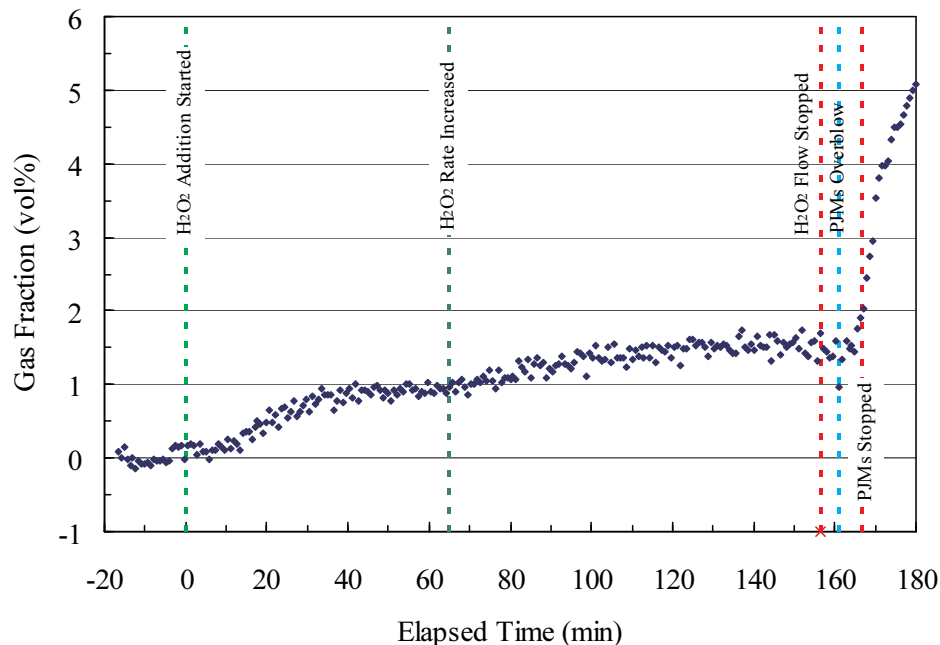


Figure 5.1. Gas Fraction as a Function of Time During and After a Gas Holdup Test in the APEL LS Prototype (Sequence 15). Events are marked on the plot by vertical lines.

waste gas generation rates (e.g., 2-4 vol%/day) by a factor of ~100 or more. Section 2.5 contains additional experimental details.

A steady-state gas fraction of ~0.9 vol% was attained after ~45 minutes. The rate of H₂O₂ addition was increased to an effective gas generation rate of 0.37 vol%/min after ~65 minutes, and a second steady-state gas holdup of 1.5 vol% was measured after ~125 minutes. The average gas holdup values in the last 10 minutes of H₂O₂ injection at each rate are tabulated in Table 5.1. The table also shows the standard deviation of the results (one value per pulse cycle, as shown in Figure 5.1).

As would be expected for a well-mixed system, the measured gas holdup in lag storage increased with increasing gas generation (H₂O₂ addition) rate.^(a) Figure 5.2 and Table 5.2 summarize the gas holdup experimental results for the two UFP prototype test sequences (5 and 6). A single relatively high equivalent gas generation rate was used in these tests (0.4 to 0.5 vol%/min).

Table 5.1. Summary of Gas Holdup in the LS Vessel (Sequence 15, 8-PJM cluster with 7 45° plus one vertical nozzles at ~12 m/s; 4-nozzle recirculation at ~120 gpm; 0.74 H/D; Bingham plastic rheology: 35-37 Pa yield stress, 26-27 cP consistency)

Experimental Gas Generation Rate (vol%/min)	Measured Gas Holdup±Standard Deviation (vol%)
0.18	0.93±0.06
0.37	1.5±0.1

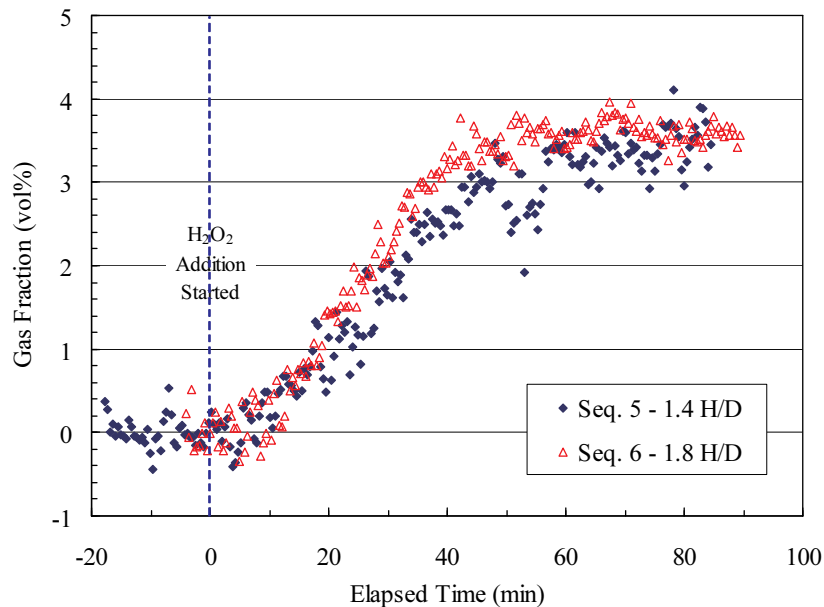


Figure 5.2. Gas Holdup Test Results in APEL UPF Prototype Using Two Sets of Operating Conditions: 1) Seq. 5, ~1.4 H/D, 4 PJMs + recirculation pump; and 2) Seq. 6, ~1.8 H/D, 4 PJMs + 1 sparger)

(a) Scaling arguments (not reported) suggest the holdup gas fraction should be proportional to the specific gas generation rate and the vessel scale factor (e.g., relative height for geometrically scaled vessels).

Table 5.2. Summary of Gas Holdup in UFP Vessel (Bingham plastic rheology: 33-36 Pa yield stress, 19-20 cP consistency)

Configuration	Experimental Gas Generation Rate (vol%/min)	Measured Gas Holdup±Standard Deviation (vol%)
Sequence 5: 1.4 H/D; 4 PJMs + recirculation pump at ~90 gpm	0.46	3.5±0.3
Sequence 6: 1.8 H/D; 4 PJMs + 1 sparge tube at ~3 cfm	0.41	3.6±0.1

5.3 Gas Release after Mixing System Restart

During a shutdown in which the air supply to PJMs and spargers is interrupted and recirculation pumps are idled, generated gas is expected to accumulate in the quiescent waste. In the extreme, all gas generated during the outage will be retained in the waste slurry. Upon restart of the mixing apparatus, accumulated gas is likely to be released. The release rate is dependent on many factors including waste rheology and mixing energy. Examples of gas release from gelled clay resulting from the restart of PJMs and spargers in the LS and UFP prototypes are provided below. In each of these tests the clay rheology exceeded the upper bounding Bingham plastic yield stress (>30 Pa). Based on preliminary matrix experiments conducted in the APEL 4PJM system, gas release rates may be faster as the simulant or waste slurry is thinned (lower rheological parameters).

Figure 5.3 shows the results of two gas release tests in the LS prototype. In the “overnight growth” test, H₂O₂ was introduced the day before the release began, and in the “30-min growth” test, the release experiment was started shortly after a preceding gas holdup test. The figure indicates relatively rapid initial gas release in both experiments. Nearly complete gas release was obtained after ~20 minutes (~27 pulses at 45 s/pulse cycle) in the overnight growth test with an initial gas volume fraction of ~4.5 vol%. Starting at a somewhat higher initial gas fraction (~5.8 vol%), gas was released to a retained gas volume fraction of ~1.8 vol% in 40 min in the “30-min growth” experiment, after which the gas fraction decreased slowly in time. In general, the characteristics of the initial gas release profiles (e.g., exponential decay) in the two experiments are similar. However, as noted above, the gas release rate decayed significantly in the “30-min growth” case before the retained gas was fully released.

Differences in gas release characteristics shown in Figure 5.3 are not fully explained at this point. Several contributing factors are under consideration: 1) differences in coincidental gas generation due to residual H₂O₂ decomposition; 2) differences in simulant rheological properties (e.g., strength) due to gel time, aging effects, and other factors (e.g., initial gas fraction); 3) differences in nominal bubble size, which may be a function of aging (bubble ripening), initial gas fraction, and rate of nucleation (a function of H₂O₂ concentration during bubble formation); 4) differences in initial gas fraction, which may make certain regions of the tank more difficult to mix due to buoyancy effects; 5) level sensors that do not measure tank level over the entire surface and therefore do not represent the total average gas fraction (note, however, that the sensor positions were not changed significantly between tests); and 6) other unaccounted differences in experimental variables such as sparger flow rate (e.g., no individual pressure gauges available on sparge tubes in the overnight growth test) and initial simulant depth (~5-cm lower in the overnight growth test).

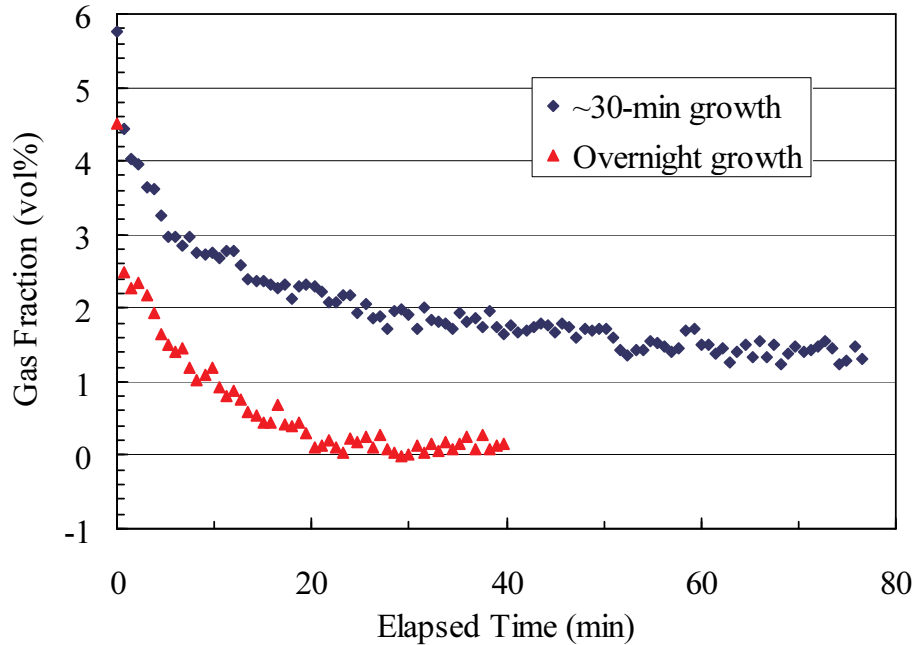


Figure 5.3. Gas Release from Gelled Clay in the APEL LS Prototype (Sequence 15, eight PJMs + four spargers).

After a near steady-state gas fraction (~ 1.4 vol%) was achieved in the “30-min. aging” test, the LS mixing system was stopped temporarily and restarted using eight (instead of four) sparge tubes at ~ 3 cfm each for ~ 10 min. These data are shown at long durations in Figure 5.4. The data indicate that retained gas volume fraction was reduced by ~ 1 vol% with the increased number of spargers.

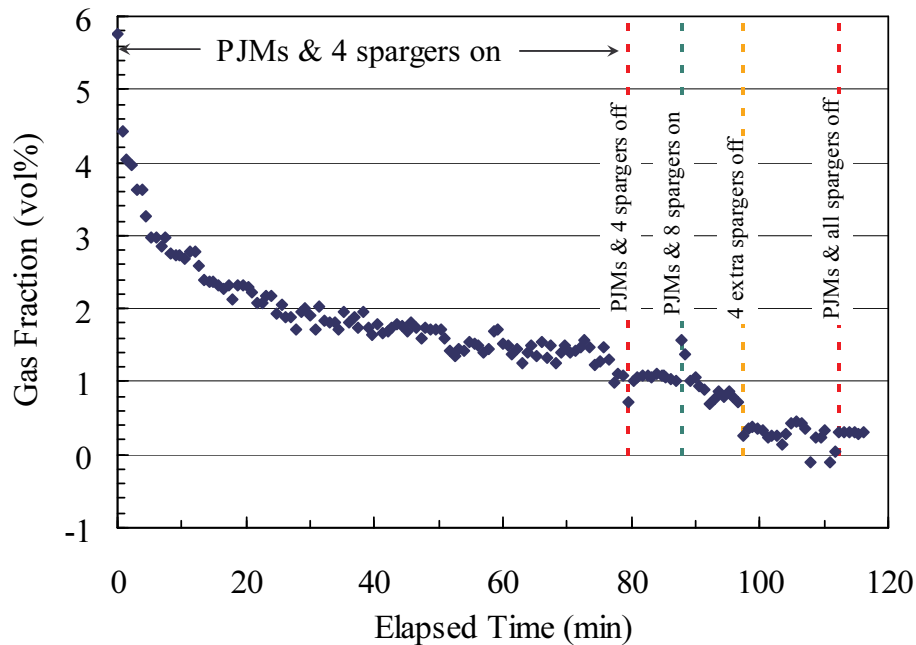


Figure 5.4. Gas Release from Gelled Clay in the APEL LS Prototype Showing Additional Gas Release Resulting from Operation of Eight Spargers (Sequence 15)

Gas release tests in the UFP prototypes were conducted with initial simulant loading to 1.4 and 1.8 H/D. The results are shown in Figures 5.5 and 5.6, respectively. The four-PJM tri-foil and single central sparge tube (~3 scfm) configuration was used in each test. As in the LS test, additional gas was released in some tests (e.g., Sequence 5, “~30-min. growth” shown in Figure 5.5) by using more spargers. However, Figures 5.5 and 5.6 only show the results for the specified baseline sparger operation (single sparge tube). At a given initial simulant loading (H/D value), the initial gas release profiles (i.e., change in gas fraction as a function of time) are consistent for the short and long growth cases. Differences at longer times, if any, may be due to factors identified above in the discussion of LS gas release tests.

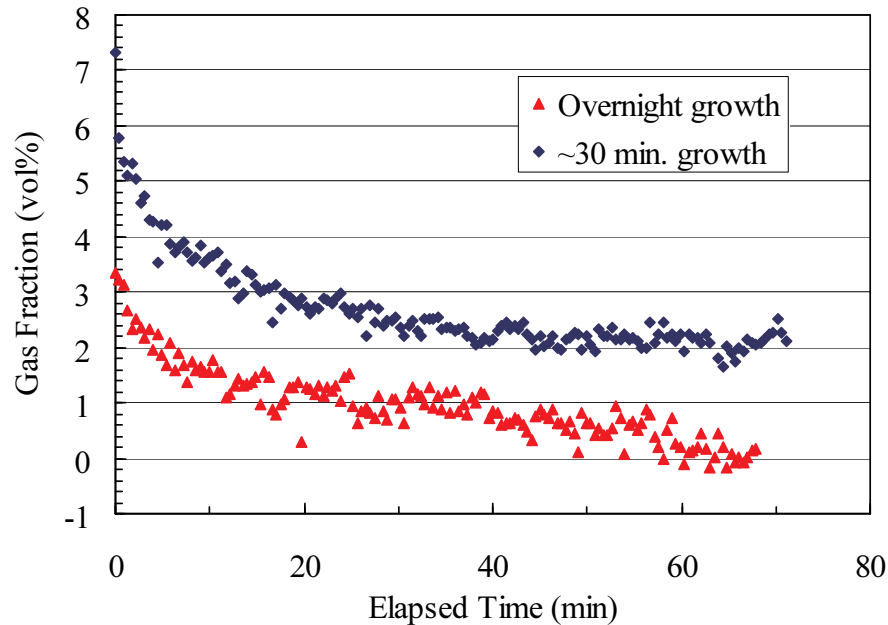


Figure 5.5. Gas Release from Gelled Clay at 1.4 H/D in the APEL UFP Prototype (Sequence 5)

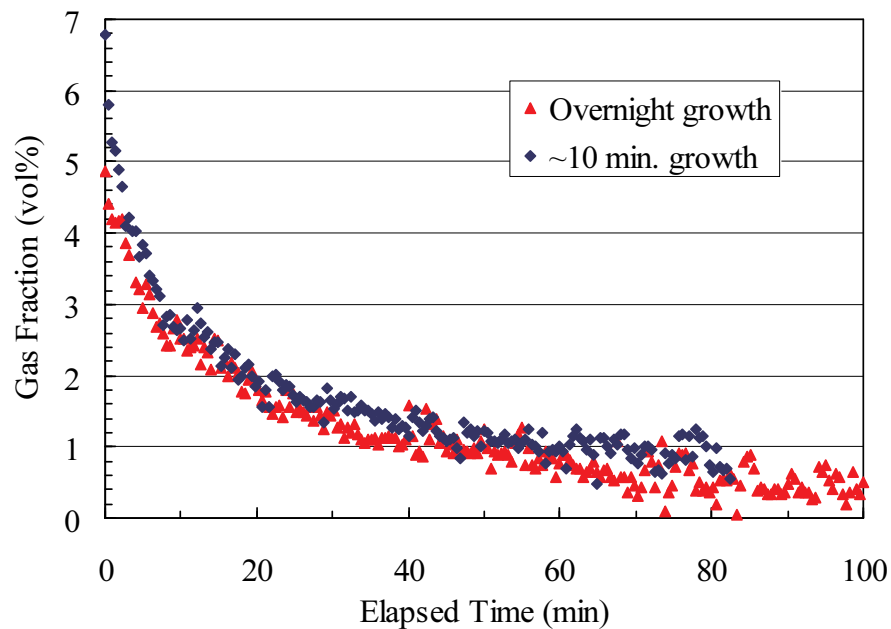


Figure 5.6. Gas Release from Gelled Clay at 1.8 H/D in the APEL UFP Prototype (Sequence 6)

6.0 References

- Atiemo-Obeng VA, P Armenante, and WR Penney. 2003. "Solid Liquid Mixing." *Handbook of Industrial Mixing*, Ch. 10, pp. 543–582. EL Paul, SM Kresta, and VA Atiemo-Obeng (eds). Wiley and Sons, New York.
- Bontha JR, JM Bates, CW Enderlin, and MG Dodson. 2003. *Large Tank Experimental Data for Validation of the Fluent CFD Model of Pulsed Jet Mixers*. PNWD-3303, Battelle – Pacific Northwest Division, Richland, WA.
- Brown DAR, PN Jones, and JC Middleton. 2003. "Experimental Methods." *Handbook of Industrial Mixing*, Ch. 4, pp. 145–201. EL Paul, SM Kresta, and VA Atiemo-Obeng (eds). Wiley and Sons, New York.
- CCN 065607, "Rheology Design Basis for non-Newtonian Treated Waste," November 17, 2003.
- CCN 069099, "R&T Response to Engineering Review of AZ-102 HLW Pretreated Sludge Rheological Data and Rheological Recommendation for Consideration," October 17, 2003.
- CCN 082255, "High-Level Waste Rheology in the Waste Treatment Plant," February 17, 2004.
- Poloski A. 2004. *Technical Basis for HLW Vitrification Stream Physical and Rheological Property Bounding Conditions*. WTP-RPT-100 Rev. 0, Battelle – Pacific Northwest Division, Richland, WA.
- Speers RA, KR Holme, MA Tung, and WT Williamson. 1987. "Drilling fluid shear stress overshoot behavior." *Rheologica Acta*, Vol. 26, pp. 447-452.
- Zwietering TN. 1958. "Suspending of Solid Particles in Liquids." *Chem. Eng. Sci.*, Vol. 8, p. 244.

Appendix A

Technical Basis for Scaled Testing of WTP Mixing Vessels with Non-Newtonian Slurries

Appendix A

Technical Basis for Scaled Testing of WTP Mixing Vessels with Non-Newtonian Slurries

A.1 Introduction

Small-scale testing is a common approach used successfully in the many varied fields of applied fluid dynamics. The success of the approach depends greatly on the fact that system performance depends on certain non-dimensional groupings of physical parameters. If these parameter groupings can be preserved at different geometric scales (i.e., large and small), the essential behavior of the system will be the same at both scales. This principle is referred to as *similarity* in the theory of fluid dynamics engineering. Limitations of scaled testing are attributed to the inability to match important non-dimensional parameter groupings at both scales. In complex fluid dynamic problems, there can be many non-dimensional parameter groups; however, often the essential behavior of the phenomenon is dominated by only a few key groups. In this situation small-scale testing can produce results that are very close to large-scale behavior.

This appendix presents the approach used to establish the scalability of the scaled prototypic mixing tests. Section A.2 gives a brief introduction to the basics of pulse jet mixer (PJM) operation. Section A.3 gives a summary of the important properties and parameters involved in PJM mixing of non-Newtonian materials. Section A.4 explains the geometric scaling approach and how velocities and time are scaled. Section A.5 discusses the important non-dimensional parameters which, ideally, are to be preserved during scaled testing. Finally, Section A.6 summarizes the basis for scaled-testing.

A.2 Principles of PJM Operation

A schematic of a typical PJM system in a vessel is shown in Figure A.1. The tank has diameter D_T , volume V_T , and an operating level H . There are N PJMs in the tank, each with diameter D_{PT} and volume V_{PT} . Each PJM has a conical nozzle with diameter d_0 . For the baseline design, the total volume of the pulse tubes $N V_{PT}$ is approximately 10% the operating volume of the vessel.

There are three phases to the operation of the PJM. During the drive phase, the tube is pressurized and a volume of slurry is discharged. The level change in the tube during discharge is ΔL . The corresponding increase in waste level is ΔH where

$$\Delta H = N\Delta L \left(\frac{D_{PT}^2}{D_T^2 - ND_{PT}^2} \right) \quad (\text{partially submerged PJMs}) \quad (\text{A.1})$$

or

$$\Delta H = N\Delta L \frac{D_{PT}^2}{D_T^2} \quad (\text{fully submerged PJMs}) \quad (\text{A.2})$$

Typical values of ΔH are about 10% of the operating level H . The average velocity u_0 discharged during the drive phase is given by

$$u_0 = \frac{D_{PT}^2 \Delta L}{d_0^2 t_D} \quad (A.3)$$

where t_D is the drive time.

The drive pressure, p_D , required to produce the discharge velocity is given by

$$p_D = p_e + \frac{C_L}{2} \rho u_0^2 \quad (A.4)$$

where p_e is the pressure head at the exit of the nozzle, C_L is the nozzle loss coefficient, and ρ is the slurry density. The other two phases of PJM operation are the vent phase and suction phase.

Immediately after the drive phase, a vent is opened and excess pressure is allowed to vent to the atmosphere. During the suction phase, vacuum is applied to the pulse tube. The tube fills due to a combination of the applied vacuum and the difference in hydrostatic head between the waste level and the level in the tube. The vent time and suction time are given by t_V and t_S , respectively. The total cycle time for PJM operation is given by

$$t_C = t_D + t_V + t_S \quad (A.5)$$

It is important to emphasize that the average drive velocity given by Eq. (3) is both spatially and temporally averaged. Spatially, the velocity will vary over the cross section of the nozzle. Temporally, the velocity varies due to inertial effects. When the drive phase is over, some fluid continues to discharge due to the inertia of the moving column of fluid. These inertial effects are dependent on the physical size of the system. The actual velocity varies somewhat over the operating cycle, as shown in Figure A.2.

For comparing PJM operation at different scales, various average velocities can be considered. One is the area-averaged velocity, given by

$$\bar{u}_{\text{area}} = \frac{1}{t_P - t_m} \int_{t_m}^{t_D} u \, dt \quad (A.6)$$

Another is the true average velocity given by

$$\bar{u}_{\text{disch}} = \frac{D_{PT}^2 \Delta L_A}{d_0^2 t_{DA}} \quad (A.7)$$

where ΔL_A and t_{DA} are the actual measured level change and drive times in the pulse tube. Generally, Equation (A.6) will produce higher velocities than Equation (A.7).

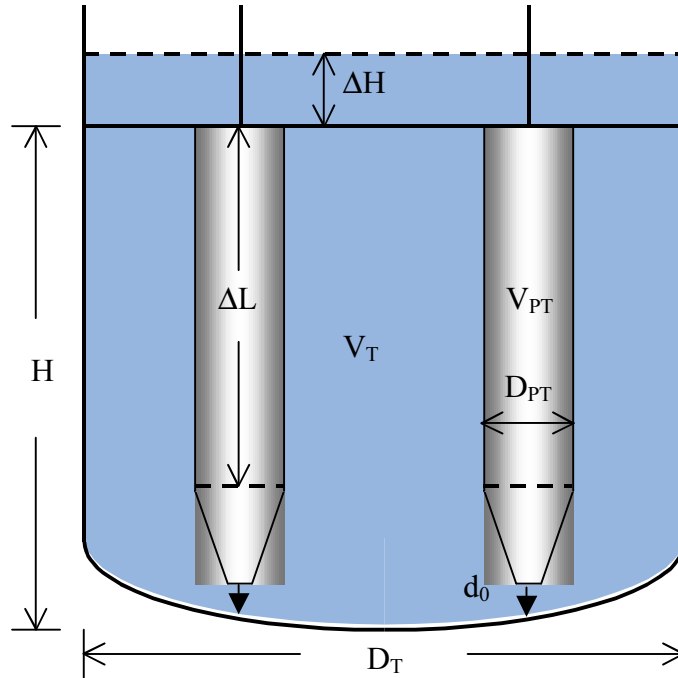


Figure A.1. Illustration of a Typical PJM System in a Waste Treatment Plant Vessel

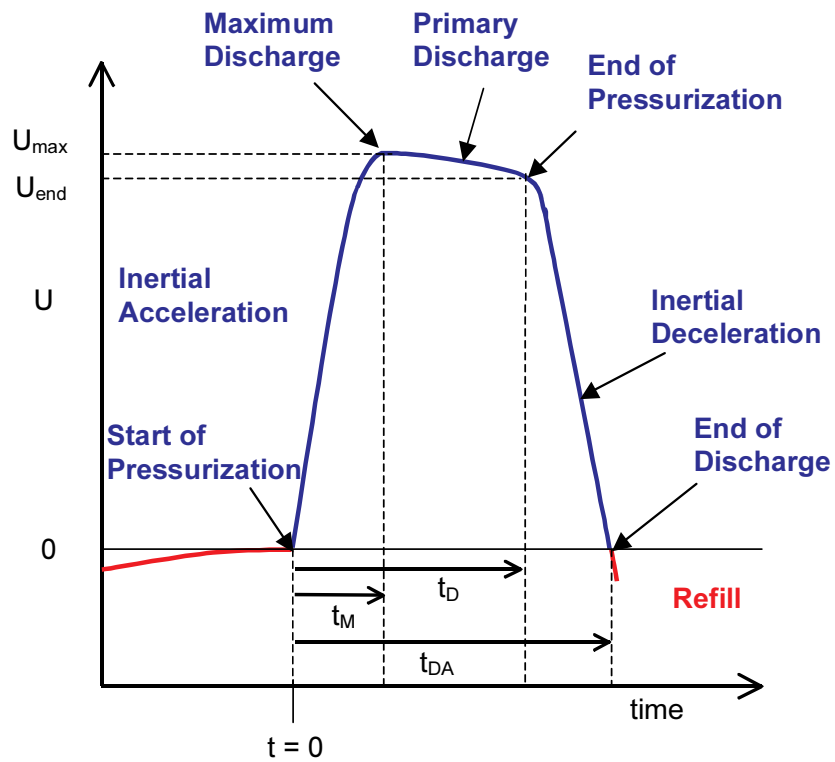


Figure A.2. Illustration of Temporal Variation of Velocity During PJM Operation

A.3 Important Properties, Parameters, and Non-Dimensional Groups

The following is a list of pertinent waste properties and system parameters to be used in forming non-dimensional parameter groups:

- Waste properties
 - ρ slurry density (kg/m^3) (assumes well-mixed slurry with no settling)
 - τ_s slurry shear strength (Pa)
 - τ_0 laminar flow yield stress (Pa) (from Bingham plastic fit of waste rheogram)
 - K laminar flow consistency (mPa-s) (assumed to be effective Newtonian viscosity (μ) in turbulent region)
 - t_{rel} slurry relaxation time (s) (characteristic response time of gelled slurry to an impulse)

- Physical parameters
 - u_0 nominal PJM jet velocity (m/s) (may be replaced with an averaged velocity)
 - d_0 PJM nozzle diameter (m)
 - t_D PJM nominal drive time (s) (or actual drive time)
 - t_c cycle time (s)
 - H waste fill level (m)
 - V vessel volume (m^3)
 - V_{PT} pulse tube volume (m^3)
 - p average hydrostatic pressure $\rho g H / 2$ (Pa)
 - Q_0 PJM flow rate (per pulse) $(\pi / 4) u_0 d_0^2$ (m^3/s)
 - P_0 PJM hydraulic power (per pulse) $(\pi / 8) \rho u_0^3 d_0^2$ (W)

The relevant non-dimensional parameter groups for the physical system are as follows:

Yield Reynolds number:
$$\text{Re}_\tau = \frac{\rho u_0^2}{\tau_s}$$

This is the ratio of dynamic stress to slurry strength which directly affects size of the mixing cavern. It is considered a dominant non-dimensional parameter.

Jet Reynolds number:
$$\text{Re}_0 = \frac{\rho u_0 d_0}{\mu}$$

This is the ratio of dynamic stress to viscous stress. It affects the degree of turbulence in the mixed region as well as weakly affecting stresses at the cavern and boundary layers. It is considered a secondary non-dimensional parameter.

Non-Newtonian stress ratio: $N_{\tau} = \frac{\tau_s}{\tau_0}$

This is the ratio of shear strength to Bingham yield stress. It may affect boundary layer structure and possibly the friction coefficient at the cavern boundary. The importance of this parameter is considered low.

Strouhal number: $S_0 = \frac{t_D u_0}{d_0}$

This is the ratio of pulse time to flow time scale. It affects the degree to which flow approaches steady jet behavior and is considered a primary non-dimensional parameter. In the limit of steady jet flows, the Strouhal Number become infinite, and the effects of pulsation are no longer present. For small Strouhal number, the mixing behavior will be highly dominated by pulsation effects.

Deborah number: $D_0 = \frac{t_D}{T_s}$

This is the ratio of pulse time to material response time. It affects how well non-steady flow at cavern mobilizes gelled slurry and is considered a secondary non-dimensional parameter.

Pressure ratio: $\frac{p_a}{\rho g H}$

This is the ratio of ambient pressure to static head. It affects the scaling of gravity refill of a PJM but should not affect the discharge flow.

Densimetric Froude number: $F_0 = \frac{\rho u_0^2}{\Delta \rho g H}$

This is the ratio of the potential energy to kinetic energy of flow. It requires density stratification and affects the ability of a jet to transport material upward. The importance of this parameter is considered low due to minimal solids settling in the turbulent region.

A.4 Geometric Scaling Approach

The non-Newtonian test program uses geometric scaling. We define the geometric scale factor s as

$$s = \frac{L_L}{L_S} \quad (\text{A.8})$$

where L_L is any characteristic linear dimension of the large-scale system (such as tank diameter, nozzle diameter, waste level, etc.). At small scale, every linear dimension, L_S , is reduced or *scaled* by s

(i.e., $d_{0s} = d_{0L} / s$, $D_{Ts} = D_{TL} / s$, $H_s = H_L / s$). Hence the ideal small-scale test is an exact geometric miniature of the large system, with all areas scaled according to

$$A_s = \frac{1}{s^2} A_L \quad (\text{A.9})$$

and all volumes scaled according to

$$V_s = \frac{1}{s^3} V_L \quad (\text{A.10})$$

Typically in scaled fluid mixing tests, scale factors up to about 10 are considered acceptable, that is, much of the important physics can be captured at small scale. For the non-Newtonian test program, conservative scale factors in the range of 4 to 5 were selected due to the relatively new nature of the tests and the importance of the outcome.

When testing at small scale, one must determine how to scale velocity (i.e., PJM drive velocity u_0). One choice is to scale velocity by the scale factor. This is problematic, however, because it tends to reduce the Reynolds number by $1/s^2$ and introduce further difficulties with the scaling of time. A better choice is to keep jet velocity constant at both scales:

$$u_{0s} = u_{0L} \quad (\text{A.11})$$

With geometric scaling and constant velocity scaling, nozzle flow rates per pulse scale according to

$$Q_{0s} = Q_{0L} / s^2 \quad (\text{A.12})$$

Jet hydraulic power also scales similarly. However, power per unit volume scales according to

$$\left. \frac{P_0}{V} \right)_S = s \left. \frac{P_0}{V} \right)_L \quad (\text{A.13})$$

For steady jet mixing, time does not come into play. However, PJM operation is a periodic process. Therefore, the scaling of time must be addressed.

If velocity is held constant and the geometry is scaled, then it follows that all imposed time scales must be reduced at small scale. Similarly, to keep the jet discharge velocity the same while scaling pulse volume geometrically, the pulse time will be reduced by the scale factor according to

$$t_{Ds} = \frac{1}{s} t_{DL} \quad (\text{A.14})$$

Hence the PJM drive time (as well as refill time and cycle time) are all reduced by s at small scale.

A.5 Scaling Non-Dimensional Parameters

In general, for a given non-Newtonian PJM mixing test, the non-dimensional cavern position should depend on all of the non-dimension parameter groups:

$$\frac{H_C}{D_T} = f(\text{Re}_\tau, \text{Re}_0, N_\tau, S_0, D_0, F_0) \quad (\text{A.15})$$

Similarly, non-dimensional mixing time (time to steady cavern formation, time to break through, or time to full mobilization) should depend on the same parameters:

$$\frac{t_M}{t_D} = g(\text{Re}_\tau, \text{Re}_0, N_\tau, S_0, D_0, F_0) \quad (\text{A.16})$$

The ideal small-scale test is one where the measured non-dimensional cavern height and mixing time are the same as those at full scale. Hence, the extent to which the non-dimensional parameters scale will determine the success of the small scale test approach.

To this end, we consider how each of the non-dimensional parameters scale with the geometric scale factor s :

Yield Reynolds Number: $\text{Re}_{\tau_S} = \text{Re}_{\tau_L}$

The yield Reynolds number will be the same at both scales so long as the simulant used has the same shear strength τ_s :

Jet Reynolds Number: $\text{Re}_{0_S} = \frac{1}{s} \text{Re}_{0_L}$

The Reynolds number at small scale is reduced by the geometric scale factor. This should introduce only minor differences in test results since the Reynolds numbers in both tests are quite large. Whether the reduction in Reynolds number produces conservative results (i.e., lower caverns) at small scale is not clear due to the competing effects of Reynolds number on jet structure and friction coefficients. The potential need for a minor Reynolds number correction to small-scale results should be evident from the scaling tests. If necessary, the Reynolds number can be matched at small scale by reducing the consistency or viscosity by the factor $1/s$.

Non-Newtonian stress ratio: $N_{\tau_S} = N_{\tau_L}$

The non-Newtonian stress ratio will be the same at both scales if the same simulant is used.

Strouhal number: $S_{0_S} = S_{0_L}$

The Strouhal number will be the same at both scales.

Deborah number:
$$D_{0S} = \frac{1}{s} D_{0L}$$

The Deborah number will be smaller in the small-scale tests. If the Deborah number is large overall, the effect will be negligible. If Deborah is close to unity, then the small-scale results will be conservative.

Densimetric Froude number:
$$F_{0S} = sF_{0L}$$

The densimetric Froude number will be larger at small scale. This would produce non-conservative results at small scale should the effect be important. So long as simulants with very slow particle settling are used, this effect should be negligible.

A.6 Summary of Scaled Test Approach

By way of summary, the primary non-dimensional parameters required for small-scale testing are the yield Reynolds number Re_{τ} , and the Strouhal number S_0 . If these are matched at large and small scale, then we expect, to first order, non-dimensional cavern heights and mixing times to be the same:

$$\left. \frac{H_C}{D_T} \right)_S \approx \left. \frac{H_C}{D_T} \right)_L \quad (\text{A.17})$$

and

$$\left. \frac{t_M}{t_D} \right)_S \approx \left. \frac{t_M}{t_D} \right)_L \quad (\text{A.18})$$

Given that full-scale cavern heights are adequately predicted by reduced-scale testing, it follows that specification of PJM operation parameters sufficient to achieve complete mixing (no stagnant regions) at reduced scale will produce designs that also provide complete mixing at full-scale. Further, testing at reduced scale will provide a degree of conservatism so long as the consistency, k , of the simulant is the same as the full-scale bounding value. This is true since the jet Reynolds number will be smaller in the scaled-test than in the full-scale system:

$$Re_{0S} = \frac{1}{s} Re_{0L} \quad (\text{A.19})$$

If adequate mixing is achieved in a reduced-scale test, then it can be expected that the degree of turbulence will be greater in the full-scale vessel due the associated effect of increased jet Reynolds number.

Appendix B

Dye Method

Appendix B

Dye Method

The concentration of dye [in this case Food Dye Color No. 1, (Brilliant Blue FCF) (BB FCF)] in an aqueous sample was determined through the correlation shown in Figure B.1. This correlation follows Beer's law, which says that the dye concentration is proportional to the optical absorbance value of the dye at the mode wavelength. The mode wavelength for BB FCF is approximately 633 nm. The results are only valid over a certain region of dye concentration. From visual inspection of Figure B.1, the linear region is present up to an absorbance value of 1.5 (~9 ppm FCD1). When the dye concentration is above this level the sample must be diluted with water and remeasured. The original dye concentration can be calculated by knowing the quantity of water used for the dilution.

Beer's Law Chart of Brilliant Blue (FD&C Blue 1) in Water

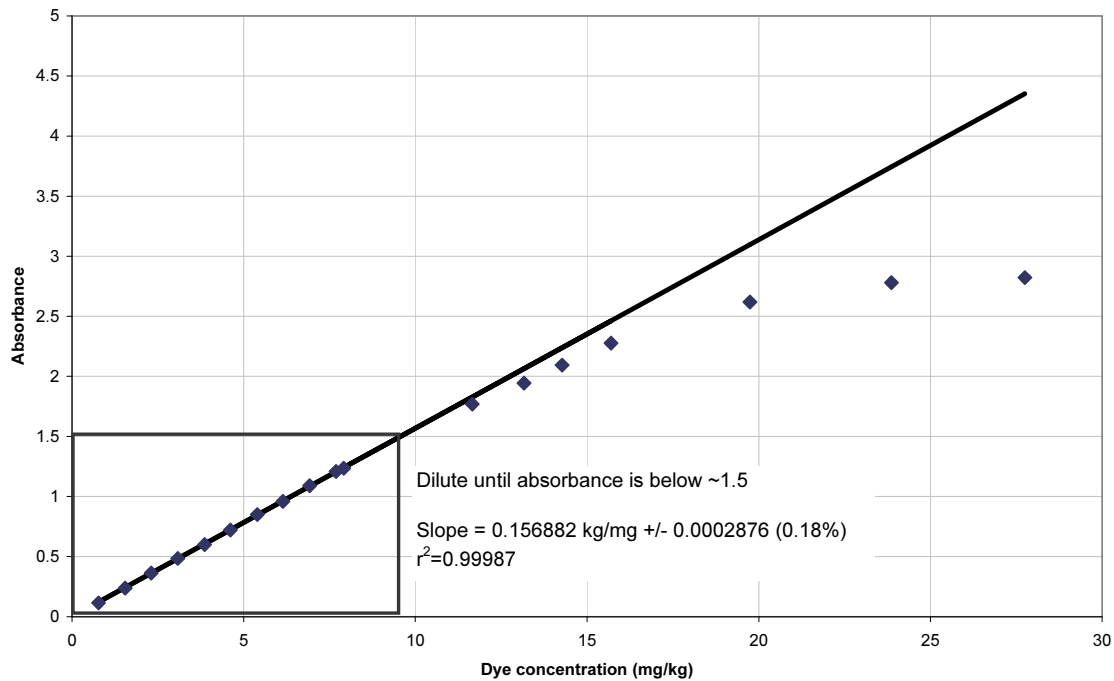


Figure B.1. Beer's Law Correlation of Optical Absorbance to BB FCF Dye Concentration in Water

Absorption of dye onto the surface of the clay particles can be estimated through a linear approximation. This correlation is shown in Figure B.2, where the dye concentration in the liquid phase is plotted against the dye concentration in the solid phase. Due to batch to batch variations of the clay composition, small differences in the amount of dye absorbed were measured from sample to sample. The linear isotherm assumption allows for the use of Equation B.1 to calculate percent mixed in a PJM test.

$$X_j = \frac{A_f - A_0}{A_j - A_0} \quad (\text{B.1})$$

where

X_j	is the fraction mixed of the j-th tank sample
A_f	is the optical absorbance of the final homogenized simulant
A_0	is the optical absorbance of the initial baseline simulant
A_j	is the optical absorbance of the j-th tank sample

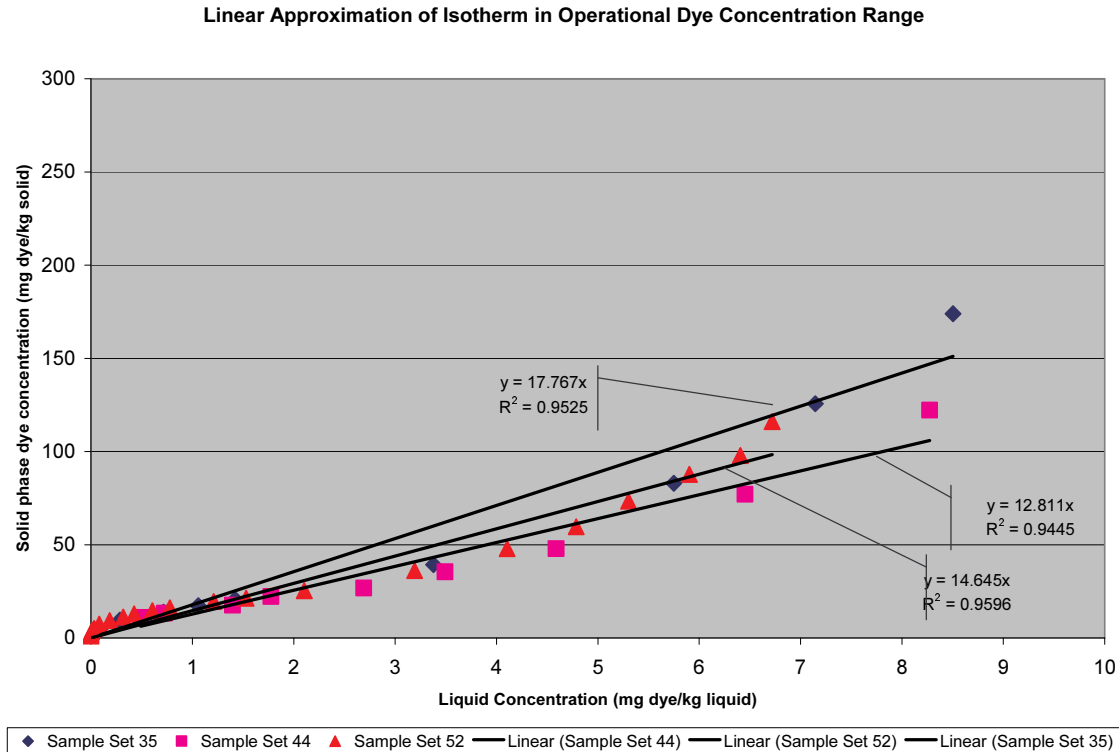


Figure B.2. Linear Fit of Isotherm Data over the Linear Beer's Law Region

A polynomial fit to one of the isotherm data sets is shown in Figure B.3. Use of this fit allows for an estimation of the error incurred through the assumption of a linear isotherm. This error is estimated by calculating the difference in the percent mixed between Equations B.1 and B.2. To perform this calculation the correlation shown in Figure B.3 is used to calculate the K_d values of each sample in the calculation. A conservative estimation of the solids loading in each sample is assumed at 30 wt% solids 70 wt% liquid.

$$X_j = \frac{Y_l (A_f - A_0) + Y_s (K_{df} A_f - K_{do} A_0)}{Y_l (A_j - A_0) + Y_s (K_{dj} A_j - K_{do} A_0)} \quad (\text{B.2})$$

where

K_{df}	is the distribution coefficient at the homogenized tank tracer concentration
K_{do}	is the distribution coefficient at the initial baseline tracer concentration
K_{dj}	is the distribution coefficient at the j-th tank sample tracer concentration

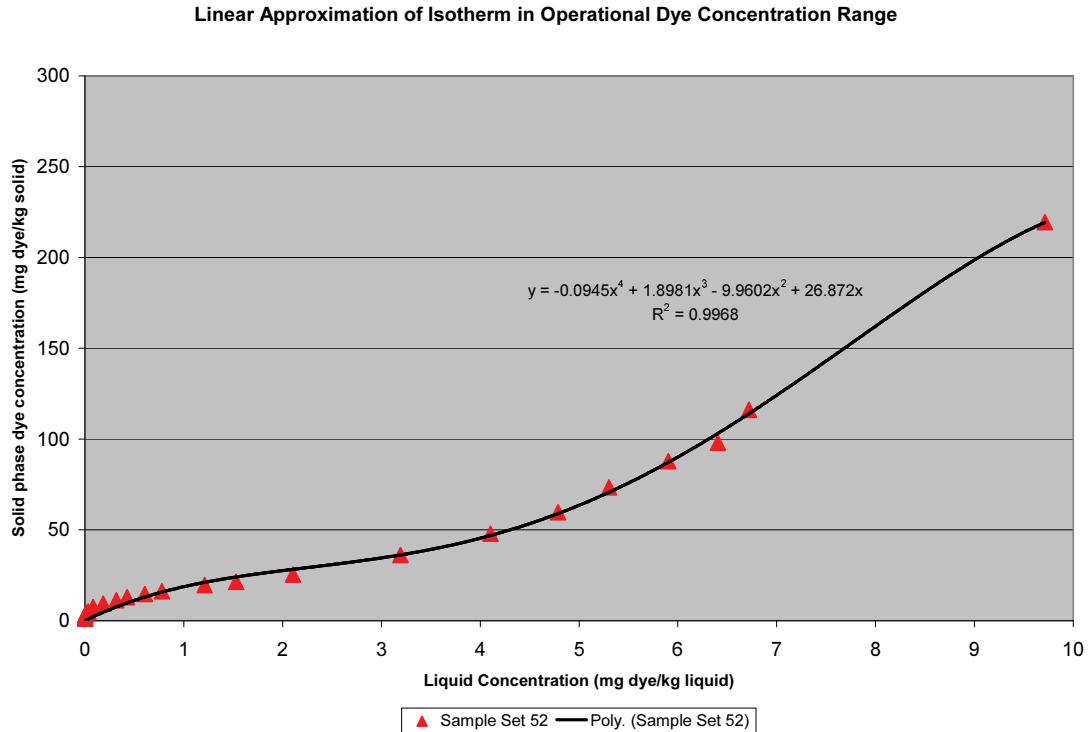


Figure B.3. Polynomial Fit of Isotherm Data over the Linear Beer’s Law Region

During prototype testing, Equation B.1 was used to calculate a fraction mixed for each sample at each sample location. These samples were drawn from different locations in the testing vessel. Sample locations 1, 2, and 3 are from separate pulse tubes and represent the composition of the mixing cavern (see Section 1.4.6). Locations 4 and 5 were located near the tank wall at low and high elevations, respectively. During the first run of a test sequence, samples from locations 1, 4, and 5 were taken approximately every 10 minutes after completion of dye injection. After 50 minutes of operation, samples were drawn from all sample locations and the next run experimental condition was employed. During subsequent run conditions, samples from locations 1, 4, and 5 were taken every 15 minutes. After 45-90 minutes of operation, samples were drawn from all sample locations and the next run experimental condition was employed. The fraction of the tank mixed calculated from each sample is shown in Figures B.4 through B.7 for LS test sequences 4, 7, 11, and 20, respectively. Figures B.8 and B.9 show the fraction mixed results for UFP test sequences 2 and 3B.

The final fraction mixed value was determined as the minimum fraction mixed from the locations 1, 2, and 3 of the last sample of a test run. This represents the fraction mixed value associated with highest dye concentration in the cavern after approximately 45–50 minutes of operation. As discussed above, the error associated with the linear isotherm approximation is estimated through the use of Equation B.3. In the worst case, typical errors due to this assumption are approximately less than ± 0.15 fraction mixed; the error goes to zero as the fraction mixed approaches unity. The final fraction of the tank mixed calculated from each run is shown in Tables B.1 through B.4 for LS test sequences 4, 7, 11, and 20, respectively. Tables B.5 and B.6 show the fraction mixed results for UFP test sequences 2 and 3B. Although the NaCl tracer technique is discussed in this document, the NaCl tracer results are supplementary to the BB dye results and will be discussed in a future report.

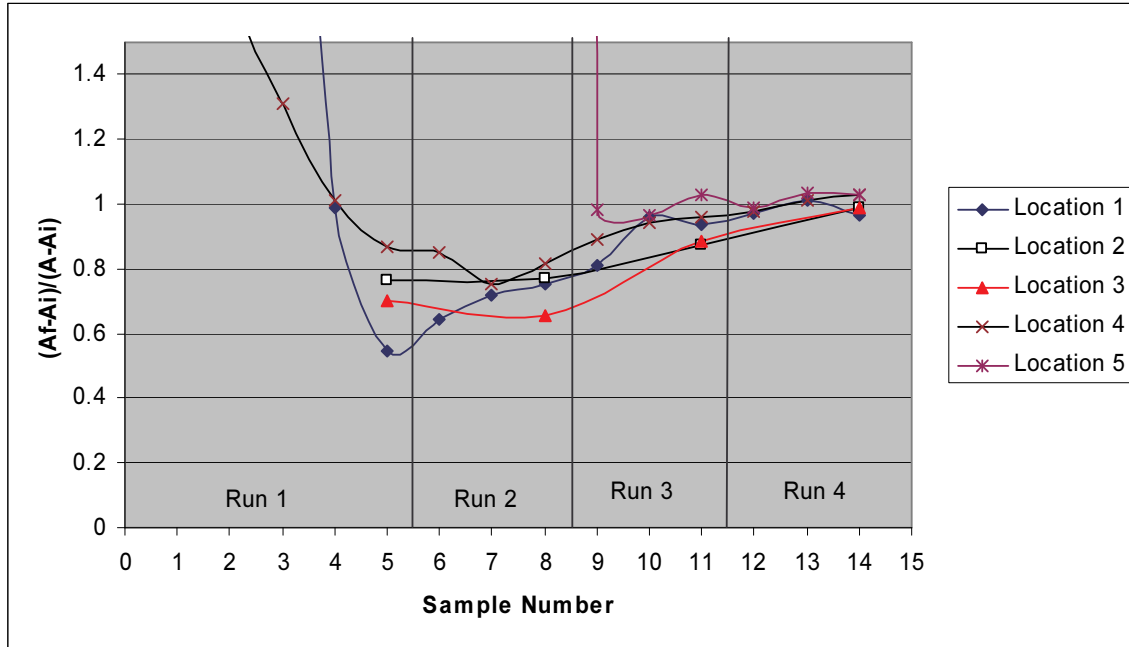


Figure B.4. Fraction Mixed Chart for LS Test Sequence 4

Table B.1. Final Fraction Mixed and Error Estimate Due to Linear Isotherm Assumption for LS Test Sequence 4

Run	Fraction Mixed	Linear Isotherm Estimated Error (\pm) ^(a)
1	0.54	0.15
2	0.65	0.13
3	0.87	0.052
4	0.97	0.014

(a) Estimated error due to assumption of linear isotherm for dye absorption. Experimental error not included.

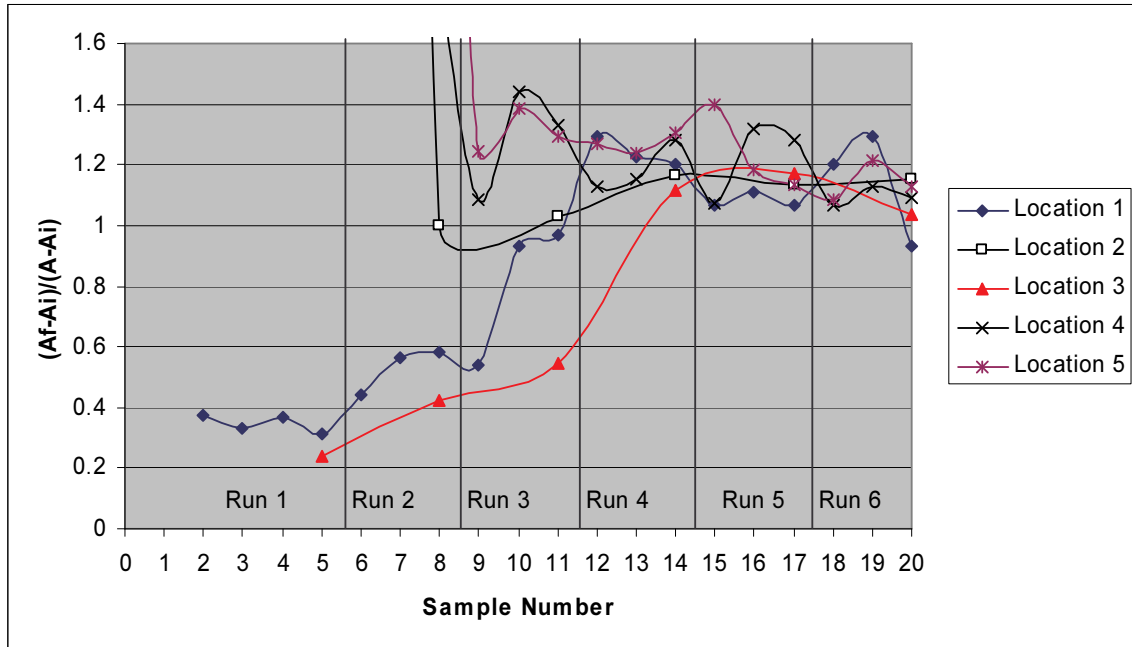


Figure B.5. Fraction Mixed Chart for LS Test Sequence 7

Table B.12. Final Fraction Mixed and Error Estimate Due to Linear Isotherm Assumption for LS Test Sequence 7

Run	Fraction Mixed	Linear Isotherm Estimated Error (\pm) ^(a)
1	0.24	0.11
2	0.42	0.085
3	0.55	0.060
4	1.1	0.010
5	1.1	0.0058
6	0.93	0.0067

(a) Estimated error due to assumption of linear isotherm for dye absorption. Experimental error not included.

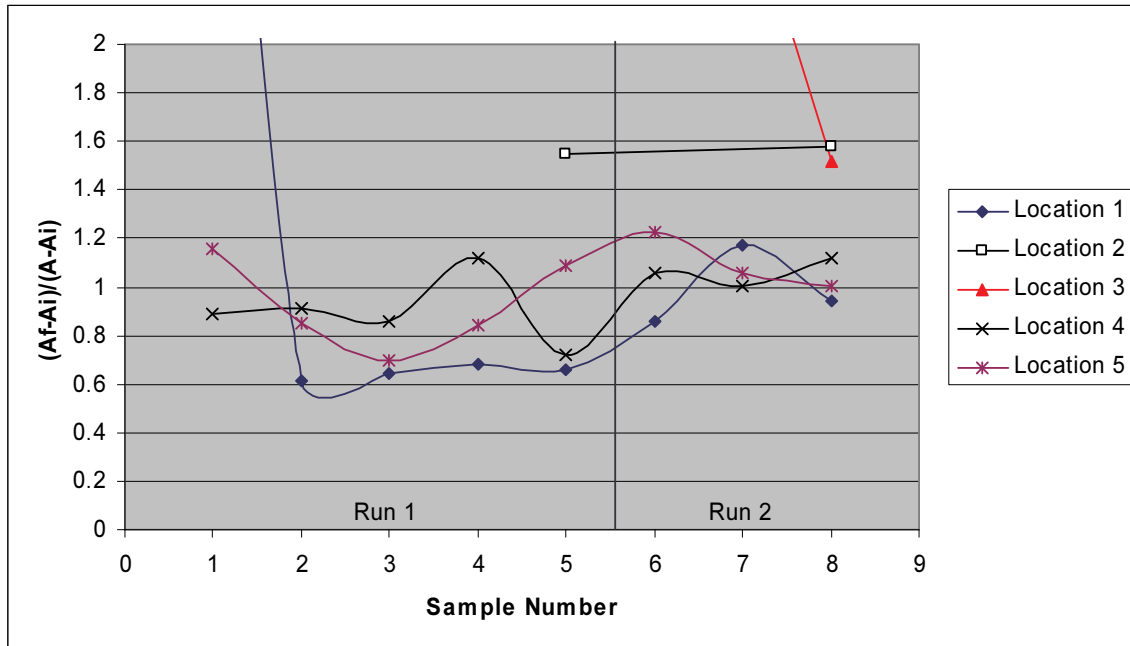


Figure B.6. Fraction Mixed Chart for LS Test Sequence 11

Table B.3. Final Fraction Mixed and Error Estimate Due to Linear Isotherm Assumption for LS Test Sequence 11

Run	Fraction Mixed	Linear Isotherm Estimated Error (\pm) ^(a)
1	0.66	0.033
2	0.95	0.0055

(a) Estimated error due to assumption of linear isotherm for dye absorption. Experimental error not included.

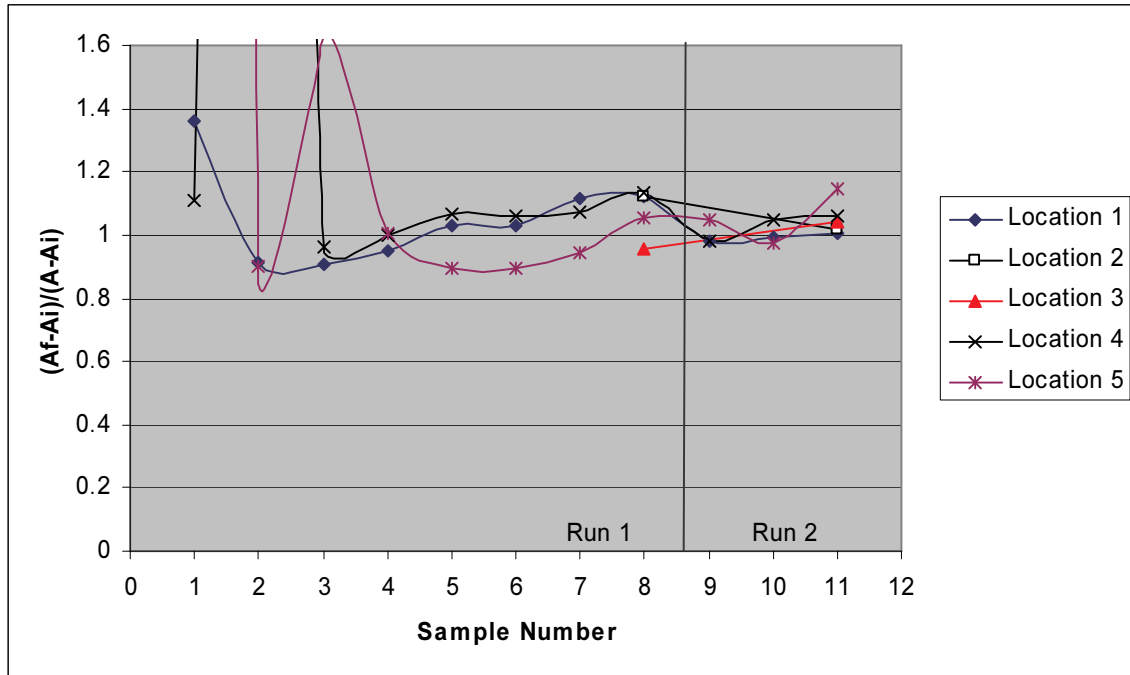


Figure B.7. Fraction Mixed Chart for LS Test Sequence 20

Table B.4. Final Fraction Mixed and Error Estimate Due to Linear Isotherm Assumption for LS Test Sequence 20

Run	Fraction Mixed	Linear Isotherm Estimated Error (\pm) ^(a)
1	0.96	0.0097
2	1.0	0.00069

(a) Estimated error due to assumption of linear isotherm for dye absorption. Experimental error not included.

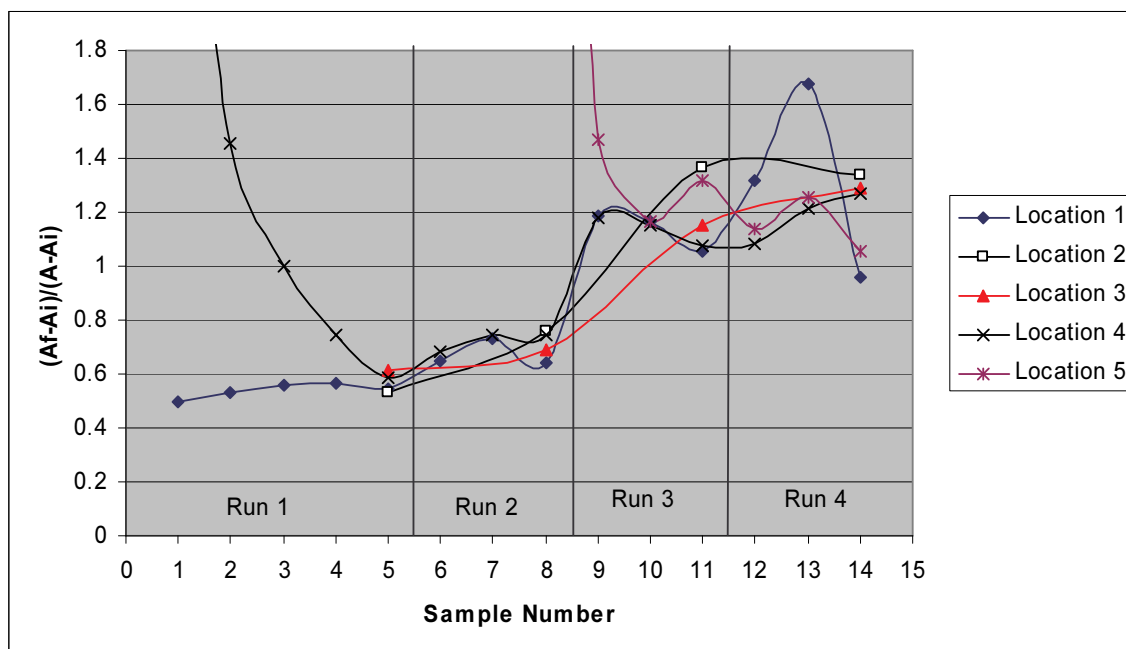


Figure B.8. Fraction Mixed Chart for UFP Test Sequence 2

Table B.5. Final Fraction Mixed and Error Estimate Due to Linear Isotherm Assumption for UFP Test Sequence 2

Run	Fraction Mixed	Linear Isotherm Estimated Error (\pm) ^(a)
1	0.53	0.093
2	0.64	0.074
3	1.1	0.013
4	0.96	0.0088

(a) Estimated error due to assumption of linear isotherm for dye absorption. Experimental error not included.

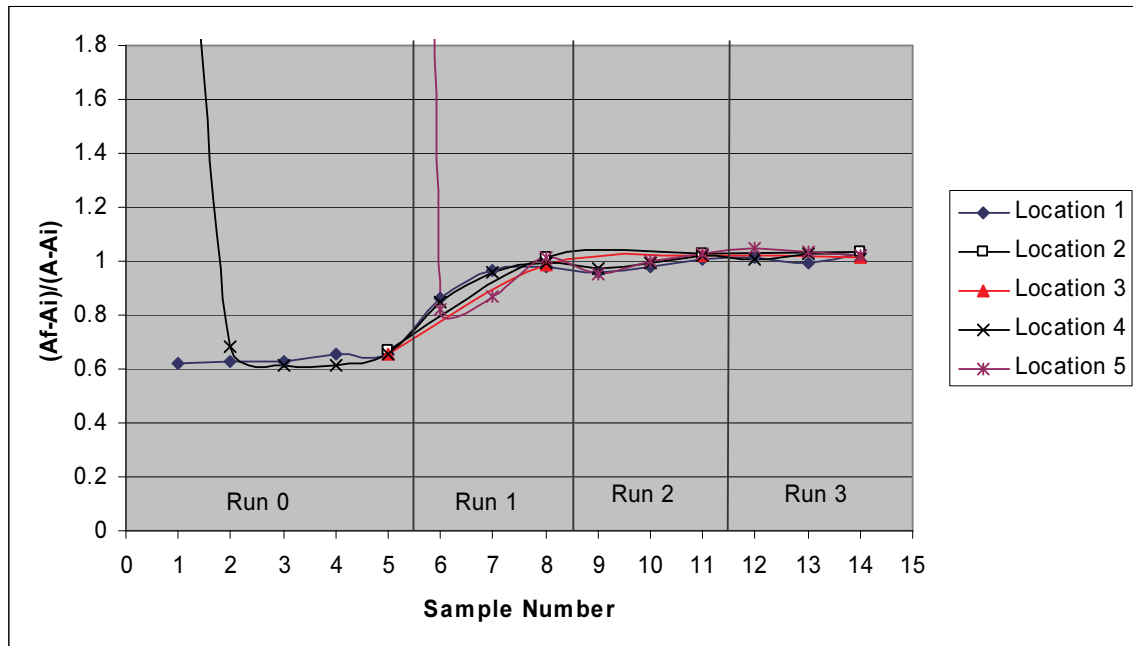


Figure B.9. Fraction Mixed Chart for UFP Test Sequence 3B

Table B.6. Final Fraction Mixed and Error Estimate Due to Linear Isotherm Assumption for UFP Test Sequence 3B

Run	Fraction Mixed	Linear Isotherm Estimated Error (\pm) ^(a)
1	0.65	0.12
2	0.98	0.0074
3	1.0	0.0019
4	1.0	0.0038

(a) Estimated error due to assumption of linear isotherm for dye absorption. Experimental error not included.